Critical phenomena in (2+1)-dimensional relativistic fermion systems

Dissertation

zur Erlangung des akademischen Grades
doctor rerum naturalium (Dr. rer. nat.)

vorgelegt dem Rat der Physikalisch-Astronomischen Fakultät
der Friedrich-Schiller-Universität Jena

von Dipl.-Phys. Lukas Janssen,
geboren am 15. Oktober 1983 in Aachen

Gutachter:

1. Prof. Dr. Holger Gies, Friedrich-Schiller-Universität Jena
2. PD Dr. Lorenz von Smekal, Technische Universität Darmstadt
3. Prof. Dr. I. Herbut, Simon Fraser University, B.C., Canada

Tag der Disputation: 28.06.2012

To Maria

Contents

1 Introduction

"It's also common to hear the opinion that science leads to atheism. This is an opinion that I can't share; I even find it somewhat absurd."

Walter Thirring [1]

Phase transitions are omnipresent in everyday experience: a steaming cup of hot coffee, the formation of clouds upon a cooling of humid air, the melting of ice due to the frictional heat of a skate blade, the little piece of chocolate in the child's warm hand. Moreover, phase transitions embody the most intriguing and challenging puzzles of modern physics: Though being clearly indicated both experimentally and by computer simulations, theoretists already for decades try to understand the confinement-deconfinement phase transition in the theory of quark matter. Moreover, with few exceptions the whole phase diagram of quantum chromodynamics (QCD) is to a large extent unknown, both theoretically and experimentally. Tremendous efforts are expended on its exploration in heavy-ion collider experiment at RHIC, LHC, and the forthcoming FAIR complex. The electroweak phase transition gives rise to the Higgs boson, which is hunted at the two main experiments at the LHC due to its importance for our understanding of the weak-gauge-boson masses. Likewise in condensed matter physics, many of the most exciting challenges are related to phase transitions, often with fascinating applications of potentially high technological relevance. In particular, the unconventional superconducting transition observed in certain strongly-correlated electron systems so far defies any thorough theoretical explanation.

A small but particular interesting subset of all phase transitions are the continuous ones. In the vicinity of a continuous phase transition, thermodynamic quantities and correlation functions typically behave as power laws characterized by critical exponents. The phenomenon of *universality*, after which very dissimilar systems exhibit the same critical behavior with universal critical exponents, has been one of the most fascinating observations of the twentieth century. The microscopic explanation for this phenomenon was the substantial progress of Wilson's work on the renormalization group (RG) [2–7] for which he was awarded the Nobel Prize in 1982. Besides leading to a deep understanding of systems at criticality, the RG has also provided a systematic method for explicitly calculating critical exponents in cases where mean-field theory fails [8]. In fact, RG predictions are in phenomenal agreement with the experiments and often ahead in precision. Phase transitions and their accompanying critical phenomena are determined by fluc-

tuations on all scales. The RG approach is an extremely successful strategy for dealing with such many coupled degrees of freedom; for pedagogical introductions see [9–11]. In the last decades, it has therefore stimulated enormous progress in various fields of physics. In quantum field theory, the RG has led to a substantial new view on the essential concept of renormalization [7]. It has played a key role in the development of quantum chromodynamics and the discovery of asymptotic freedom [12, 13] (Nobel Prize 2004). The RG method describes the mechanism of spontaneous symmetry breaking [14–16] (Nobel Prize 1972 and 2008), which is of intrinsic importance both in particle as well as condensed-matter physics. With this in mind, it is sometimes said that the RG has nowadays achieved the status of a meta-theory, that is to say, a "theory about theories" [17].

In the present work, we apply the RG approach to critical phenomena in $(2+1)$-dimensional relativistic fermion systems. These systems have lately been extensively investigated in a variety of scenarios. On the one hand, they are *per se* rich models that were proposed to confront important puzzles of quantum field theory and thus deserve to be studied on their own right. On the other hand, they allow for fascinating applications to condensed-matter systems. In particular, three-dimensional quantum electrodynamics (QED_3) or the Thirring model [18] are actively discussed, e.g., as effective theories describing different regions of the phase diagram of high-T_c cuprate superconductors [19–24] and, recently, the electronic properties of graphene [25–31]. Especially graphene since its first synthesis in 2004 [32,33] (Nobel Prize 2010) is being lively discussed in the rapidly growing literature on this subject, also because it offers the appealing opportunity of a comparatively simple experimental realization of some up to now unobserved quantum relativistic phenomena, such as the Klein paradox [34,35] or Zitterbewegung [36–38]; for reviews, see [39–42].

However, QED_3 [43–59] and the three-dimensional Thirring model [60–73] are likewise intrinsically interesting: In these models the number of fermion flavors N_f serves as a continuous control parameter for a (possible) quantum phase transition at a critical value N_f^cr. Several approximate solutions of the Dyson-Schwinger equations (DSE) predict that chiral symmetry breaking (χSB) is prohibited for arbitrary large coupling if $N_\mathrm{f} > N_\mathrm{f}^\mathrm{cr}$ [63–66]. A similar quantum critical phenomenon has also been identified in many-flavor QCD_4 [74–78], being currently under intense investigation also because of its potential relevance for technicolor scenarios [79–82] and its implications for the thermal phase boundary [83–87].

The search for the quantum critical point in the Thirring model has so far been rather challenging: different DSE approaches, e.g., have yielded values between $N_\mathrm{f}^\mathrm{cr} \simeq 3.24$ [63] and $N_\mathrm{f}^\mathrm{cr} = \infty$ [64]. By constructing an effective potential for the chiral order parameter, up to leading order of the $1/N_\mathrm{f}$ expansion $N_\mathrm{f}^\mathrm{cr} = 2$ has been found [67]. Recent extensive lattice simulations now point to $N_\mathrm{f}^\mathrm{cr} \simeq 6.6$ [72]. For physical graphene and cuprates, the number of flavors is $N_\mathrm{f} = 2$, such that the true value of N_f^cr may be of profound importance for physical effects corresponding to chiral symmetry breaking in the effective (strongly-coupled) theories. In fact, a dynamically induced mass gap in the band structure of graphene, corresponding to a semimetal-Mott insulator quantum

phase transition, could provide extraordinary applications for graphene-based electronics, offering a possible new candidate material to take over from Si-based technology [39, 40].

Even more than the significant quantitative discrepancies, a more detailed comparison of the critical behavior close to $N_{\rm f}^{\rm cr}$ reported in those studies reveals our insufficient understanding of fermionic field theories in the nonperturbative domain: Kondo [67] reports a *second-order* phase transition with the usual power-law behavior as a function of the control parameter $N_{\rm f}$. By contrast, in the DSE studies [65, 66] an essential scaling behavior of the Kosterlitz-Thouless type has been found, that is to say, the phase transition is of *infinite* order. There[a], the nature of the transition appears to depend on whether the strong-coupling limit is taken before or after $N_{\rm f} \nearrow N_{\rm f}^{\rm cr}$. The scaling analysis on the lattice [72, 73] is consistent with a power-law behavior corresponding to a second-order phase transition which qualitatively confirms, but quantitatively significantly contradicts the Kondo-scenario [67].

The RG approach is *per constructionem* exceedingly powerful to describe systems at criticality, allowing high-precision computations of the corresponding critical exponents. A prominent benchmark example for field-theoretical tools is set by the 3d bosonic O(N) models, which are probably the most simple systems exhibiting spontaneous symmetry breaking where no exact solution is available. The critical exponents are known to considerable high accuracy from high-temperature expansions, resummations of perturbation theory, various implementations of the RG approach, Monte Carlo simulations, and experiments; see [88–91] for recent overviews. The fermionic counterpart of the O(N) models with respect to simplicity is given by the three-dimensional $\mathbb{Z}_2$-symmetric Gross-Neveu (GN) model [92] and its U(1)-symmetric generalizations[b]. From the $1/N_{\rm f}$ expansion [96, 100–102] (together with conformal techniques [103]) and Monte Carlo simulations [97–99, 104] the critical exponents are well known for large and intermediate flavor number, respectively. However, while numerical simulations may become inefficient for increasing flavor number $N_{\rm f}$, the results of the $1/N_{\rm f}$ expansion are not reliable for small $N_{\rm f}$. The RG approach by contrast provides a uniform framework describing both the small and the large-$N_{\rm f}$ domain. The critical behavior of the $\mathbb{Z}_2$-symmetric GN model as a function of $N_{\rm f}$ has been computed

[a] This fact has been argued in Ref. [72].

[b] We note that there is some ambiguity in the terminology of three-dimensional chiral fermion models in the literature. The chiral symmetric model in *four* dimensions has been proposed by Nambu and Jona-Lasinio to describe spontaneous symmetry breaking and dynamical mass generation in QCD [93,94]. There, the symmetry group is the U(1). However, as we shall see below, in three dimension (in a reducible representation of the Dirac algebra), there exist in fact *three* chiral generators. In agreement with [27, 42, 95] we therefore refer to the 3d Nambu-Jona-Lasinio (NJL) model as the fermionic theory which is invariant under *all three* chiral transformations, forming (together with the usual phase rotations) for each flavor a global U(2) symmetry, cf. Chap. 4. As is the case in four dimensions, the symmetry groups of NJL and Thirring model then coincide. The three-dimensional four-fermion theory invariant under only *one* of the three chiral transformations in this convention is often termed chiral GN model [96–99].

in various RG studies to high accuracy [101,105–107], agreeing well with the $1/N_{\rm f}$-studies for large $N_{\rm f}$ and the lattice results for intermediate $N_{\rm f}$. The available Monte Carlo studies [97,99,104] employ *staggered* lattice fermions [108,109], which face the doubling problem [110]; without further ado (see e.g., [71]), they are hence limited to even number of flavors. The only study we know of which computes the critical behavior of the GN model with solely one (two-component) fermion flavor is Ref. [106]; it employs the *functional RG* approach. The functional RG and associated RG flow equations such as the Wetterich equation [111] are a versatile tool to investigate strongly-interacting field theories in general and critical phenomena in particular. With the Wetterich equation being an exact equation, consistent approximation schemes can be devised that allow for a systematic nonperturbative investigation of a given system. For reviews on this very fruitful and rapidly developing approach, see [17,112–120]. In the context of the bosonic O(N) models, the method has exhaustively been investigated and used with a remarkable quantitative success; the results for critical exponents have reached an accuracy which is comparable if not superior to that of, e.g., lattice simulations and high-order ϵ expansions, see [89,90] for comparisons.

We have been motivated by these developments to confront the functional RG with the puzzles given by the 3d chiral fermion systems at criticality. The question is: What is the nature of the χSB phase transition being controlled by either the bare coupling g (for fixed $N_{\rm f} \leq N_{\rm f}^{\rm cr}$) or the number of flavors $N_{\rm f}$ (for fixed $g > g_{\rm cr}$)? What are, if applicable, the corresponding exponents determining the critical behavior? Naively, a universal answer may not be apparent as 3d fermion models are perturbatively nonrenormalizable. However, rather than inherent inconsistencies, this difficulty may reflect the failure of the perturbative approach [121–124]. In fact, renormalizability to any order in a large-$N_{\rm f}$ expansion has been shown both for the 3d GN model [60,125,126] as well as the 3d Thirring [60–64], corresponding to an interacting fixed point of the RG. This has been taken as an indication that these models can indeed be defined nonperturbatively in 3d, providing the same amount of universality as any perturbatively renormalizable theory. In any case, a profound understanding of the χSB phase transition in these models requires a quantitative control of fluctuating chiral fermions in the nonperturbative domain. This is a challenging problem, which applies well beyond our 3d models. A probably wise approach to the complicated issues related to χSB in the standard model of particle physics or the superconducting transition in the cuprates may be to first get a grasp of the mechanism in somewhat simpler (lower-dimensional and higher-symmetric, resp.) systems before tackling the really painful matter. In this spirit, we believe that quantitative predictions for the critical behavior of the 3d fermion models investigated in this work can serve as benchmark examples, where nonperturbative techniques can prove their validity.

The work is organized as follows: After a brief review of the functional RG approach in the formulation of the *effective average action* in Chap. 2, we construct in Chap. 3 a generalization of the chiral GN model exhibiting a $\mathrm{U_L}(N_{\rm L}) \otimes \mathrm{U_R}(1)$ symmetry. These models support a left-

right asymmetry similar to a crucial building block of the standard model of particle physics: the Higgs-Yukawa sector. If they undergo a phase transition to an ordered phase with broken chiral symmetry this transition can be viewed as an analogue of the electroweak phase transition in 3d. The corresponding critical behavior defines new universality classes, the properties of which are a pure prediction of the system.

In Chap. 4 we turn our focus to a systematic investigation of 3d fermion theories in the maximally symmetric case. The 3d Thirring as well as the 3d Nambu-Jona-Lasinio (NJL) model is of this type. Universality and, more profoundly, UV completeness can, in fact, be analyzed within Weinberg's scenario of asymptotic safety [127–130], in which a UV complete infinite-cutoff limit can be taken at a potentially non-Gaußian fixed point. The resulting theories are predictive and exhibit universality, if the number of RG relevant directions at the fixed point are finite. In Chap. 4, we re-examine renormalizability from this viewpoint by taking a full basis of fermionic four-point functions invariant under the 3d Thirring symmetry into account. We show that the UV fixed point structure can indeed be mapped out, on the one hand confirming the large-N_f results, but also revealing interesting deviations from the large-N_f asymptotics. For instance, we can identify a non-Gaußian UV fixed point that defines a "Thirring universality class" which governs (at least in our RG scheme) the critical behavior of both the Thirring model as well as the NJL model. However, we show that only in the strict large-N_f limit it corresponds to a pure Thirring coupling. In addition, we find further fixed points, which may be associated with phase transitions, e.g., towards a parity broken phase, corresponding to the $\mathbb{Z}_2$-symmetric GN universality class.

With the insight gained from the analysis of the UV structure we develop the long-range behavior of the 3d Thirring model in Chap. 5. By including composite degrees of freedom by means of a scale-dependent Hubbard-Stratonovich transformation we are able to investigate a competition between different interaction channels and to identify a critical flavor number above which χSB is prohibited. We compute the critical behavior in terms of the universal exponents ν, η_ϕ, β, and γ and explicitly verify the hyperscaling relations. We also discuss the phase transition for fixed $g > g_\mathrm{cr}$ with N_f as control parameter, pointing to a scenario with a second-order phase transition at $N_\mathrm{f}^\mathrm{cr} \simeq 5.1(7)$. Finally, we attempt to unravel the plethora of different results for the critical behavior given in the literature and relate them to our findings. We give a summary in Chap. 6.

The compilation of this thesis is solely due to the author. However, parts of this work have been developed in collaboration with colleagues from the Institute of Theoretical Physics in Jena. The results on the chiral Gross-Neveu model in Chap. 3 have been obtained in collaboration with H. Gies, S. Rechenberger (now University of Mainz), and M. Scherer (now RWTH Aachen University) and have already been reported in [131–133]. The UV structure of the Thirring model as described in Chap. 4 has been worked out together with my supervisor H. Gies; our findings have been published in [134]. Chap. 5 contains as yet unpublished materials, which have also been developed in collaboration with H. Gies.

2 Functional renormalization group approach to critical phenomena

2.1 Quantum effective action

All physical information of a field theory is stored in correlation functions which in turn can be extracted from a generating functional

$$Z[J] \equiv \mathrm{e}^{W[J]} = \int \mathcal{D}\varphi \, \mathrm{e}^{-S[\varphi]+\int J\varphi}, \tag{2.1}$$

with source term $\int J\phi \equiv \int \mathrm{d}^d x \, J(x)\varphi(x)$. For notational simplicity, we consider a theory of a single scalar field φ. The generalization to higher-spin fields, for instance, fermionic fields or vector fields is straightforward; see, e.g., Ref. [10]. We assume the functional integral in Eq. (2.1) to be regularized by an UV cutoff Λ. Connected n-point correlators are obtained by suitable differentiation of the Schwinger functional $W[J] = \ln Z[J]$. E.g., the connected 2-point function is given by

$$\left.\frac{\delta^2 W[J]}{\delta J(x)\delta J(y)}\right|_{J=0} = \langle\varphi(x)\varphi(y)\rangle - \langle\varphi(x)\rangle\langle\varphi(y)\rangle. \tag{2.2}$$

A differentiable Schwinger functional $W[J]$ is strictly convex, since its second derivative $W^{(2)}(x,y) \equiv \delta^2 W/\delta J(x)\delta J(y)$ is the kernel of a positive operator,

$$W^{(2)}(x,y) = \langle(\varphi(x) - \langle\varphi(x)\rangle_J)\,(\varphi(y) - \langle\varphi(y)\rangle_J)\rangle_J\,, \qquad \int J(x)W^{(2)}(x,y)J(y) > 0. \tag{2.3}$$

Here we adopted the notation

$$\langle\mathcal{O}(\varphi)\rangle_J = \frac{\int \mathcal{D}\varphi\, \mathcal{O}(\varphi)\, \mathrm{e}^{-S[\varphi]+\int J\varphi}}{\int \mathcal{D}\varphi\, \mathrm{e}^{-S[\varphi]+\int J\varphi}} \tag{2.4}$$

for the expectation value of the observable $\mathcal{O}(\varphi)$ in the presence of an external source J [135]. Typically, for systems with spontaneous symmetry breaking, the Schwinger function however has a kink at $J = 0$, reflecting the degeneracy of the vacuum state. Thus, in general $W[J]$ is only convex for large arguments $|J|$, not necessarily for all J. The effective action $\Gamma[\phi]$ (generating functional of one-particle irreducible (1PI) correlation functions) is defined as the Legendre transform of the

Schwinger functional $W[J]$,

$$\Gamma[\phi] = \sup_J \left(\int J\phi - W[J] \right). \tag{2.5}$$

For any given ϕ, the source J for which $\int J\phi - W[J]$ approaches its supremum is its conjugate variable. ϕ then corresponds to the expectation value of φ in the presence of the conjugate source J,

$$\phi(x) = \frac{\delta W[J]}{\delta J(x)}, \tag{2.6}$$

which is unique for differentiable $W[J]$. For the conjugate pair (ϕ, J) we find the quantum equation of motion

$$J(x) = \frac{\delta \Gamma[\phi]}{\delta \phi(x)}, \tag{2.7}$$

The field expectation value for vanishing source is thus given by the homogeneous field $\phi = \phi_0$, for which the effective action is minimal, $\Gamma[\phi_0] \leq \Gamma[\phi]$. For differentiable $W[J]$ the minimum ϕ_0 is unique. From Eqs. (2.6)–(2.7) we infer for conjugate (J, ϕ)

$$\frac{\delta^2 W[J]}{\delta J(x) \delta J(y)} = \frac{\delta \phi(x)}{\delta J(y)}, \qquad \frac{\delta^2 \Gamma[\phi]}{\delta \phi(x) \delta \phi(y)} = \frac{\delta J(x)}{\delta \phi(y)}, \tag{2.8}$$

and thus

$$\int \mathrm{d}^d z \, \frac{\delta^2 \Gamma[\phi]}{\delta \phi(x) \delta \phi(z)} \frac{\delta^2 W[J]}{\delta J(z) \delta J(y)} = \delta(x - y). \tag{2.9}$$

Thus, at the minimum $\phi = \phi_0$ the proper 2-vertex $\Gamma^{(2)}|_{\phi_0} \coloneqq \delta^2 \Gamma / \delta \phi^2|_{\phi_0}$ is the inverse of the full connected propagator $G = W^{(2)}|_{J=0}$. Analogously, proper n-vertices for $n > 2$ are related to (amputated) correlation functions by

$$W^{(n)}_{\text{amp.}} = -\Gamma^{(n)} + \text{reducible terms}, \qquad n > 2, \tag{2.10}$$

see [10] for details.

2.2 RG flow equation

In the spirit of Wilson's approach to the renormalization group (RG), we introduce the scale-dependent partition function [111]

$$Z_k[J] = \mathrm{e}^{W_k[J]} \coloneqq \int \mathcal{D}\varphi \, \mathrm{e}^{-S[\varphi] - \Delta S_k[\varphi] + \int J\phi}, \tag{2.11}$$

where we added the regulator term

$$\Delta S_k[\varphi] = \int \frac{\mathrm{d}^d q}{(2\pi)^d} \, \varphi(-q) R_k(q) \varphi(q), \tag{2.12}$$

which serves as an additional IR cutoff, ensuring that momentum modes $\varphi(q)$ above the scale k, i.e., for $k \lesssim q \leq \Lambda$, are integrated out. This is indeed possible, if the regulator function $R_k(q)$ screens the IR modes for $q \ll k$, i.e.,

$$R_k(q \to 0) = C_k > 0 \quad \text{for } k > 0. \tag{2.13}$$

For $k \to 0$ we demand that all modes should be integrated out and thus

$$R_{k\to 0}(q) = 0. \tag{2.14}$$

At the IR scale the k-dependent partition function thus exactly coincides with the usual functional integral in Eq. (2.1), $Z_{k\to 0}[J] = Z[J]$. At the UV scale $k \to \Lambda$ the regulator function has to satisfy

$$R_{k\to\Lambda}(q) \to \infty \quad \text{for } \Lambda \to \infty. \tag{2.15}$$

We define the *effective average action* Γ_k as the Legendre transform of $W_k = \ln Z_k$ with an additional regulator term,

$$\Gamma_k[\phi] \coloneqq \sup_J \left(\int J\phi - W_k[J] \right) - \Delta S_k[\phi], \tag{2.16}$$

such that the quantum equation of motion for conjugate (J, ϕ) with $\phi = \delta W_k / \delta J$ receives a regulator modification,

$$\frac{\delta \Gamma_k[\phi]}{\delta \phi(x)} = J(x) - \int \frac{\mathrm{d}^d q}{(2\pi)^d} \, \mathrm{e}^{\mathrm{i}qx} \, R_k(q) \phi(q). \tag{2.17}$$

Hence, the inverse of the scale-dependent full propagator $G_k = W_k^{(2)}|_{J=0}$ is given by $G_k^{-1} = \Gamma_k^{(2)}|_{\phi_0} + R_k$, with ϕ_0 denoting the (in general scale-dependent) minimizing field configuration. From Eq. (2.16) we can straightforwardly derive an equation for Γ_k,

$$\mathrm{e}^{-\Gamma_k[\phi]} = \int \mathcal{D}\varphi \, \mathrm{e}^{-S[\phi+\varphi] - \Delta S_k[\varphi] + \int \frac{\delta \Gamma_k}{\delta \phi} \varphi} \, . \tag{2.18}$$

In the UV limit $k \to \infty$ the cutoff function R_k diverges and the regulator term $\mathrm{e}^{-\Delta S[\varphi]}$ behaves as a delta functional $\propto \delta[\varphi]$. Hence, the effective average action in this limit coincides with the bare action,

$$\Gamma_{k\to\Lambda}[\phi] = S[\phi] + \text{const.} \quad \text{for } \Lambda \to \infty. \tag{2.19}$$

In the IR we have $\Delta S_{k\to 0}[\phi] = 0$ and $W_{k\to 0}[J] = W[J]$ such that Γ_k approaches the full quantum effective action,

$$\Gamma_{k\to 0}[\phi] = \Gamma[\phi], \tag{2.20}$$

taking all quantum fluctuations into account. For intermediate scales $0 < k < \Lambda$ the effective average action includes all quantum effects of the UV modes with momentum $q \gtrsim k$. The change of Γ_k under an infinitesimal RG step from k to $k - dk$ is governed by the Wetterich equation [111]

$$\partial_t \Gamma_k[\phi, \psi, \dots] = \frac{1}{2} \operatorname{STr} \left(\frac{\partial_t R_k}{\Gamma_k^{(2)}[\phi, \psi, \dots] + R_k} \right), \qquad \partial_t \equiv k \partial_k, \tag{2.21}$$

where for completeness we reintroduced a possible dependence of Γ_k on fermionic and other higher-spin fields $\psi, \dots$ Again, $\Gamma_k^{(2)}$ denotes the second functional derivative with respect to the fields. Due to its Grassmann nature, the fermionic sector contributes to the flow with an additional minus sign, which is taken into account by the supertrace $\operatorname{STr} \coloneqq \operatorname{Tr}|_{\phi,\dots} - \operatorname{Tr}|_{\psi,\dots}$. The solution to the flow equation (2.21) provides an RG trajectory in theory space, interpolating between the bare action $\Gamma_{k=\Lambda} = S$ to be quantized and the full quantum action $\Gamma_{k=0} = \Gamma$.

As a functional differential equation, the Wetterich equation can exactly be solved only in very special cases; see, e.g., [136, 137]. However, various systematic approximation schemes beyond perturbation theory are available which can be summarized under the *method of truncations*. One of the most frequently employed schemes is the operator expansion. It is obtained by expanding Γ_k in operators of increasing mass dimension; in particular, derivative operators. In this context, the expansion is also referred to as *derivative expansion*. E.g., for a scalar field theory we obtain up to second order

$$\Gamma_k[\phi] = \int \mathrm{d}^d x \left(U_k(\phi) + \frac{1}{2} Z_k(\phi) (\partial_\mu \phi)^2 + \mathcal{O}(\partial^4) \right), \tag{2.22}$$

with the scale-dependent effective potential $U_k(\phi)$ and the wave function renormalization $Z_k(\phi)$. The derivative expansion is particularly convenient for highly-symmetric systems, in which case up to a given order only a very limited number of operators at all can occur in Γ_k. Another widely used approximation scheme is given by the *vertex expansion*

$$\Gamma_k[\phi] = \sum_{n=0}^{\infty} \frac{1}{n!} \int \mathrm{d}^d x_1 \dots \mathrm{d}^d x_n \, \Gamma_k^{(n)}(x_1, \dots, x_n) \phi(x_1) \dots \phi(x_n), \tag{2.23}$$

with the scale-dependent vertex functions $\Gamma_k^{(n)}$, interpolating between the bare vertices of the UV action S and the fully dressed 1PI proper vertices $\Gamma^{(n)}$. Further approximation schemes are obtained by suitable systematic combinations of the two above. For reviews on the functional renormalization group approach both to condensed-matter as well as high-energy physics, we refer to the review articles in [112–120] and the textbook [17].

Due to the absence of an obvious small expansion parameter in strongly-correlated systems, the challenge is to find a truncation which still incorporates the most relevant degrees of freedom of a given problem. As for all nonperturbative analytical tools, it is often hard to control the systematic error induced by the neglected contributions. On the one hand, one can study the

quantitative influence of higher-order effects through enlargement of the truncation. This is often a tedious task; moreover, it also does not give a rigorous upper bound on the error. On the other hand, a rough estimate can possibly already be obtained very easily by comparing the flow in different regularization schemes. In a full computation, all IR quantities are of course regulator independent. However, this not necessarily remains true for the truncated flow. Thus, the amount of dependence on the regulator function R_k may give an indication on the order of the truncation-induced error. Let us discuss this suggestion in some more detail: Within a given order of the expansion, different regularization schemes may lead to differently accurate results. In fact, it has been shown [116, 138–143] that there are specific classes of regulator functions, for which the error within a truncation is minimized. For the derivative expansion, such an optimized regulator is given by the linear cutoff, which reads for the bosonic sector

$$R_{\phi,k}(q) = Z_{\phi,k} q^2 r_{\phi,k}(q^2), \qquad r^{\mathrm{opt}}_{\phi,k}(q^2) = \left(\frac{k^2}{q^2} - 1\right)\Theta(k^2 - q^2), \tag{2.24}$$

with bosonic wave-function renormalization $Z_{\phi,k}$ and for the fermionic sector

$$R_{\psi,k}(q) = -Z_{\psi,k} \not{q} r_{\psi,k}(q^2), \qquad r^{\mathrm{opt}}_{\psi,k}(q^2) = \left(\sqrt{\frac{k^2}{q^2}} - 1\right)\Theta(k^2 - q^2), \tag{2.25}$$

with fermionic wave-function renormalization $Z_{\psi,k}$. Here, we have used the common notation using the regulator shape functions r_k. Loosely speaking, the optimized flow within a given truncation corresponds to the "shortest" RG trajectory in theory space. In contrast, the sharp cutoff reads

$$r^{\mathrm{sc}}_{\phi,k}(q^2) = a\left(\frac{k^2}{q^2} - 1\right)\Theta(k^2 - q^2), \tag{2.26}$$

$$r^{\mathrm{sc}}_{\psi,k}(q^2) = \left(\sqrt{a\left(\frac{k^2}{q^2} - \frac{a-1}{a}\right)} - 1\right)\Theta(k^2 - q^2), \qquad \text{with} \quad a \to \infty. \tag{2.27}$$

We demand for definiteness that the sharp-cutoff limit $a \to \infty$ is to be taken *after* the integration over the internal momentum q, in agreement with [144]. For practical reasons, we have chosen the definition of the fermionic shape function $r^{\mathrm{sc}}_{\psi,k}$ such that for all $a \geq 1$ we have $q^2(1 + r^{\mathrm{sc}}_{\phi,k}) = q^2(1 + r^{\mathrm{sc}}_{\psi,k})^2$, in accordance with the linear cutoff. In terms of optimization, the sharp cutoff represents the opposite of the linear cutoff: in a sense, it leads to the "longest" RG trajectory, possibly yielding the poorest results within a given truncation. In what follows, we will therefore think of the results obtained with the linear regulator as our most accurate ones (the "measured" value), whereas the difference to the results obtained with the sharp regulator is thought of as very rough estimate on the truncation error: since for a nonoptimized regulator compared to optimized flows a higher order of the expansion is needed to achieve similar predictive power, different regularization schemes (very loosely speaking) effectively "probe" different orders of the expansion [145]. Of course, this identification is by no means rigorous and could turn out to be very sensitive to the respective observable; the corresponding error estimate should therefore be interpreted

with caution. However, studies of the derivative expansion in the context of three-dimensional scalar field theories, where the critical behavior is known to extremely high accuracy, show indeed that the regulator-dependence gives a good estimate on the truncation-induced error; see [89] for a recent overview. Similar conclusions can be drawn from works on the three-dimensional Gross-Neveu model at next-to-leading order in the derivative expansion [105, 106].

Once a particular expansion of the effective action with corresponding truncation has been fixed, the flow of the individual terms present in Γ_k are straightforwardly obtained by appropriate projections of the Wetterich equation (2.21). E.g., for a scalar field theory, the flow equation for the effective potential is given by evaluating $\partial_t \Gamma_k$ for constant fields,

$$\partial_t U_k(\phi) = \frac{1}{2\Omega_d} \operatorname{STr}\left(\frac{\partial_t R_k}{\Gamma_k^{(2)}[\phi] + R_k}\right)\Bigg|_{\phi=\text{const.}}, \tag{2.28}$$

with d-dimensional space-time volume $\Omega_d = \int \mathrm{d}^d x$. In general, the flow equations for all couplings can be acquired by rewriting (2.21) as

$$\partial_t \Gamma_k = \frac{1}{2}\,\tilde{\partial}_t \operatorname{STr} \ln\left(\Gamma_k^{(2)} + R_k\right), \tag{2.29}$$

where $\tilde{\partial}_t$ is defined to act only on the regulator's t-dependence,

$$\tilde{\partial}_t \coloneqq \int \frac{\mathrm{d}^d q}{(2\pi)^d}\, \partial_t R_{\phi,k}(q) \frac{\delta}{\delta R_{\phi,k}(q)} \tag{2.30}$$

We split $\Gamma_k^{(2)}[\phi]$ into a field-independent and a fluctuating part,

$$\Gamma_k^{(2)}[\phi] = \Gamma_{k,0}^{(2)} + \Delta\Gamma_k^{(2)}[\phi], \quad \text{with} \quad \Gamma_{k,0}^{(2)} \coloneqq \Gamma_k^{(2)}[\phi_0] \quad \text{and} \quad \Delta\Gamma_k^{(2)}[\phi] \coloneqq \Gamma_k^{(2)}[\phi] - \Gamma_k^{(2)}[\phi_0], \tag{2.31}$$

where ϕ_0 denotes the field configuration which minimizes Γ_k. Note that the field-independent part is the inverse of the full propagator $G_k^{-1} = \Gamma_{k,0}^{(2)} + R_k$. In the regime of spontaneous symmetry breaking, the minimum ϕ_0 is in general scale-dependent and not unique. The flow equations for the individual couplings are easily obtained by comparing the coefficients in the expansion

$$\partial_t \Gamma_k[\phi] = \frac{1}{2}\,\tilde{\partial}_t \operatorname{STr} \ln\left(\Gamma_{k,0}^{(2)} + R_k\right) + \frac{1}{2}\,\tilde{\partial}_t \operatorname{STr}\left[\sum_{n=1}^{\infty} \frac{(-1)^{n+1}}{n}\left(\frac{\Delta\Gamma_k^{(2)}[\phi]}{\Gamma_{k,0}^{(2)} + R_k}\right)^n\right], \tag{2.32}$$

$$= \frac{1}{2} \operatorname{STr}\left(\frac{\partial_t R_k}{\Gamma_{k,0}^{(2)} + R_k}\right) + \frac{1}{2} \operatorname{STr}\left[\sum_{n=1}^{\infty} (-1)^n \left(\frac{\Delta\Gamma_k^{(2)}[\phi]}{\Gamma_{k,0}^{(2)} + R_k}\right)^n \frac{\partial_t R_k}{\Gamma_{k,0}^{(2)} + R_k}\right]. \tag{2.33}$$

For a scalar field theory in the symmetric regime, the flow of the 2-vertex is given by the terms quadratic in ϕ,

$$\partial_t \Gamma_k^{(2)}[\phi_0] = -\frac{1}{2} \operatorname{STr}\left(\frac{\Delta\Gamma_k^{(4)}[\phi_0]}{\Gamma_{k,0}^{(2)} + R_k} \frac{\partial_t R_k}{\Gamma_{k,0}^{(2)} + R_k}\right), \tag{2.34}$$

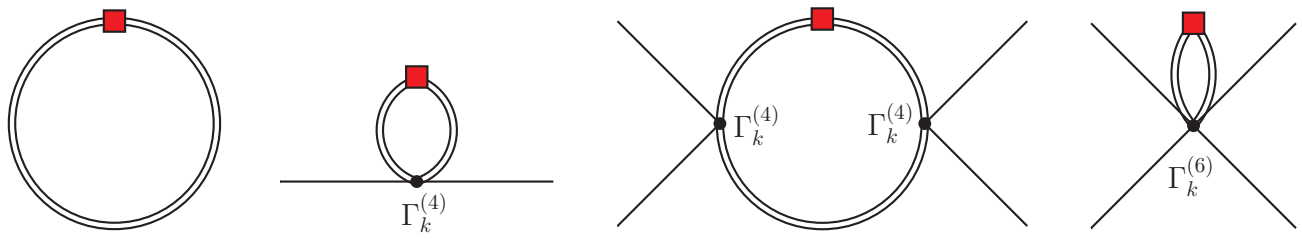

Figure 2.1 Representation of flow equations for effective potential, 2-vertex, and 4-vertex; cf. Eqs. (2.28), (2.34), (2.35). Inner double lines correspond to full average propagators $(\Gamma_{k,0}^{(2)} + R_k)^{-1}$, vertices represent the full vertices $\Gamma_k^{(n)}$, $n > 2$. Regulator insertions $\partial_t R_k$ are depicted by red squares.

which involves the average 4-vertex $\Gamma_k^{(4)}$, whose flow is given by the terms quartic in ϕ,

$$\partial_t \Gamma_k^{(4)}[\phi_0] = \mathrm{STr}\left[\left(\frac{\Delta\Gamma_k^{(4)}[\phi_0]}{\Gamma_{k,0}^{(2)} + R_k}\right)^2 \frac{\partial_t R_k}{\Gamma_{k,0}^{(2)} + R_k}\right] - \frac{1}{2}\,\mathrm{STr}\left(\frac{\Delta\Gamma_k^{(6)}[\phi_0]}{\Gamma_{k,0}^{(2)} + R_k}\frac{\partial_t R_k}{\Gamma_{k,0}^{(2)} + R_k}\right), \tag{2.35}$$

involving the 6-vertex $\Gamma_k^{(6)}$, and so on. In the style of perturbative Feynmans graphs, the flow equations can be interpreted diagrammatically: The full average propagators $G_k = (\Gamma_{k,0}^{(2)} + R_k)^{-1}$ correspond to double inner lines and the 1PI n-point functions $\Gamma^{(n)}$ for $n > 2$ are represented graphically by n-vertices. The regulator insertion $\partial_t R_k$ is depicted by a filled square. As an example, we give in Fig. 2.1 the diagrams for the flow equations (2.28)[a], (2.34), and (2.35). All beta functions can thus be computed straightforwardly in close analogy to the perturbative Feynman graphs by summing up all possible 1-loop diagrams and replacing the bare vertices by full vertices $\Gamma_k^{(n)}$ and the bare propagators by full propagators G_k. We note however that the number of possible vertices $\Gamma_k^{(n)}$ is in general much larger than the number of bare vertices present in the bare action S, since during the renormalization procedure additional terms (compatible with the symmetries) may be generated by the flow. We emphasize that in spite of the structural similarities to the perturbative series, the resulting flow equations are fully nonperturbative, incorporating effects of arbitrarily high loop order as well as genuinely nonperturbative effects like instantons in QCD [112].

2.3 Critical behavior and RG scaling

Consider the field theory consisting of N scalar fields ϕ^a with effective average action of Ginzburg-Landau-Wilson type

$$\Gamma_k[\phi] = \int \mathrm{d}^d x \left[\frac{Z_k}{2}(\partial_\mu \phi^a)(\partial_\mu \phi^a) + \frac{\bar{\lambda}_k}{8}\left(\phi^a\phi^a - \phi_{0,k}^a \phi_{0,k}^a\right)^2\right], \qquad a = 1, \ldots, N, \tag{2.36}$$

[a] The diagrammatical representation of Eq. (2.28) involves a slight abuse of notation: here, the inner line corresponds to the propagator $(\Gamma_k^{(2)} + R_k)^{-1}$ evaluated at *arbitrary* constant field ϕ, not necessarily at the minimum ϕ_0.

exhibiting O(N) symmetry

$$\phi^a \mapsto O^{ab}\phi^b, \qquad \text{with} \qquad O^{ac}O^{bc} = \delta^{ab}. \tag{2.37}$$

As is well known, for $2 < d \leq 4$ and above some critical initial parameters the O(N) symmetry is spontaneously broken down to O($N-1$), corresponding to a nontrivial fixed point of the RG transformations, known as Wilson-Fisher fixed point [146]. In the broken phase, the spectrum of the theory contains one massive mode (in QCD we would call it the ρ-meson) and $N-1$ massless Goldstone modes (the pions). The universal critical behavior of many statistical systems is described by the O(N) models: For $N = 1$ the theory belongs to the Ising universality class with discrete symmetry $Z_2 \equiv \mathrm{O}(1)$, determining the gas-liquid transition at the critical point. For $N = 2$ the theory describes the superfluid phase transition (XY models), for $N = 3$ the ferromagnetic phase transition (Heisenberg models), etc.

In simple truncations, one studies the beta functions given by the flow equations of the dimensionless renormalized couplings $\lambda \coloneqq Z_k^{-2}k^{d-4}\bar{\lambda}_k$ and $\kappa \coloneqq Z_k k^{2-d}\phi^a_{0,k}\phi^a_{0,k}/2$, i.e., $\beta_i(g) \coloneqq \partial_t g_i$ with $g \equiv (\kappa, \lambda)$. We define the scale-dependent anomalous dimension as the flow of the wave function renormalization, $\eta(g) \coloneqq -\partial_t \ln Z_k$. A fixed point $g^* = (\kappa^*, \lambda^*)$ is given by a simultaneous zero of all beta functions,

$$\forall i: \qquad \beta_i(g^*) = 0. \tag{2.38}$$

Starting the RG flow below the nontrivial fixed point with $g^* \neq 0$, the field expectation value in the IR (the order parameter) remains zero, $\phi_{0,k\to 0} = \langle\varphi\rangle = 0$, whereas for a UV coupling above the fixed point spontaneous symmetry breaking occurs with a finite order parameter $\langle\varphi\rangle \neq 0$. The corresponding critical exponents are universal and can be related to the flow in the vicinity of the fixed point g^*: The correlation length ξ is given by the inverse of the renormalized mass $\bar{m}_{\mathrm{R}} = \lim_{k\to 0}\sqrt{\bar{\lambda}_k/Z_k}\phi_{0,k}$,

$$\xi = \bar{m}_{\mathrm{R}}^{-1} = f_\pm|\delta g|^{-\nu}\left(1 + b_\pm|\delta g|^{\omega\nu} + \dots\right), \tag{2.39}$$

with $\delta g \coloneqq g_\Lambda - g^*$ measuring the distance from its critical value ("reduced temperature"). "+" ("−") refers to "above" ("below") criticality. The index ν characterizes the divergence of ξ close to the critical point, whereas ω determines the leading correction to the power-law scaling behavior. Both exponents ν and ω are universal, while for the amplitudes this is the case only for ratios like f_+/f_-. In the regime of the fixed point g^*, the RG flow can be linearized,

$$\partial_t g_i = B_i{}^j(g_j - g_j^*) + \mathcal{O}((g-g^*)^2), \qquad \text{with} \qquad B_i{}^j \coloneqq \left.\frac{\partial\beta_i}{\partial g_j}\right|_{g=g^*}. \tag{2.40}$$

The Jacobian $B_i{}^j$ defines the *stability matrix*. The associated eigenvectors v_I govern the evolution of small deviations from the fixed point according to $\partial_t v_I = Bv_I = -\Theta_I v_I$, with corresponding

eigenvalues (with additional minus sign) Θ_I. The index I labels the order of the negative eigenvalues according to their real part, starting with the largest one, i.e., $\Theta_1 > \Theta_2 > \dots$ The solution to the linearized flow $v_I \propto k^{-\Theta_I}$ implies that positive $\Theta_I > 0$ correspond to RG relevant, i.e., infrared repulsive, directions and negative $\Theta_I < 0$ correspond to RG irrelevant, i.e., infrared attractive, directions. In the models we consider, there is typically (for $J = 0$, i.e., without external "magnetic" field) one relevant direction with $\Theta_1 > 0$ and an infinite set of irrelevant directions with $\Theta_I < 0$, $I = 2, \dots$ By truncating the effective action we obtain of course only a finite subset.

Let $G(p; v_1, v_2, \dots,)$ denote the full propagator in Fourier space, obtained from the flow with initial dimensionless couplings $g = g^* + \sum_I v_I$ at the UV scale Λ. Performing an RG step from Λ to $k = \Lambda/b$, we can express the scaling hypothesis close to the critical point as [147–149],

$$G(p; v_1, v_2, \dots) = Z_k^{-1} b^2 G(bp; b^{\Theta_1} v_1, b^{\Theta_2} v_2, \dots), \qquad b \coloneqq \frac{\Lambda}{k}, \tag{2.41}$$

which may be motivated by simple dimensional analysis and the field rescaling under RG transformations $\phi \to \sqrt{Z_k}\phi$. Directly at the critical point $v_I = 0$ on the one hand, we obtain

$$G(p; 0, \dots) \propto \frac{1}{p^{2-\eta^*}}. \tag{2.42}$$

where we have chosen $b = \Lambda/p$ and defined $\eta^* \coloneqq \eta(g^*) = -\partial_t \ln Z_k$, such that $Z_k = b^{\eta^*}$. In real space the correlation function at the critical point becomes long range,

$$G(x; 0, \dots) \propto \frac{1}{|x|^{d-2+\eta^*}}, \qquad \text{for } |x| \to \infty. \tag{2.43}$$

Thus, our definition for the anomalous dimension η^* at the fixed point coincides with the usual definition for the critical exponent η. If for $v_I \neq 0$ the correlation length $\xi = \bar{m}_{\mathrm{R}}^{-1}$ is the only relevant length scale, we expect asymptotically for large distances an exponential decay (in general modulated by some power-law behavior)

$$G(x, v_1, v_2, \dots) \sim \mathrm{e}^{-|x|/\xi}, \qquad \text{for } |x| \to \infty. \tag{2.44}$$

We now fix the RG scale by requiring $b^{\Theta_1}|v_1| = 1$, i.e.,

$$G(p, v_1, v_2, \dots) = |v_1|^{-(2-\eta^*)/\Theta_1} G(p|v_1|^{-1/\Theta_1}; \operatorname{sgn} v_1, v_2|v_1|^{-\Theta_2/\Theta_1}, \dots). \tag{2.45}$$

The asymptotic behavior (2.44) is only possible if ξ obeys the power-law scaling

$$\xi = f_\pm |\delta g|^{-1/\Theta_1} \left(1 + b_\pm |\delta g|^{-\Theta_2/\Theta_1} + \dots\right). \tag{2.46}$$

Comparing with the definition of the critical exponents ν and ω in Eq. (2.39), we find

$$\nu = \frac{1}{\Theta_1} > 0 \qquad \text{and} \qquad \omega = -\Theta_2 > 0. \tag{2.47}$$

The scaling of the order parameter ("magnetization") is determined by the exponent β,

$$\langle\varphi\rangle = \left.\frac{\delta W}{\delta J}\right|_{J=0} = \phi_0 \propto \delta g^\beta (1 + \dots), \qquad \delta g \geq 0, \tag{2.48}$$

with the "bare" field expectation value $\phi_0 = \lim_{k\to 0} \phi_{0,k}$. We suppressed the corrections to scaling for simplicity. The susceptibility χ is given by the response of the order parameter under a change of the external source J,

$$\chi = \left.\frac{\delta^2 W}{\delta J^2}\right|_{J=0} = \left(\Gamma^{(2)}\big|_{\phi_0}\right)^{-1} = \bar{m}^{-2} \propto |\delta g|^{-\gamma}(1 + \dots). \tag{2.49}$$

with the "unrenormalized" mass $\bar{m} = \sqrt{Z}\bar{m}_\mathrm{R} = \lim_{k\to 0} \sqrt{\bar{\lambda}_k}\phi_{0,k}$. [150].

Provided the hyperscaling relation (2.41), together with the scaling assumption for the singular part of the effective potential $U = \Gamma|_{\phi=\text{const.}}/\Omega_d$,

$$U_\mathrm{sing}(v_1, v_2, \dots) = b^{-d} U_\mathrm{sing}(b^{\Theta_1} v_1, b^{\Theta_2} v_2, \dots), \tag{2.50}$$

both β and γ are uniquely determined by the anomalous dimension η and the correlation length exponent ν,

$$\beta = \frac{\nu}{2}(d - 2 + \eta^*), \qquad\qquad \gamma = \nu(2 - \eta^*). \tag{2.51}$$

Furthermore, we can relate η and ν also to the critical exponents δ and α, characterizing the scaling of magnetization $\langle\varphi\rangle_J \propto |J|^{1/\delta} \operatorname{sgn} J$, $(\delta g = 0)$ and the specific heat $\partial^2\Gamma/\partial\delta g^2|_{\phi_0} \propto |\delta g|^{-\alpha}$, respectively,

$$\alpha = 2 - d\nu, \qquad\qquad \delta = \frac{d + 2 - \eta^*}{d - 2 + \eta^*}. \tag{2.52}$$

3 Chiral Gross-Neveu model with left-right asymmetry

We begin the main part of this work by constructing a generalization of the 3d chiral Gross-Neveu (GN) model exhibiting a $\mathrm{U_L}(N_\mathrm{L}) \otimes \mathrm{U_R}(1)$ chiral symmetry reminiscent of the Higgs-Yukawa sector of the standard model of particle physics. We classify all possible four-fermion interaction terms and the corresponding discrete symmetries. For sufficiently strong correlations in a scalar parity-conserving channel, the system can undergo a second-order phase transition to a chiral-symmetry broken phase which can be viewed as a 3d analog of the electroweak phase transition[a]. We determine the critical behavior of this phase transition in terms of the correlation-length exponent and the fermion and scalar anomalous dimensions as a function of the number of left-handed fermions $N_\mathrm{L} \geq 1$. This external parameter, which controls the left-right asymmetry of our models, allow us to modulate the relative amplitude of boson and fermion fluctuations and therewith to vary the fixed-point properties of the RG flow. This implies a variation of the critical properties of these systems. In particular, the fixed-point potential for the bosonic order parameter can be in the symmetric regime for small N_L or in the broken regime for larger N_L. The small N_L regime turns out to be particularly interesting, as the anomalous dimensions of all fields have to satisfy a sum rule within our truncation, in order to give rise to a nontrivial fixed point in the Yukawa coupling.

The quantitative reliability of our results for the critical properties can be checked by a reduction of our model to a corresponding purely bosonic $\mathrm{O}(N)$ model, for which our method has been used with a remarkable quantitative success [89,90,153]. Our inclusion of fermions can reliably be based on this footing, as our models approach an $\mathrm{O}(2N_\mathrm{L})$ model in the limit of large N_L; this is because the composite scalar degrees of freedom dominate the fluctuation contributions as a result of the chiral structure. For smaller N_L, our results show quantitative as well as qualitative differences to $\mathrm{O}(N)$ models, as expected due to the fermionic contributions. We also discuss the dependence of our findings on the regularization scheme, which might be thought of as rough error estimate (cf. Sec. 4.2).

[a] This chapter has partly been inspired by a recently discovered asymptotic-safety scenario for the Higgs-Yukawa sector of the standard model, which aims at a solution of the triviality and an improvement of the hierarchy problem of the standard-model Higgs sector [151,152].

The resulting models and quantitative findings constitute and characterize a new set of universality classes, classified by the chiral-symmetry content. In particular, we provide for quantitative predictions for the critical exponents for these universality classes, which have not been investigated with any other method so far. We believe that these can serve as a first benchmark for other nonperturbative methods, which are urgently needed for a study of chiral phase transitions in strongly correlated chiral fermions.

3.1 Classical action and symmetry transformations

Let us first consider a general fermionic model in $d = 2 + 1$ Euclidean dimensions with local quartic self-interaction, being invariant under chiral $\mathrm{U_L}(N_\mathrm{L}) \otimes \mathrm{U_R}(N_\mathrm{R})$ transformations and satisfying Osterwalder-Schrader positivity [154]. For the latter, we require invariance of the action under generalized complex conjugation defined by $\psi^\dagger \coloneqq \mathrm{i}\bar{\psi}\gamma_3$ and a simultaneous reflection of the Euclidean time coordinate, which we choose to be x_3. For a detailed discussion of our chiral conventions, see Ref. [155, 156]. The Dirac algebra

$$\{\gamma_\mu, \gamma_\nu\} = 2\delta_{\mu\nu}, \tag{3.1}$$

could minimally be realized by an irreducible representation in terms of 2×2 matrices. As this representation does not permit a chiral symmetry, the massless theory could not be separated from the massive theory by an order-disorder transition. We therefore work with a 4×4 *reducible* representation of the Dirac algebra

$$\gamma_\mu = \begin{pmatrix} 0 & -\mathrm{i}\sigma_\mu \\ \mathrm{i}\sigma_\mu & 0 \end{pmatrix}, \qquad \mu = 1, 2, 3, \tag{3.2}$$

reminiscent of the chiral representation in four dimensions. Here, $\{\sigma_\mu\}_{\mu=1,2,3}$ denote the standard 2×2 Pauli matrices. In this formulation, the Dirac fermions thus have four components. In the light of condensed-matter applications, this is very common in three dimensions: it is in fact the natural language of the effective theories describing the electronic interactions on graphene's honeycomb lattice [25–31] and in the cuprates [19–24]. There are now *two* other 4×4 matrices, which anticommute with all γ_μ as well as with each other,

$$\gamma_4 = \begin{pmatrix} 0 & \mathbb{1}_2 \\ \mathbb{1}_2 & 0 \end{pmatrix} \qquad \text{and} \qquad \gamma_5 = \gamma_1\gamma_2\gamma_3\gamma_4 = \begin{pmatrix} \mathbb{1}_2 & 0 \\ 0 & -\mathbb{1}_2 \end{pmatrix}. \tag{3.3}$$

Together with

$$\mathbb{1}_4, \quad \gamma_{\mu\nu} \coloneqq \frac{\mathrm{i}}{2}[\gamma_\mu, \gamma_\nu] \quad \text{for} \quad \mu < \nu, \quad \mathrm{i}\gamma_\mu\gamma_4, \quad \mathrm{i}\gamma_\mu\gamma_5, \quad \gamma_{45} \coloneqq \mathrm{i}\gamma_4\gamma_5, \tag{3.4}$$

these 16 matrices form a complete basis of the 4×4 Dirac algebra,

$$\{\gamma_A\}_{A=1,\ldots,16} = \{\mathbb{1}_4, \gamma_\mu, \gamma_4, \gamma_{\mu\nu}, \mathrm{i}\gamma_\mu\gamma_4, \mathrm{i}\gamma_\mu\gamma_5, \gamma_{45}, \gamma_5\}. \tag{3.5}$$

Now, we define chiral projectors

$$P^{(5)}_{\mathrm{L/R}} \coloneqq \frac{1}{2}(\mathbb{1}_4 \pm \gamma_5) \tag{3.6}$$

that allow us to decompose a Dirac fermion ψ into the left- and right-handed Weyl spinors ψ_L and ψ_R,

$$\psi_{\mathrm{L/R}} = P^{(5)}_{\mathrm{L/R}}\psi, \quad \bar{\psi}_{\mathrm{L/R}} = \bar{\psi}P^{(5)}_{\mathrm{R/L}}. \tag{3.7}$$

(ψ and $\bar{\psi}$ are considered as independent field variables in our Euclidean formulation.) Note that there is a certain freedom of choice of the notion of chirality here: we could have chosen just as well $P^{(4)}_{\mathrm{L/R}} \coloneqq (\mathbb{1} \pm \gamma_4)/2$ or $P^{(45)}_{\mathrm{L/R}} \coloneqq (\mathbb{1} \pm \gamma_{45})/2$ as chiral projectors. This would have led us to different definitions of the decomposition into Weyl spinors. All these chiralities remain conserved under Lorentz transformations since all three projectors commute with the generators of the Lorentz transformation of the Dirac spinors, $[\gamma_5, \gamma_{\mu\nu}] = [\gamma_4, \gamma_{\mu\nu}] = [\gamma_{45}, \gamma_{\mu\nu}] = 0$. We will further develop this issue in Chap. 4, where we investigate the theories invariant under *all three* chiral transformations. In that case, the full symmetry group (including the usual phase rotations) for each flavor is a U(2); see below.

Here, we stick to the definition given by Eq. (3.6). We consider N_R right-handed and N_L left-handed fermions, where the numbers of which not necessarily coincide. We impose a chiral $\mathrm{U_L}(N_\mathrm{L}) \otimes \mathrm{U_R}(N_\mathrm{R})$ symmetry with corresponding field transformations acting independently on the left- and right-handed parts,

$$\mathrm{U_L}(N_\mathrm{L}): \qquad \psi^a_\mathrm{L} \mapsto U^{ab}_\mathrm{L}\psi^b_\mathrm{L}, \qquad \bar{\psi}^a_\mathrm{L} \mapsto \bar{\psi}^b_\mathrm{L}(U^\dagger_\mathrm{L})^{ba}, \qquad U_\mathrm{L} \in \mathrm{U}(N_\mathrm{L}) \tag{3.8}$$

$$\mathrm{U_R}(N_\mathrm{R}): \qquad \psi^a_\mathrm{R} \mapsto U^{ab}_\mathrm{R}\psi^b_\mathrm{R}, \qquad \bar{\psi}^a_\mathrm{R} \mapsto \bar{\psi}^b_\mathrm{R}(U^\dagger_\mathrm{R})^{ba}, \qquad U_\mathrm{R} \in \mathrm{U}(N_\mathrm{R}). \tag{3.9}$$

For $U^{ab}_\mathrm{L} = \mathrm{e}^{\mathrm{i}\alpha}\,\delta^{ab}$ and $U^{ab}_\mathrm{R} = \mathrm{e}^{-\mathrm{i}\alpha}\,\delta^{ab}$ we obtain the usual $\mathrm{U_A}(1)$ axial transformations, whereas for $U^{ab}_\mathrm{L} = \mathrm{e}^{\mathrm{i}\alpha}\,\delta^{ab}$ and $U^{ab}_\mathrm{R} = \mathrm{e}^{\mathrm{i}\alpha}\,\delta^{ab}$ we get the $\mathrm{U_V}(1)$ phase rotations. Thus, the symmetry group may be written as

$$\mathrm{U_L}(N_\mathrm{L}) \otimes \mathrm{U_R}(N_\mathrm{R}) \cong \mathrm{SU_L}(N_\mathrm{L}) \otimes \mathrm{SU_R}(N_\mathrm{R}) \otimes \mathrm{U_A}(1) \otimes \mathrm{U_V}(1), \tag{3.10}$$

with chiral $\mathrm{SU}(N_{\mathrm{L,R}})$ factors.

Because of the reducible representation of the Dirac algebra, there is some freedom in the definition of the discrete transformations [63]. Charge conjugation may be implemented by either

$$\mathcal{C}: \qquad \psi^a_{\mathrm{L/R}} \mapsto \left(\bar{\psi}^a_{\mathrm{L/R}}C\right)^T, \qquad \bar{\psi}^a_{\mathrm{L/R}} \mapsto -\left(C^\dagger\psi^a_{\mathrm{L/R}}\right)^T, \qquad C = \gamma_2\gamma_5, \tag{3.11}$$

or

$$\tilde{\mathcal{C}}: \qquad \psi^a_{\mathrm{L/R}} \mapsto \left(\bar{\psi}^a_{\mathrm{R/L}}\tilde{C}\right)^T, \qquad \bar{\psi}^a_{\mathrm{L/R}} \mapsto -\left(\tilde{C}^\dagger\psi^a_{\mathrm{R/L}}\right)^T, \qquad \tilde{C} = \gamma_2\gamma_4, \tag{3.12}$$

or a unitary combination of the two of these. In contrast to the 4d case, in three dimensions the parity transformation is commonly [157][b] defined by a reflection of solely *one* of the spacial

[b] We note that this definition is however not so common in the condensed-matter literature, where $\mathcal{P}$ is often associated with an inversion of *both* spacial coordinates; see, for instance, Ref. [31] for a discussion on this peculiarity. We thank D. Mesterhazy and L. von Smekal for pointing this fact out to us.

Table 3.1 Properties of fermion bilinears under discrete transformations. For parity, the arguments of the transformed fields are $\hat{x} = (-x_1, x_2, x_3)$. The bilinears with $(\mathrm{L} \leftrightarrow \mathrm{R})$ transform analogously.

	$\mathcal{C}$	$\tilde{\mathcal{C}}$	$\mathcal{P}$	$\tilde{\mathcal{P}}$	$\mathcal{T}$	$\tilde{\mathcal{T}}$
$\bar{\psi}^a_{\mathrm{L}}\psi^b_{\mathrm{R}}$	$\bar{\psi}^b_{\mathrm{R}}\psi^a_{\mathrm{L}}$	$\bar{\psi}^b_{\mathrm{L}}\psi^a_{\mathrm{R}}$	$\bar{\psi}^a_{\mathrm{L}}\psi^b_{\mathrm{R}}$	$\bar{\psi}^a_{\mathrm{R}}\psi^b_{\mathrm{L}}$	$\bar{\psi}^a_{\mathrm{L}}\psi^b_{\mathrm{R}}$	$\bar{\psi}^a_{\mathrm{R}}\psi^b_{\mathrm{L}}$
$\bar{\psi}^a_{\mathrm{L}}\gamma_\mu\psi^b_{\mathrm{L}}$	$-\bar{\psi}^b_{\mathrm{L}}\gamma_\mu\psi^a_{\mathrm{L}}$	$-\bar{\psi}^b_{\mathrm{R}}\gamma_\mu\psi^a_{\mathrm{R}}$	$\bar{\psi}^a_{\mathrm{L}}\hat{\gamma}_\mu\psi^b_{\mathrm{L}}$	$\bar{\psi}^a_{\mathrm{R}}\hat{\gamma}_\mu\psi^b_{\mathrm{R}}$	$-\bar{\psi}^a_{\mathrm{L}}\gamma_\mu\psi^b_{\mathrm{L}}$	$-\bar{\psi}^a_{\mathrm{R}}\gamma_\mu\psi^b_{\mathrm{R}}$
$\bar{\psi}^a_{\mathrm{L}}\gamma_{\mu\nu}\psi^b_{\mathrm{R}}$	$-\bar{\psi}^b_{\mathrm{R}}\gamma_{\mu\nu}\psi^a_{\mathrm{L}}$	$-\bar{\psi}^b_{\mathrm{L}}\gamma_{\mu\nu}\psi^a_{\mathrm{R}}$	$\bar{\psi}^a_{\mathrm{L}}\hat{\gamma}_{\mu\nu}\psi^b_{\mathrm{R}}$	$\bar{\psi}^a_{\mathrm{R}}\hat{\gamma}_{\mu\nu}\psi^b_{\mathrm{L}}$	$-\bar{\psi}^a_{\mathrm{L}}\gamma_{\mu\nu}\psi^b_{\mathrm{R}}$	$-\bar{\psi}^a_{\mathrm{R}}\gamma_{\mu\nu}\psi^b_{\mathrm{L}}$
$\bar{\psi}^a_{\mathrm{L}}\gamma_4\psi^b_{\mathrm{L}}$	$\bar{\psi}^b_{\mathrm{L}}\gamma_4\psi^a_{\mathrm{L}}$	$-\bar{\psi}^b_{\mathrm{R}}\gamma_4\psi^a_{\mathrm{R}}$	$-\bar{\psi}^a_{\mathrm{L}}\gamma_4\psi^b_{\mathrm{L}}$	$\bar{\psi}^a_{\mathrm{R}}\gamma_4\psi^b_{\mathrm{R}}$	$-\bar{\psi}^a_{\mathrm{L}}\gamma_4\psi^b_{\mathrm{L}}$	$\bar{\psi}^a_{\mathrm{R}}\gamma_4\psi^b_{\mathrm{R}}$
$\bar{\psi}^a_{\mathrm{L}}\mathrm{i}\gamma_\mu\gamma_4\psi^b_{\mathrm{R}}$	$\bar{\psi}^b_{\mathrm{R}}\mathrm{i}\gamma_\mu\gamma_4\psi^a_{\mathrm{L}}$	$-\bar{\psi}^b_{\mathrm{L}}\mathrm{i}\gamma_\mu\gamma_4\psi^a_{\mathrm{R}}$	$-\bar{\psi}^a_{\mathrm{L}}\mathrm{i}\hat{\gamma}_\mu\gamma_4\psi^b_{\mathrm{R}}$	$\bar{\psi}^a_{\mathrm{R}}\mathrm{i}\hat{\gamma}_\mu\gamma_4\psi^b_{\mathrm{L}}$	$-\bar{\psi}^a_{\mathrm{L}}\mathrm{i}\gamma_\mu\gamma_4\psi^b_{\mathrm{R}}$	$\bar{\psi}^a_{\mathrm{R}}\mathrm{i}\gamma_\mu\gamma_4\psi^b_{\mathrm{L}}$

coordinates,$(x_1, x_2, x_3) \mapsto (-x_1, x_2, x_3) =: \hat{x}$. The parity transformation then reads either

$$\mathcal{P}: \qquad \psi^a_{\mathrm{L/R}}(x) \mapsto P\psi^a_{\mathrm{L/R}}(\hat{x}), \qquad \bar{\psi}^a_{\mathrm{L/R}}(x) \mapsto \bar{\psi}^a_{\mathrm{L/R}}(\hat{x})P^\dagger, \qquad P = \gamma_1\gamma_4, \tag{3.13}$$

or

$$\tilde{\mathcal{P}}: \qquad \psi^a_{\mathrm{L/R}}(x) \mapsto \tilde{P}\psi^a_{\mathrm{R/L}}(\hat{x}), \qquad \bar{\psi}^a_{\mathrm{L/R}}(x) \mapsto \bar{\psi}^a_{\mathrm{R/L}}(\hat{x})\tilde{P}^\dagger, \qquad \tilde{P} = \gamma_1\gamma_5. \tag{3.14}$$

Time reversal is given by an antiunitary operator, that is to say, it includes a complex conjugation. In Euclidean field theory however, the (generalized) complex conjugation is given by the usual complex conjugation *together* with a reflection of the Euclidean time coordinate x_3 [154, 155]. Therefore, time reversal in Euclidean space simply complex conjugates c-numbers without reversing x_3 [158][c]. The fermion fields then transform as

$$\mathcal{T}: \qquad \psi^a_{\mathrm{L/R}} \mapsto T\psi^a_{\mathrm{L/R}}, \qquad \bar{\psi}^a_{\mathrm{L/R}} \mapsto \bar{\psi}^a_{\mathrm{L/R}}T^\dagger, \qquad T = \gamma_2\gamma_4, \tag{3.15}$$

or

$$\tilde{\mathcal{T}}: \qquad \psi^a_{\mathrm{L/R}} \mapsto \tilde{T}\psi^a_{\mathrm{R/L}}, \qquad \bar{\psi}^a_{\mathrm{L/R}} \mapsto \bar{\psi}^a_{\mathrm{R/L}}\tilde{T}^\dagger, \qquad \tilde{T} = \gamma_2\gamma_5. \tag{3.16}$$

In order to derive the explicit transformation properties of the bilinears, it is useful to recall that in our representation γ_1 and γ_3 are antisymmetric and purely imaginary, whereas γ_2, γ_4, and γ_5 are symmetric and real. The results are listed in Table 3.1, where we have introduced

$$\hat{\gamma}_\mu \coloneqq (-\gamma_1, \gamma_2, \gamma_3)_\mu, \qquad (\hat{\gamma}_{12}, \hat{\gamma}_{13}, \hat{\gamma}_{23}) \coloneqq (-\gamma_{12}, -\gamma_{13}, \gamma_{23}). \tag{3.17}$$

These transformation properties facilitate a discussion of possible bilinears and 4-fermi terms in the action of our model. In addition to Lorentz invariance, we impose an invariance of our theory under $\mathrm{U_L}(N_\mathrm{L}) \otimes \mathrm{U_R}(N_\mathrm{R})$ chiral transformations, $\mathcal{C}$ charge conjugation, $\mathcal{P}$ parity inversion, and $\mathcal{T}$ time reversal, all of which are compatible with our left-right asymmetry $N_\mathrm{L} \geq N_\mathrm{R}$. The theory then automatically is also invariant under the combined discrete transformations $\tilde{\mathcal{C}}\tilde{\mathcal{P}}$, $\tilde{\mathcal{P}}\tilde{\mathcal{T}}$, and $\tilde{\mathcal{C}}\tilde{\mathcal{T}}$, since $\tilde{\mathcal{C}}\tilde{\mathcal{P}} = \mathcal{C}\mathcal{P}$, $\tilde{\mathcal{P}}\tilde{\mathcal{T}} = \mathcal{P}\mathcal{T}$, and $\tilde{\mathcal{C}}\tilde{\mathcal{T}} = \mathcal{C}\mathcal{T}$. (The equivalence holds up to $\mathrm{U_V}(1)$ phase rotations of the spinors.)

[c] This is in contrast to our definition of $\mathcal{T}$, $\tilde{\mathcal{T}}$ in [131].

As a consequence of our symmetry, no bilinears to zeroth order in derivatives are permitted in the effective action. To first order, only the standard chiral kinetic terms

$$\bar{\psi}^a_{\mathrm{L}} \mathrm{i}\partial_\mu \gamma_\mu \psi^a_{\mathrm{L}} \qquad \text{and} \qquad \bar{\psi}^a_{\mathrm{R}} \mathrm{i}\partial_\mu \gamma_\mu \psi^a_{\mathrm{R}} \tag{3.18}$$

can appear. In particular, all possible mass terms are excluded by symmetry: $\bar{\psi}^a_{\mathrm{L}}\psi^a_{\mathrm{R}}$ and $\bar{\psi}^a_{\mathrm{R}}\psi^a_{\mathrm{L}}$ are not chiral symmetric, and $\bar{\psi}^a_{\mathrm{L}}\gamma_4\psi^a_{\mathrm{L}}$ as well as $\bar{\psi}^a_{\mathrm{R}}\gamma_4\psi^a_{\mathrm{R}}$ are not invariant under $\mathcal{P}$ and $\mathcal{T}$ transformations. The same holds for terms involving γ_{45}. On the level of 4-fermi operators, the interaction terms must have the form

$$\left(\bar{\psi}^a_{\mathrm{L}}\gamma_A\psi^b_{\mathrm{L}}\right)\left(\bar{\psi}^b_{\mathrm{L}}\gamma_A\psi^a_{\mathrm{L}}\right), \qquad \left(\bar{\psi}^a_{\mathrm{R}}\gamma_A\psi^b_{\mathrm{R}}\right)\left(\bar{\psi}^b_{\mathrm{R}}\gamma_A\psi^a_{\mathrm{R}}\right), \qquad \text{with} \quad \gamma_A \in \{\gamma_\mu, \gamma_4\}, \tag{3.19}$$

$$\left(\bar{\psi}^a_{\mathrm{L}}\gamma_B\psi^b_{\mathrm{R}}\right)\left(\bar{\psi}^b_{\mathrm{R}}\gamma_B\psi^a_{\mathrm{L}}\right), \qquad \text{with} \quad \gamma_B \in \{\mathbb{1}, \mathrm{i}\gamma_\mu\gamma_4\}, \tag{3.20}$$

or, with inverse flavor structure,

$$\left(\bar{\psi}^a_{\mathrm{L}}\gamma_A\psi^a_{\mathrm{L}}\right)\left(\bar{\psi}^b_{\mathrm{L}}\gamma_A\psi^b_{\mathrm{L}}\right), \qquad \left(\bar{\psi}^a_{\mathrm{R}}\gamma_A\psi^a_{\mathrm{R}}\right)\left(\bar{\psi}^b_{\mathrm{R}}\gamma_A\psi^b_{\mathrm{R}}\right), \qquad \left(\bar{\psi}^a_{\mathrm{R}}\gamma_A\psi^a_{\mathrm{R}}\right)\left(\bar{\psi}^b_{\mathrm{L}}\gamma_A\psi^b_{\mathrm{L}}\right). \tag{3.21}$$

Terms with $\gamma_A \in \{\mathrm{i}\gamma_\mu\gamma_5, \gamma_{45}\}$ or $\gamma_B \in \{\gamma_5, \gamma_{\mu\nu}\}$ are equal to these up to a possible sign, since ψ_{L} and ψ_{R} are eigenvectors of γ_5, and $\gamma_{\mu\nu} = -\epsilon_{\mu\nu\rho}\gamma_\rho\gamma_{45}$. Terms with $\gamma_A \in \{\mathbb{1}, \gamma_5, \mathrm{i}\gamma_\mu\gamma_4, \gamma_{\mu\nu}\}$ or $\gamma_B \in \{\gamma_\mu, \mathrm{i}\gamma_\mu\gamma_5, \gamma_4, \gamma_{45}\}$ are identically zero, since $P_{\mathrm{R}}P_{\mathrm{L}} = P_{\mathrm{L}}P_{\mathrm{R}} = 0$. Moreover, the terms in Eq. (3.21) are not independent of the terms in Eqs. (3.19), (3.20), but are related by the Fierz identities (cf. App. A):

$$\left(\bar{\psi}^a_{\mathrm{L}}\gamma_\mu\psi^a_{\mathrm{L}}\right)\left(\bar{\psi}^b_{\mathrm{L}}\gamma_\mu\psi^b_{\mathrm{L}}\right) = \frac{1}{2}\left(\bar{\psi}^a_{\mathrm{L}}\gamma_\mu\psi^b_{\mathrm{L}}\right)\left(\bar{\psi}^b_{\mathrm{L}}\gamma_\mu\psi^a_{\mathrm{L}}\right) + \frac{3}{2}\left(\bar{\psi}^a_{\mathrm{L}}\gamma_4\psi^b_{\mathrm{L}}\right)\left(\bar{\psi}^b_{\mathrm{L}}\gamma_4\psi^a_{\mathrm{L}}\right), \tag{3.22}$$

$$\left(\bar{\psi}^a_{\mathrm{L}}\gamma_4\psi^a_{\mathrm{L}}\right)\left(\bar{\psi}^b_{\mathrm{L}}\gamma_4\psi^b_{\mathrm{L}}\right) = \frac{1}{2}\left(\bar{\psi}^a_{\mathrm{L}}\gamma_\mu\psi^b_{\mathrm{L}}\right)\left(\bar{\psi}^b_{\mathrm{L}}\gamma_\mu\psi^a_{\mathrm{L}}\right) - \frac{1}{2}\left(\bar{\psi}^a_{\mathrm{L}}\gamma_4\psi^b_{\mathrm{L}}\right)\left(\bar{\psi}^b_{\mathrm{L}}\gamma_4\psi^a_{\mathrm{L}}\right), \tag{3.23}$$

$$\left(\bar{\psi}^a_{\mathrm{R}}\gamma_\mu\psi^a_{\mathrm{R}}\right)\left(\bar{\psi}^b_{\mathrm{L}}\gamma_\mu\psi^b_{\mathrm{L}}\right) = -\frac{3}{2}\left(\bar{\psi}^a_{\mathrm{R}}\psi^b_{\mathrm{L}}\right)\left(\bar{\psi}^b_{\mathrm{L}}\psi^a_{\mathrm{R}}\right) - \frac{1}{2}\left(\bar{\psi}^a_{\mathrm{R}}\mathrm{i}\gamma_\mu\gamma_4\psi^b_{\mathrm{L}}\right)\left(\bar{\psi}^b_{\mathrm{L}}\mathrm{i}\gamma_\mu\gamma_4\psi^a_{\mathrm{R}}\right), \tag{3.24}$$

$$\left(\bar{\psi}^a_{\mathrm{R}}\gamma_4\psi^a_{\mathrm{R}}\right)\left(\bar{\psi}^b_{\mathrm{L}}\gamma_4\psi^b_{\mathrm{L}}\right) = -\frac{1}{2}\left(\bar{\psi}^a_{\mathrm{R}}\psi^b_{\mathrm{L}}\right)\left(\bar{\psi}^b_{\mathrm{L}}\psi^a_{\mathrm{R}}\right) + \frac{1}{2}\left(\bar{\psi}^a_{\mathrm{R}}\mathrm{i}\gamma_\mu\gamma_4\psi^b_{\mathrm{L}}\right)\left(\bar{\psi}^b_{\mathrm{L}}\mathrm{i}\gamma_\mu\gamma_4\psi^a_{\mathrm{R}}\right). \tag{3.25}$$

Analogous equations hold for ($\mathrm{L} \leftrightarrow \mathrm{R}$). We thus end up with six independent 4-fermi terms preserving $\mathrm{U_L}(N_{\mathrm{L}}) \otimes \mathrm{U_R}(N_{\mathrm{R}})$ and $\mathcal{C}$, $\mathcal{P}$, and $\mathcal{T}$ symmetry,

$$\left(\bar{\psi}^a_{\mathrm{L}}\psi^b_{\mathrm{R}}\right)\left(\bar{\psi}^b_{\mathrm{R}}\psi^a_{\mathrm{L}}\right), \qquad \left(\bar{\psi}^a_{\mathrm{L}}\gamma_4\psi^b_{\mathrm{L}}\right)\left(\bar{\psi}^b_{\mathrm{L}}\gamma_4\psi^a_{\mathrm{L}}\right), \qquad \left(\bar{\psi}^a_{\mathrm{R}}\gamma_4\psi^b_{\mathrm{R}}\right)\left(\bar{\psi}^b_{\mathrm{R}}\gamma_4\psi^a_{\mathrm{R}}\right), \tag{3.26}$$

$$\left(\bar{\psi}^a_{\mathrm{L}}\mathrm{i}\gamma_\mu\gamma_4\psi^b_{\mathrm{R}}\right)\left(\bar{\psi}^b_{\mathrm{R}}\mathrm{i}\gamma_\mu\gamma_4\psi^a_{\mathrm{L}}\right), \qquad \left(\bar{\psi}^a_{\mathrm{L}}\gamma_\mu\psi^b_{\mathrm{L}}\right)\left(\bar{\psi}^b_{\mathrm{L}}\gamma_\mu\psi^a_{\mathrm{L}}\right), \qquad \left(\bar{\psi}^a_{\mathrm{R}}\gamma_\mu\psi^b_{\mathrm{R}}\right)\left(\bar{\psi}^b_{\mathrm{R}}\gamma_\mu\psi^a_{\mathrm{R}}\right). \tag{3.27}$$

Note that the corresponding set in $d = 3 + 1$ dimensions would be smaller as the γ_4 terms would be constrained by a larger Lorentz symmetry.

In a (partially) bosonized language after a Hubbard-Stratonovich transformation, we encounter six boson-fermion interactions: The first one corresponding to Eq. (3.26a) couples the fermions to a scalar boson (scalar with respect to $\mathcal{P}$ parity), the second and the third (3.26b)–(3.26c) to a pseudoscalar boson, the fourth to an axialvector boson (3.27a), and the fifth and the sixth

(3.27b)–(3.27c) to a parity even vector boson. Further bosonic structures in the flavor-singlet channels appear in the corresponding Fierz transforms (3.22)–(3.25).

We expect that a general model based on these interactions exhibits a rich phase structure, being controlled by the relative strength of the various interaction channels. Aiming at an analogue of the electroweak phase transition, we focus in this work on the $\mathcal{P}$ parity-conserving and Lorentz-invariant condensation channel, parameterized in terms of the first interaction term. Moreover, we confine ourselves to the case of $N_\mathrm{R} = 1$ right-handed fermion flavor and $N_\mathrm{L} \geq 1$ left-handed fermion flavors, allowing for a left-right asymmetry similar to the standard model of particle physics (where $N_\mathrm{L} = 2$). The microscopic action of our model in the purely fermionic language then reads

$$S_{\chi\mathrm{GN}} = \int \mathrm{d}^3x \left[\bar{\psi}^a_\mathrm{L} \mathrm{i}\partial\!\!\!/ \psi^a_\mathrm{L} + \bar{\psi}_\mathrm{R} \mathrm{i}\partial\!\!\!/ \psi_\mathrm{R} + g\left(\bar{\psi}^a_\mathrm{L}\psi_\mathrm{R}\right)\left(\bar{\psi}_\mathrm{R}\psi^a_\mathrm{L}\right)\right]. \tag{3.28}$$

Via Hubbard-Stratonovich transformation, we obtain the equivalent Yukawa action

$$S_\mathrm{Yukawa} = \int \mathrm{d}^3x \left[\frac{1}{g}\phi^{a\dagger}\phi^a + \bar{\psi}^a_\mathrm{L} \mathrm{i}\partial\!\!\!/ \psi^a_\mathrm{L} + \bar{\psi}_\mathrm{R} \mathrm{i}\partial\!\!\!/ \psi_\mathrm{R} + \phi^{a\dagger}\bar{\psi}_\mathrm{R}\psi^a_\mathrm{L} - \phi^a\bar{\psi}^a_\mathrm{L}\psi_\mathrm{R}\right], \tag{3.29}$$

where the complex scalar ϕ^a serves as an auxiliary field. The purely fermionic model can be recovered by use of the algebraic equations of motion for ϕ^a and $\phi^{a\dagger}$,

$$\phi^a = -g\bar{\psi}_\mathrm{R}\psi^a_\mathrm{L}, \qquad\qquad \phi^{a\dagger} = g\bar{\psi}^a_\mathrm{L}\psi_\mathrm{R}. \tag{3.30}$$

Here, we can read off the transformation properties of the scalar field under the chiral symmetry,

$$\mathrm{U_L}(N_\mathrm{L}) \otimes \mathrm{U_R}(1): \qquad \phi^a \mapsto U^{ab}_\mathrm{L}\phi^b U^\dagger_\mathrm{R}, \qquad \phi^{a\dagger} \mapsto U_\mathrm{R}\phi^{b\dagger}(U^\dagger_\mathrm{L})^{ba}, \tag{3.31}$$

with $U_\mathrm{L} \in \mathrm{U}(N_\mathrm{L})$ and $U_\mathrm{R} \in \mathrm{U}(1)$. The composite scalar field ϕ^a represents an order parameter for an order-disorder transition. As long as ϕ^a has a vanishing expectation value, the system is in the symmetric phase with full chiral symmetry

$$\mathrm{U_L}(N_\mathrm{L}) \otimes \mathrm{U_R}(1) \simeq \mathrm{SU_L}(N_\mathrm{L}) \otimes \mathrm{U_A}(1) \otimes \mathrm{U_V}(1). \tag{3.32}$$

The fermions are massless, whereas the scalars are generically massive as determined by the symmetry-preserving effective potential for the scalars. A finite vacuum expectation value of ϕ^a spontaneously breaks the chiral symmetry according to the pattern

$$\mathrm{SU_L}(N_\mathrm{L}) \otimes \mathrm{U_A}(1) \to \mathrm{U}(N_\mathrm{L} - 1). \tag{3.33}$$

In the broken phase, the spectrum consists of one massive Dirac fermion, one massive bosonic radial mode, $N_\mathrm{L} - 1$ massless left-handed Weyl fermions and $2N_\mathrm{L} - 1$ massless Goldstone bosons.

Near the phase transition, we expect the order-parameter fluctuations to dominate the critical behavior of the system. Universality suggests that the degrees of freedom parameterized by the

action (3.29) are sufficient to quantify the critical behavior of this transition, independently of the presence of further microscopic fermionic interactions of Eqs. (3.26b), (3.26c), (3.27). Concentrating on the action (3.29), we observe that the purely scalar sector, i.e., the scalar mass term, has a larger symmetry group of $\mathrm{O}(2N_\mathrm{L})$-type. It is therefore instructive to compare the critical behavior of our fermionic model with that of a standard scalar $\mathrm{O}(2N_\mathrm{L})$ model, which is known to undergo a second-order phase transition associated with a Wilson-Fisher fixed point. Differences in the corresponding critical behaviors can then fully be attributed to fermionic fluctuations near the phase transition.

3.2 Partially bosonized RG flow

Integrating out fluctuations momentum shell by momentum shell near the phase transition described above, the effective average action is expected to acquire all possible operators of mixed scalar and fermionic nature compatible with the symmetries of the action (3.29). Here, we constrain the flow of this action functional to lie in the subspace of the full theory space spanned by the following ansatz valid at an RG scale k:

$$\begin{aligned}\Gamma_k = \int_x \Big[& Z_{\mathrm{L},k}\bar{\psi}^a_\mathrm{L}\mathrm{i}\partial\!\!\!/\psi^a_\mathrm{L} + Z_{\mathrm{R},k}\bar{\psi}_\mathrm{R}\mathrm{i}\partial\!\!\!/\psi_\mathrm{R} + Z_{\phi,k}\left(\partial_\mu\phi^{a\dagger}\right)\left(\partial^\mu\phi^a\right) + U_k(\phi^{a\dagger}\phi^a) \\ & + \bar{h}_k\bar{\psi}_\mathrm{R}\phi^{a\dagger}\psi^a_\mathrm{L} - \bar{h}_k\bar{\psi}^a_\mathrm{L}\phi^a\psi_\mathrm{R}\Big].\end{aligned} \tag{3.34}$$

The fermion fields ψ^a_L and ψ_R have standard kinetic terms but can pick up different wave function renormalizations $Z_{\mathrm{L},k}$ and $Z_{\mathrm{R},k}$. The index a runs from 1 to N_L. The bosonic sector involves a standard kinetic term with wave function renormalization $Z_{\phi,k}$ and an effective potential $U_k(\rho)$, where $\rho = \phi^{a\dagger}\phi^a$. All parameters in the average action are understood to be scale dependent, indicated by the momentum-scale index k. The scale-dependence is governed by the Wetterich equation (2.21), the solution of which provides an RG trajectory in theory space, interpolating between the bare action to be quantized, $\Gamma_{k\to\Lambda} = S_\mathrm{Yukawa}$, and the full quantum effective action, $\Gamma_{k\to 0} = \Gamma$, cf. Sec. 2.2. The ansatz (3.34), in fact, represents the next-to-leading order (NLO) in a systematic derivative expansion. (The leading-order (LO) is obtained by setting all wave function renormalizations $Z_{\phi/\mathrm{L/R},k} = \text{const.}$) This expansion can consistently be extended to higher orders and thus defines a legitimate and controllable nonperturbative approximation scheme. It has indeed proved its quantitative reliability already in a number of examples involving Yukawa sectors [105–107, 159–170].

In order to fix the standard RG invariance of field rescalings, we define the renormalized fields as

$$\tilde{\phi} \coloneqq Z^{1/2}_{\phi,k}\phi, \qquad \tilde{\psi}_\mathrm{L/R} \coloneqq Z^{1/2}_{\mathrm{L/R},k}\psi_\mathrm{L/R}, \qquad \tilde{\bar{\psi}}_\mathrm{L/R} \coloneqq Z^{1/2}_{\mathrm{L/R},k}\bar{\psi}_\mathrm{L/R}. \tag{3.35}$$

For the search for a fixed point, where the system is scale invariant, it is useful to introduce dimensionless renormalized quantities. In order to display the dimension dependence, we perform the analysis in d spacetime dimensions, where the dimensionless renormalized field and scalar potential read

$$\tilde{\rho} \coloneqq Z_{\phi,k} k^{2-d} \rho, \qquad u(\tilde{\rho}) \coloneqq k^{-d} U_k(Z_{\phi,k}^{-1} k^{d-2} \tilde{\rho}), \tag{3.36}$$

and the dimensionless Yukawa coupling

$$h^2 = Z_{\phi,k}^{-1} Z_{\mathrm{L},k}^{-1} Z_{\mathrm{R},k}^{-1} k^{d-4} \bar{h}_k^2. \tag{3.37}$$

Here and in the following, we suppress the index k denoting the scale-dependence of the dimensionless quantities. The presence of this scale dependence is implicitly understood. The flow of the wave function renormalizations $Z_{\phi,k}$, $Z_{\mathrm{L},k}$, and $Z_{\mathrm{R},k}$ can be expressed in terms of scale-dependent anomalous dimensions

$$\eta_\phi = -\partial_t \ln Z_{\phi,k}, \qquad \eta_{\mathrm{L/R}} = -\partial_t \ln Z_{\mathrm{L/R},k}\,. \tag{3.38}$$

With these preliminaries, we can compute the flow of the effective potential (see Sec. 2.2)

$$\begin{aligned} \partial_t u = {} & -du + (d - 2 + \eta_\phi)\tilde{\rho} u' + 2v_d \left[(2N_\mathrm{L} - 1)\, \ell_0^{(\mathrm{B})d}(u'; \eta_\phi) + \ell_0^{(\mathrm{B})d}(u' + 2\tilde{\rho} u''; \eta_\phi) \right] \\ & - 2v_d d_\gamma \left[(N_\mathrm{L} - 1)\, \ell_0^{(\mathrm{F})d}(0; \eta_\mathrm{L}) + \ell_0^{(\mathrm{F})d}(\tilde{\rho} h^2; \eta_\mathrm{L}) + \ell_0^{(\mathrm{F})d}(\tilde{\rho} h^2; \eta_\mathrm{R}) \right], \end{aligned} \tag{3.39}$$

where $v_d^{-1} \coloneqq 2^{d+1} \pi^{d/2} \Gamma(d/2) = 8\pi^2$ for $d = 3$ and $d_\gamma = 2$ is the number of components of the Weyl fermions[d]. The flow involves the threshold functions $\ell_0^{(\mathrm{B/F})}(\dots)$, which encode the details of the regularization scheme; their definitions and explicit forms for both linear and sharp cutoff are listed in App. B.

Whereas the flow of the Yukawa coupling is unambiguous in the symmetric regime, the Goldstone and radial modes can generally develop different couplings in the broken regime. Here, we concentrate on the Goldstone-mode Yukawa coupling to the fermions, as the radial mode becomes massive and decouples in the broken regime. In both regimes, the flow of the Yukawa coupling can be written as

$$\partial_t h^2 = (d - 4 + \eta_\phi + 2\eta_\psi) h^2 - 8 v_d \kappa u''\, \ell_{1,1,1}^{(\mathrm{FB})d}(\kappa h^2, u' + 2\kappa u'', u'; \eta_\psi, \eta_\phi)\, h^4, \tag{3.40}$$

where we introduced $\eta_\psi \coloneqq (\eta_\mathrm{L} + \eta_\mathrm{R})/2$. Here, the scalar-potential terms have to be evaluated on the k-dependent minimum of the potential $\tilde{\rho}_{\min} \equiv \kappa$. In the symmetric regime, we have, of course, $\kappa = 0$. At next-to-leading order in the derivative expansion, it is important to distinguish

[d] By contrast, we have chosen $d_\gamma = 4$ in [131].

between $Z_{\mathrm{L},k}$ and $Z_{\mathrm{R},k}$ as they acquire different loop contributions, see below. The flows of the anomalous dimensions read[e]

$$\eta_\phi = \frac{8v_d d_\gamma}{d} m_4^{(\mathrm{F})d}(\kappa h^2;\eta_\psi)\, h^2 + \frac{8v_d d_\gamma}{d}\kappa\, m_2^{(\mathrm{F})d}(\kappa h^2;\eta_\psi)\, h^4 + \frac{16v_d}{d}\kappa u''^2\, m_{2,2}^{(\mathrm{B})d}(u'+2\kappa u'', u';\eta_\phi), \tag{3.41}$$

$$\eta_\mathrm{L} = \frac{4v_d}{d}\left[m_{1,2}^{(\mathrm{FB})d}(\kappa h^2, u'+2\kappa u'';\eta_\psi,\eta_\phi) + m_{1,2}^{(\mathrm{FB})d}(\kappa h^2, u';\eta_\psi,\eta_\phi)\right] h^2, \tag{3.42}$$

$$\eta_\mathrm{R} = \frac{4v_d}{d}\Big[m_{1,2}^{(\mathrm{FB})d}(\kappa h^2, u'+2\kappa u'';\eta_\psi,\eta_\phi) + m_{1,2}^{(\mathrm{FB})d}(\kappa h^2, u';\eta_\psi,\eta_\phi) + 2(N_\mathrm{L}-1)\, m_{1,2}^{(\mathrm{FB})d}(0, u';\eta_\psi,\eta_\phi)\Big] h^2, \tag{3.43}$$

where the potential is again evaluated at $\tilde{\rho}_{\min} = \kappa$. The definitions of the threshold functions $\ell_{\dots}^{(\mathrm{B/F})d}(\dots)$ can again be found in App. B.

3.3 Fixed points and critical exponents

The Wetterich equation provides us with the flow of the generalized couplings $\partial_t g_i = \beta_i(g_1, g_2, \dots)$ of our truncation, where the g_i correspond to Yukawa coupling, expansion coefficients of the scalar potential, etc. In the vicinity of a fixed point g^*, defined by a simultaneous zero of all beta functions, $\beta_i(g_1^*, g_2^*, ...) = 0$, the flow is governed by the stability matrix $B_i{}^j = \partial\beta_i/\partial g_j|_{g^*}$. If the fixed point separates the disordered from an ordered phase, it is a candidate for a second-order phase transition. The critical behavior in terms of the correlation-length-exponent ν and the corrections-to-scaling-exponent ω then is given by

$$\nu = \frac{1}{\Theta_1} \qquad \text{and} \qquad \omega = -\Theta_2, \tag{3.44}$$

where Θ_1 and Θ_2 denote the largest and second-largest eigenvalues of the stability matrix $B_i{}^j$, cf. Eq. (2.47). For a fixed point with solely one RG relevant direction, both ν and ω are positive. As long as hyperscaling is fulfilled, the full set of critical exponents can then be obtained by ν and the anomalous dimension $\eta_\phi^* = \eta_\phi(g^*)$ at the fixed point; see Eqs. (2.51)–(2.52).

In order to analyze the fixed point structure of this model, we will distinguish two different regimes of the system, namely, the symmetric regime (SYM), where the vacuum expectation value (VEV) of the boson field is zero, and the regime of spontaneously broken symmetry (SSB), where it is nonzero. As boson and fermion fluctuations generically contribute with opposite sign, the existence of a fixed point requires a balancing between both contributions together with potential dimensional scaling terms [such as, e.g., the first term on the right-hand side of Eq. (3.40)]. We observe that this balancing is indeed possible in both regimes, depending on the number of left-handed fermion flavors. The origin of this flavor-number dependence is illustrated for the running of the scalar mass term or vacuum expectation value in Fig. 3.1. Whereas the scalar loop carries

[e] At this point, we like to draw attention to a missing factor 1/2 in the equations for $\eta_{\mathrm{L/R}}$ in our publication [131].

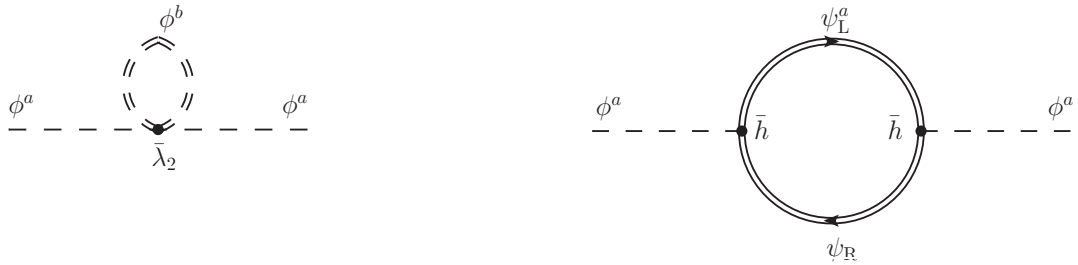

Figure 3.1 Loop contributions to the RG flow of the mass or the VEV. (For simplicity, we suppressed the regulator insertions $\partial_t R_k$, cf. Fig. 2.1.) The left loop involves only inner boson lines. The vertex $\bar{\lambda}_2$ allows for a coupling between all available boson components. This implies a linear dependence on N_{L} for the renormalization of the boson contribution, see below. On the right panel, we depict the corresponding fermion loop contribution. The incoming boson ϕ_a fully determines the structure of the fermion loop and does not allow for other left-handed inner fermions than ψ^a_{L}, inhibiting an N_{L} dependence of the algebraic weight of this loop.

a weight $\sim N_{\mathrm{L}}$ as all scalar degrees of freedom can contribute, the left-right asymmetry structure leads to a weight $\sim \mathcal{O}(1)$ for the fermion loops in Fig. 3.1. In the following, we analyze the different regimes in detail.

The symmetric regime

From now on, we restrict our investigations to the three-dimensional case $d = 3$. In the symmetric regime, we employ the following expansion of the effective potential u

$$u(\tilde{\rho}) = \sum_{n=1}^{\infty} \frac{\lambda_n}{n!} \tilde{\rho}^n = m_\phi^2 \tilde{\rho} + \frac{\lambda_2}{2!} \tilde{\rho}^2 + \frac{\lambda_3}{3!} \tilde{\rho}^3 + \ldots, \tag{3.45}$$

with scalar mass $m_\phi^2 \equiv \lambda_1$. The minimum is assumed to be at $\tilde{\rho}_{\min} = \kappa = 0$. This implies $m_\phi^2 \geq 0$. By expanding the flow equation for the effective potential (3.39) with respect to $\tilde{\rho}$ and comparing coefficients, we obtain the beta functions for the various scalar couplings λ_n. As a consequence of the one-loop structure of the Wetterich equation (2.21), for a given order n, any coupling λ_m with $m > n + 1$ does not contribute to the flow of λ_n, i.e.,

$$\partial_t \lambda_n = f_n(\lambda_1, \ldots, \lambda_{n+1}, h^2). \tag{3.46}$$

The Yukawa coupling reduces in the SYM regime to

$$\partial_t h^2 = (\eta_\phi + \eta_{\mathrm{L}} + \eta_{\mathrm{R}} - 1) h^2, \tag{3.47}$$

telling us that an interacting fixed point ($h^* \neq 0$) necessarily requires the sum rule for the anomalous dimensions

$$\eta_\phi^* + \eta_{\mathrm{L}}^* + \eta_{\mathrm{R}}^* = 1. \tag{3.48}$$

We note that while this statement holds exactly in the present truncation it may, of course, receive corrections from higher orders. We comment further on the relevance of this sum rule in the conclusions. For the linear cutoff, the expressions for the anomalous dimensions read

$$\eta_\phi = \frac{h^2}{6\pi^2}(5-\eta_\mathrm{L}-\eta_\mathrm{R}), \qquad \eta_\mathrm{L} = \frac{h^2}{12\pi^2}\frac{4-\eta_\phi}{(1+m_\phi^2)^2}, \qquad \eta_\mathrm{R} = N_\mathrm{L}\frac{h^2}{12\pi^2}\frac{4-\eta_\phi}{(1+m_\phi^2)^2}. \tag{3.49}$$

Besides fulfilling the optimization criterion, the linear cutoff has the convenient property that the corresponding loop integrals (threshold functions) can be evaluated analytically. (This is in fact also true for the sharp cutoff.) Consequently, the present set of fixed-point equations in the SYM regime can be solved analytically. Eliminating the anomalous dimensions in Eqs. (3.49) in terms of the couplings h^2 and m_ϕ^2 yields

$$\eta_\mathrm{L} = \frac{h^2(5h^2-24\pi^2)}{h^4(N_\mathrm{L}+1)-72\pi^4\left(1+m_\phi^2\right)^2}, \qquad \eta_\mathrm{R} = N_\mathrm{L}\frac{h^2(5h^2-24\pi^2)}{h^4(N_\mathrm{L}+1)-72\pi^4\left(1+m_\phi^2\right)^2}, \tag{3.50}$$

$$\eta_\phi = \frac{4h^2\left[h^2(N_\mathrm{L}+1)-15\pi^2\left(1+m_\phi^2\right)^2\right]}{h^4(N_\mathrm{L}+1)-72\pi^4\left(1+m_\phi^2\right)^2}. \tag{3.51}$$

These expressions can be plugged into the sum rule (3.48), resulting in a necessary condition for the fixed-point values h^{*2} and m_ϕ^{*2},

$$h^{*2} = \frac{3\pi^2}{4(N_\mathrm{L}+1)}\Bigg\{7+5m_\phi^{*2}\left(2+m_\phi^{*2}\right)+2N_\mathrm{L} - \sqrt{33+m_\phi^{*2}\left(2+m_\phi^{*2}\right)\left[54+25m_\phi^{*2}\left(2+m_\phi^{*2}\right)\right]+12N_\mathrm{L}+4m_\phi^{*2}\left(2+m_\phi^{*2}\right)N_\mathrm{L}+4N_\mathrm{L}^2}\Bigg\}. \tag{3.52}$$

For another solution with a positive root, we have not been able to identify a true fixed point of the full system by numerical means. The solution with the negative root, however, does give a fixed point and will be analyzed in the following. In fact, as a function of $m_\phi^{*2} > 0$ the Yukawa coupling $h^{*2}(m_\phi^{*2})$ is always positive and, moreover, monotonously increasing. It ranges between $h^{*2}(m_\phi^{*2}=0) = \frac{3\pi^2}{4}\left(7+2N_\mathrm{L}-\sqrt{33+4N_\mathrm{L}(3+N_\mathrm{L})}\right)/(N_\mathrm{L}+1)$ and $h^{*2}(m_\phi^{*2}=\infty) = \frac{6\pi^2}{5}$, which is very convenient because it ensures that the fixed-point value h^{*2} is bounded from above and from below in a very narrow window for all m_ϕ^{*2}. A true fixed point of the system requires also a vanishing of the scalar flow equations (3.46). Together with the relation (3.52) between h^{*2} and m_ϕ^{*2} this leaves us with the problem of searching for a scalar fixed-point potential. This question is familiar from scalar theories, where the Wilson-Fisher fixed point follows from an equation similar to Eq. (3.46) (with $h^2=0$). We truncate this system of fixed-point equations at a finite order $n \leq n_\mathrm{max}$, i.e., we neglect the contributions of all higher-order couplings $\lambda_{n>n_\mathrm{max}} \equiv 0$. The resulting system can then be solved explicitly. We find suitable fixed-point solutions in the symmetric regime only for $N_\mathrm{L} < 2$. The universal values for the anomalous dimensions at the fixed point as well as the correlation-length exponent ν and the corrections-to-scaling exponent ω

Table 3.2 Nonuniversal fixed-point values and universal critical exponents in the SYM regime. Exponent δ evaluated from hyperscaling relation $\delta = (5 - \eta_\phi^*)/(1 + \eta_\phi^*)$. We depict the results obtained for the optimized cutoff; the dependence on the regularization scheme (difference to sharp-cutoff results) provide a rough error estimate. Fixed points corresponding to a second-order phase transition of the system exist in this regime only for $N_\mathrm{L} = 1$.

N_L	m_ϕ^{*2}	λ_2^*	h^{*2}	ν	ω	η_ϕ^*	η_L^*	η_R^*	δ
1	0.213	6.82	8.54	1.21(2)	0.80(31)	0.67(4)	0.16(2)	0.16(2)	2.58(9)

can be read off from Table 3.2, together with the nonuniversal fixed-point values (for optimized cutoff)[f]. For these results, we have expanded the effective potential up to 12th order in the scalar field (i.e., $n_\mathrm{max} = 6$) and have computed the corresponding stability matrix, including the Yukawa coupling flow. Note that the fixed-point equations in the present case are technically more involved in comparison with those of scalar models within a similar approximation, as the insertion of the condition (3.52) introduces a much higher degree of nonlinearity. Let us emphasize that a corresponding scalar O($2N_\mathrm{L}$) model does not exhibit a fixed-point potential in the SYM regime but only in the SSB regime. Thus, the nature of the phase transition and the corresponding critical behavior is characteristic for our fermionic model. In particular for small N_L, the fermionic fluctuations contribute with a comparatively large weight to the critical behavior, as discussed in Fig. 3.1.

A priori, the full truncation error introduced by the derivative expansion is very hard to determine. At this stage of our investigation we therefore content ourself with a rough estimate taken from the dependence of our results on the regularization scheme. In agreement to what has been found in studies of other 3d bosonic [89, 90] and fermionic [105–107] models, we find that our results for the correlation-length-exponent ν is independent of the cutoff scheme within the percent level, whereas somewhat larger variations occur for the corrections-to-scaling exponent ω and the anomalous dimensions η_ϕ and $\eta_\mathrm{R/L}$. For quantitatively more accurate predictions of the latter, more refined techniques, that allow for a better resolution of the momentum dependence, are required, e.g., as suggested in [90, 153, 171]. However, the error arising from the polynomial expansion of the effective potential can be easily obtained by studying the convergence of the results as a function of increasing truncation order $n_\mathrm{max} = 2, \ldots, 7$. We find a very satisfactory convergence with a variation among the highest-order truncations being well below the dependence on the regularization scheme.

[f] For comparison with our results in [131], cf. footnotes *d*, *e*.

The regime of spontaneous symmetry breaking

For increasing left-handed fermion number, the scalar fixed-point potential must eventually lie in the regime of spontaneous symmetry breaking. This is already obvious from the structure of the flow equations: For large N_{L}, the Goldstone-like fluctuation modes dominate the flow of the effective potential (3.39) (the N_{L}-dependent fermionic contribution in Eq. (3.39) is field independent and therefore does not contribute to the flow of the couplings). We thus expect that in the $N_{\mathrm{f}} \to \infty$ our $\mathrm{U_L}(N_{\mathrm{L}}) \otimes \mathrm{U_R}(1)$ model is in the universality class of the purely bosonic $\mathrm{O}(2N_{\mathrm{L}})$ model. The latter is known to exhibit a Wilson-Fisher fixed-point potential in the SSB regime with a nonzero $\kappa^* > 0$. For finite N_{L}, the fixed-point properties compared to the Wilson-Fisher fixed point of the analogous bosonic model are, of course, quantitatively modified by the presence of fermionic fluctuations. However, its basic characteristics are left intact. Based on these simple observations, we continue with an analysis of the fixed-point structure in the SSB regime in the remainder of this section. In the SSB regime the effective potential u is minimal at a nonzero $\kappa > 0$, and we expand

$$u(\tilde{\rho}) = \sum_{n=2}^{\infty} \frac{\lambda_n}{n!}(\tilde{\rho} - \kappa)^n = \frac{\lambda_2}{2!}(\tilde{\rho} - \kappa)^2 + \frac{\lambda_3}{3!}(\tilde{\rho} - \kappa)^3 + \dots \tag{3.53}$$

For the flow of κ, we use the fact that the first derivative of u vanishes at the minimum, $u'(\kappa) = 0$. This implies for the beta function

$$0 = \partial_t u'(\kappa) = \partial_t u'(\tilde{\rho})|_{\tilde{\rho}=\kappa} + (\partial_t \kappa) u''(\kappa) \qquad \Rightarrow \qquad \partial_t \kappa = -\frac{1}{u''(\kappa)} \partial_t u'(\tilde{\rho})|_{\tilde{\rho}=\kappa} \,. \tag{3.54}$$

The flow equations in the SSB regime are much more involved due to additional loop contributions which arise from the coupling to the VEV. This higher degree of nonlinearity inhibits a simple analytical study of the fixed-point structure at NLO in the derivative expansion. Instead, we use an iterative method, starting at the Wilson-Fisher fixed point for the analogous $\mathrm{O}(2N_{\mathrm{L}})$ model, which can be obtained in our system by setting $h^2 \equiv 0$[g]. Starting at this Wilson-Fisher fixed point of the reduced scalar system, we can then obtain a fixed point of the full $\mathrm{U_L}(N_{\mathrm{L}}) \otimes \mathrm{U_R}(1)$ system by numerical iteration. This confirms that the presence of the fermions generically shifts the scalar fixed-point values only slightly. However, our $\mathrm{U_L}(N_{\mathrm{L}}) \otimes \mathrm{U_R}(1)$ system defines for finite N_{L} a different universality class, and so the critical exponents and the anomalous dimensions are special to our system. Let us discuss the results for fixed-point positions and critical exponents as a function of N_{L} in comparison to the analogous $\mathrm{O}(2N_{\mathrm{L}})$ model; both truncated at next-to-leading order in the derivative expansion and 12th order in the polynomial expansion of the effective potential.

[g] This offers also the possibility of a cross check: a comparison of our $\mathrm{O}(2N_{\mathrm{L}})$-model results to the results which are given in [153, 172] reveals a very satisfactory precision. The remaining minor deviations can fully be attributed to the fact that we use a simple NLO-derivative expansion truncated at λ_6.

In Fig. 3.2, we depict the fixed-point values κ^* and h^{*2} for linear cutoff as a function of N_L. Note that $N_\mathrm{L} < 2$ corresponds to the fixed-point scenario in the SYM regime discussed in the previous subsection; we plot m_ϕ^{*2} instead of κ^* for $N_\mathrm{L} < 2$. At the transition from the SYM to the SSB regime the fixed-point position exhibits as a function of N_L a kink. Nevertheless, the results for our $\mathrm{U_L}(N_\mathrm{L}) \otimes \mathrm{U_R}(1)$ model (black) compared to the $\mathrm{O}(2N_\mathrm{L})$ model (gray) change only slightly. We emphasize that the fixed-point positions are nonuniversal quantities, depending on the details of the regulator. By contrast, the values of the anomalous dimensions as shown in Fig. 3.3 are universal (even though slight regulator dependencies are induced by our truncation). The left panel shows η_ϕ^* for our $\mathrm{U_L}(N_\mathrm{L}) \otimes \mathrm{U_R}(1)$ model (black) in comparison with the analogous $\mathrm{O}(2N_\mathrm{L})$ model (gray). Whereas for large N_L the scalar anomalous dimension η_ϕ^* approaches the $\mathrm{O}(2N_\mathrm{L})$ value, we find large differences for smaller N_L. Those can directly be attributed to the fermionic loop contributions. The fermion anomalous dimensions η_L^* and η_R^* are shown in the right panel. For $N_\mathrm{L} = 1$, both anomalous dimensions coincide; this corresponds to the left-right symmetric point. For larger N_L, η_R^* increases significantly, as the massless fermion and boson degrees of freedom contribute to the loop diagrams with a weight $\propto N_\mathrm{L}$, whereas η_L^* vanishes for $N_\mathrm{L} \to \infty$. In both figures, we show the results for the linear (i.e., optimized) regulator (solid curve) as well as for the sharp regulator (dashed curve). The difference (gray shaded area) might be thought of as rough error estimate. The critical exponents ν and ω are shown in Fig. 3.4. Again, the black curves represent the values for our chiral $\mathrm{U_L}(N_\mathrm{L}) \otimes \mathrm{U_R}(1)$ model for optimized (solid line) and sharp regulator (dashed). For comparison, we depict again the exponents for the analogous $\mathrm{O}(2N_\mathrm{L})$ model (gray curve). For large N_L we again find the $\mathrm{O}(2N_\mathrm{L})$ exponents. However, by lowering $N_\mathrm{L} \searrow 2$, we find that the critical exponent ν and ω rapidly change with N_L and eventually exhibit a discontinuity at the transition point $N_\mathrm{L} \simeq 2$, where the fixed-point effective potential changes from the SSB to the SYM regime. We think of this strong variation as rather natural, as the structure of the fixed-point equations changes significantly across this transition. Near this point, we also observe a comparatively large dependence on the regulator (gray shaded area). Thus, in contrast to what is known from the purely bosonic theories [89,153,172], in the vicinity of $N_\mathrm{L} \simeq 2$ it is much harder to predict the critical behavior of the correlation length than, for instance, the anomalous dimension η_ϕ. The explicit results in the SSB regime are summarized in Tab. 3.3. In the limit $N_\mathrm{f} \to \infty$, the flow equations simplify considerably; in particular, the sum rule (3.48) known from the SYM regime is fulfilled in this limit and we can again solve the fixed-point equations analytically (last line of Tab. 3.3).

It may be worthwhile comparing our results for the left-right symmetric case ($N_\mathrm{L} = N_\mathrm{R} = 1$) with those obtained in previous studies. In [96, 102], the chiral Gross-Neveu model with $N_\mathrm{f} \coloneqq N_\mathrm{L} = N_\mathrm{R}$ fermion flavors and $\mathrm{U}(1) \otimes \mathrm{U}(1)$ symmetry has been solved up to $\mathcal{O}(1/{N_\mathrm{f}}^2)$ of the large-N_f expansion. To this order, the correlation-length exponent ranges from $\nu = 0.83$ for $N_\mathrm{f} = 2$ (in terms of 4-component fermions) to $\nu = 1$ for $N_\mathrm{f} \to \infty$, with a maximum of $\nu = 1.04$ at

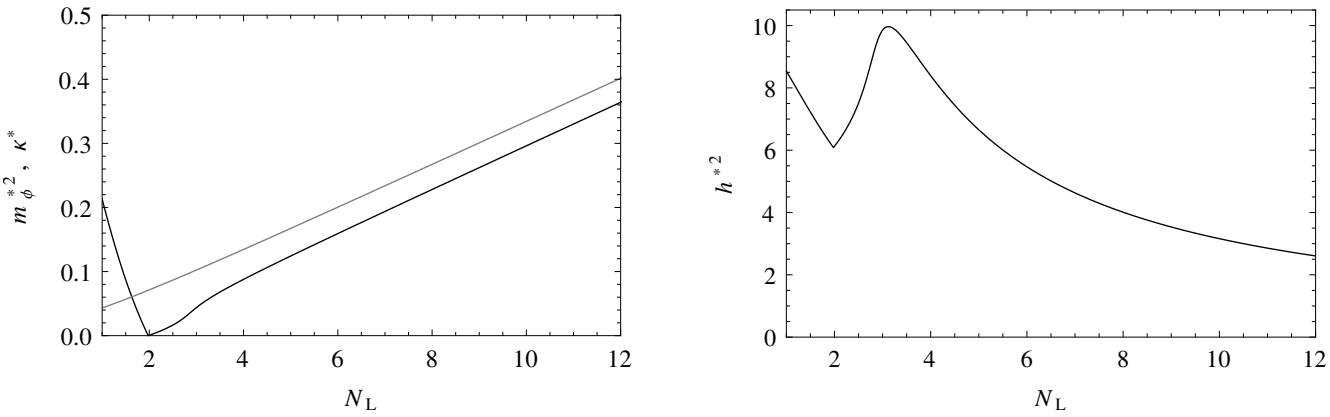

Figure 3.2 Nonuniversal fixed point values for optimized cutoff. Left panel: the potential minimum κ^* in SSB regime for $N_\mathrm{L} \geq 2$ in our $\mathrm{U_L}(N_\mathrm{L}) \otimes \mathrm{U_R}(1)$ model (black) compared with the $\mathrm{O}(2N_\mathrm{L})$ model (gray). For $N_\mathrm{L} < 2$ the fixed point is in the SYM regime and we depict m_ϕ^{*2}. The transition near $N_\mathrm{L} \simeq 2$ also causes a kink in the N_L dependence of h^{*2} (right panel).

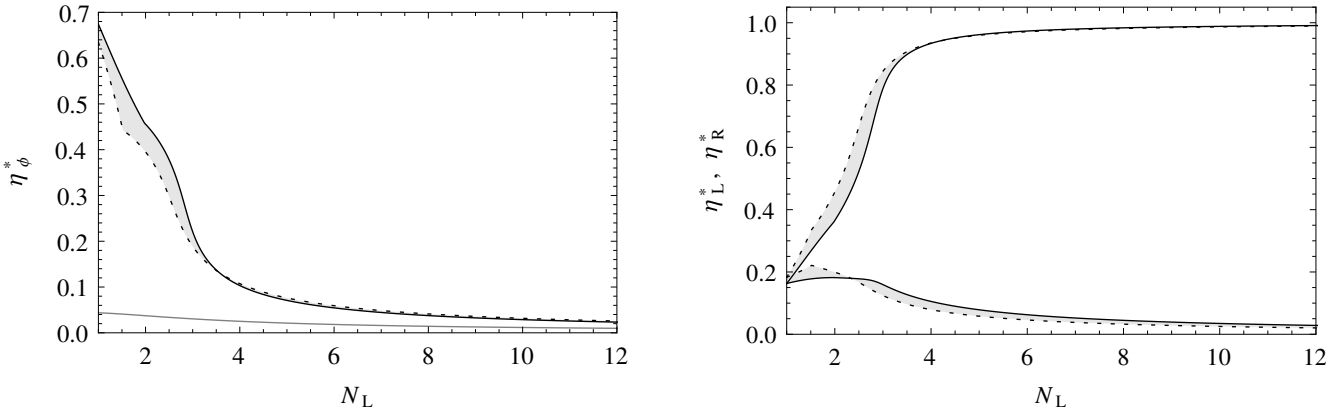

Figure 3.3 Left: η_ϕ^* in our $\mathrm{U_L}(N_\mathrm{L}) \otimes \mathrm{U_R}(1)$ model for optimized cutoff (black solid) and sharp cutoff (black dashed). The difference (shaded area) might be thought of as rough error estimate. The gray curve shows η_ϕ^* for the $\mathrm{O}(2N_\mathrm{L})$ model. Right: η_R^* (upper curves) and η_L^* (lower curves).

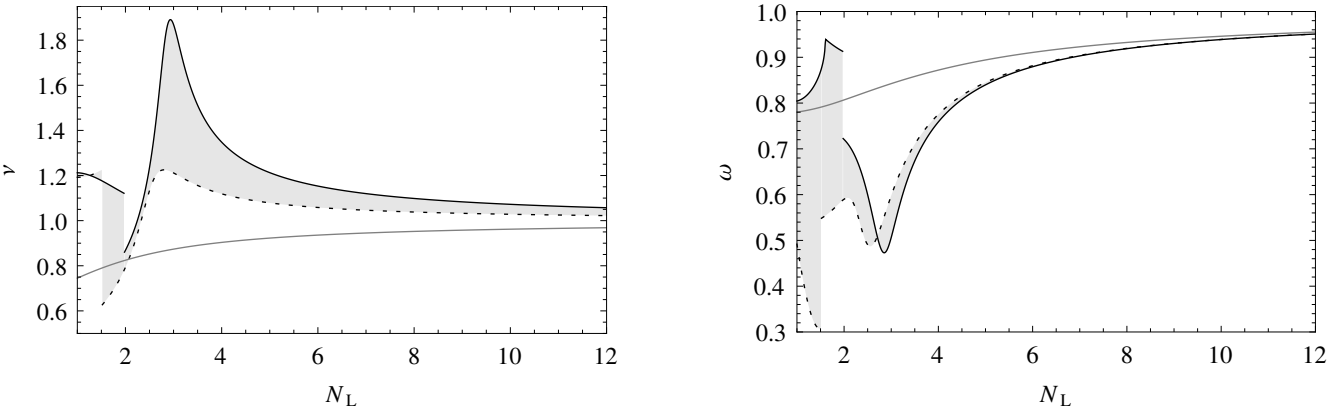

Figure 3.4 Critical exponents ν and ω in the chiral $\mathrm{U_L}(N_\mathrm{L}) \otimes \mathrm{U_R}(1)$ model (black) in comparison with those of the $\mathrm{O}(2N_\mathrm{L})$ model (gray). Shaded area: rough error estimate. The rapid change of the exponents occurs near $N_\mathrm{L} \simeq 2$, where the fixed-point potential shows a transition from the SYM to the SSB regime.

Table 3.3 Nonuniversal fixed-point values (optimized cutoff) and universal critical exponents in the SSB regime. For better visibility of the large-N_L behavior, the fixed-point couplings have been multiplied by suitable factors of N_L. The exponent δ is evaluated from the hyperscaling relation $\delta = (5 - \eta_\phi^*)/(1 + \eta_\phi^*)$. Error estimates from regulator dependence.

N_L	κ^*/N_L	$N_\mathrm{L}\lambda_2^*$	$N_\mathrm{L}h^{*2}$	ν	ω	η_ϕ^*	η_L^*	η_R^*	δ
2	0.0003	8.40	12.3	0.87(8)	0.72(13)	0.46(6)	0.18(2)	0.37(9)	3.12(17)
3	0.0146	16.7	29.6	1.87(66)	0.51(9)	0.22(3)	0.16(4)	0.79(6)	3.91(13)
4	0.0220	17.0	33.6	1.35(23)	0.76(2)	0.10(1)	0.11(3)	0.93(1)	4.44(2)
5	0.0248	16.5	33.3	1.21(13)	0.84(1)	0.07(1)	0.08(2)	0.96(1)	4.60(3)
10	0.0296	15.6	31.6	1.07(4)	0.94(1)	0.03(1)	0.03(1)	0.99(1)	4.83(2)
20	0.0317	15.2	30.6	1.03(2)	0.97(1)	0.01(1)	0.02(1)	1.00(1)	4.92(1)
50	0.0330	14.9	30.0	1.01(1)	0.99(1)	0.01(1)	0.01(1)	1.00(1)	4.97(1)
100	0.0334	14.9	29.8	1.01(1)	0.99(1)	0.00(1)	0.00(1)	1.00(1)	4.98(1)
∞	$\frac{1}{3\pi^2}$	$\frac{3\pi^2}{2}$	$3\pi^2$	1	1	0	0	1	5

$N_\mathrm{f} \simeq 7$. While it seems appealing to conclude qualitative compatibility with the general trend we find for $N_\mathrm{L} > 1$ and $N_\mathrm{R} = 1$, some caution is in order: It could well be that the fixed point, which is located in SYM regime for $N_\mathrm{L} = N_\mathrm{R} = 1$, remains in the SYM regime for larger flavor numbers N_f, if the symmetry remains $\mathrm{U}(1) \otimes \mathrm{U}(1)$. Then, the corresponding critical behavior would possibly be completely unrelated to our fixed point for $N_\mathrm{L} > N_\mathrm{R} = 1$, located in the SSB regime. Unfortunately, the $1/N_\mathrm{f}$ expansion fails for $N_\mathrm{f} = 1$ and we cannot compare to our left-right symmetric case $N_\mathrm{L} = N_\mathrm{R} = 1$.

Variants of the universality classes defined by our models have also been investigated on the lattice. In [99] the critical behavior of the $\mathrm{U}(1) \otimes \mathrm{U}(1)$ model with $N_\mathrm{f} = 4$ flavors is studied to high precision and the results agree very well with previous findings. Ref. [97] reports results on the $N_\mathrm{f} = 2$ case. The simulations give for the anomalous dimension $\eta_\phi = 0.46(11)$ and for the correlation-length exponent $\nu = 0.88(8)$, well compatible with the large-N_f results cited above. However, there is in fact some uncertainty whether the employed lattice action is a lattice version of the 3d chiral Gross-Neveu model or rather of the 3d Thirring model. Indeed, in Refs. [69–73] the same four-fermion action in three dimension is interpreted as the Thirring model. We further elaborate on this peculiarity in Sec. 5.8, where we discuss the critical behavior of the 3d Thirring model; cf. also the discussion in [97]. Here, we content ourself with just quoting the results. Ref. [69–72] finds $\delta = 2.75(9)$ ($N_\mathrm{f} = 2$), $\delta = 3.14(17)$ ($N_\mathrm{f} \simeq 3$), and $\delta = 3.76(14)$ ($N_\mathrm{f} = 4$)[h]. Assuming the hyperscaling relation, we find in our $\mathrm{U}(1) \otimes \mathrm{U}(1)$ model $\delta = 2.58(9)$ for $N_\mathrm{f} = N_\mathrm{L} =$

[h] We note that the lattice symmetry breaking pattern considered in [69–72] coincides only for the case $N_\mathrm{f} = 2$ with the one in [99]. We therefore cannot directly compare with the lattice results for $N_\mathrm{f} = 4$ cited above.

$N_{\mathrm{R}} = 1$, which seems to agree well with the reported general trend of δ as a function of N_{f}. The recent work [73] (which considers solely $N_{\mathrm{f}} = 2$) is particularly interesting, since for the first time it computes the critical behavior directly in the chiral limit, i.e., with exactly massless fermions. A finite-size scaling analysis reveals $\nu = 0.85(1)$, $\eta_\phi = 0.65(1)$, and $\eta_\psi = 0.37(1)$. All quoted lattice studies implement *staggered fermions*, in which case the chiral limit is more or less easily accessible. In three dimensions, the number of continuum four-component physical flavors is however twice the number of staggered fermion flavors [110]; unfortunately, no lattice data is hence available for $N_{\mathrm{f}} = 1$ and for a detailed comparison we have to generalize our study to larger number of right-handed fermions, in particular to the left-right symmetric case with $N_{\mathrm{L}} = N_{\mathrm{R}} > 1$. In fact, the flow equations for the latter are well-known [165], but so far have not been examined in three dimensions. This work is under way. In any case, we believe that our findings for $N_{\mathrm{L}} > N_{\mathrm{R}} = 1$ are on the whole consistent with the general trend given in the literature.

3.4 Conclusions

Let us summarize our results for the $\mathrm{U_L}(N_{\mathrm{L}}) \otimes \mathrm{U_R}(1)$ chiral Gross-Neveu models. We have designed this class of models to exhibit similarities to the Higgs-Yukawa sector of the standard model of particle physics. As a fundament of this model building, we have classified all possible four-fermion interaction terms invariant under this chiral symmetry, and also determined the corresponding discrete symmetries. We have identified a scalar parity-conserving channel similar to the standard-model Higgs scalar. For sufficiently strong correlations in this channel, a second-order phase transition into the chiral-symmetry broken phase can occur, which is a 3d analog of the electroweak phase transition. Using the functional RG, we have computed the critical behavior of this phase transition in terms of the correlation-length exponent ν, the corrections-to-scaling exponent ω, and the fermion and scalar anomalous dimensions as a function of $N_{\mathrm{L}} \geq 1$.

Whereas the standard model is defined with a fundamental Higgs scalar, we have here started with only fundamental fermion degrees of freedom. The resulting Higgs field arises as a scalar bi-fermionic composite upon strong fermionic correlations. Therefore, the relation between our original fermion model and the resulting Yukawa system is similar to that between top-quark condensation models [173–176] and the standard-model Higgs sector. From a more general RG perspective, however, the purely fermionic models can anyway be viewed as just a special case of the more general Yukawa models [177, 178] supplemented with nonuniversal compositeness conditions. As long as the compositeness scale in the deep UV remains unresolved, there is no real difference between the purely fermionic or the Yukawa-model language.

For our quantitative results, we have used a consistent and systematic expansion scheme of the effective action in terms of a nonperturbative derivative expansion. Whereas there is an extensive body of circumstantial evidence in the literature that this expansion is suitably adjusted to the

relevant degrees of freedom of Yukawa systems, a practical test for convergence is problematic in the present case. This is because the leading-order of the expansion (defined by setting all $\eta_{\phi,\mathrm{L,R}} = 0$) does not support the desired fixed point. The latter becomes visible only from next-to-leading order on, due to the structure of the Yukawa flow. This is not too surprising, as the NLO scalar anomalous dimension and the LO Yukawa coupling flow arise from technically similar diagrams; for instance, the correct one-loop Yukawa beta function receives contributions also from the anomalous dimensions. In any case, a straightforward convergence test in principle requires a NNLO calculation.

With these reservations in mind, a critical discussion of the accuracy of our NLO results can be based on the following indirect arguments: First, the large-N_L limit of our model corresponds to the purely scalar O(N) model with $N = 2N_\mathrm{L}$, which exhibits the well-known Wilson-Fisher fixed-point structure. In these models, the quantitative reliability of the derivative expansion has been verified to a high level of significance. We conjecture that this limit also provides a reasonable estimate for large finite values of N_L. Second, the derivative expansion is based on the implicit assumption that momentum dependencies of operators do not grow large. This includes the kinetic terms, such that self-consistency of the derivative expansion requires that the anomalous dimensions satisfy $\eta_{\phi,\mathrm{L,R}} \lesssim 1$, as is the case in our calculations. From the structure of the threshold functions, cf. App. B, we observe that even large anomalous dimensions of order $\eta_i \simeq 1$ do not change the LO flow qualitatively but contribute a correction on the 10-20% level to the potential flow. Third, the same NLO truncation has been used in the study of critical exponents in the 3d Gross-Neveu model [105, 106]: the resulting critical exponents are in very good quantitative agreement with the available lattice data for $N_\mathrm{f} = 4, 12$, and other methods [100, 101, 103, 104, 179, 180] even for large anomalous dimensions. Still, we emphasize that a direct quantitative estimate of the accuracy in our case requires a higher-order calculation. In particular, the anomalous dimensions and subleading exponents may acquire larger corrections. In contrast to the derivative expansion, the reliability of the polynomial expansion of the effective potential has been directly verified, and we observe very good convergence properties in this case.

We believe that the new universality classes defined by our $\mathrm{U_L}(N_\mathrm{L}) \otimes \mathrm{U_R}(1)$ models can serve as a useful testing ground for other nonperturbative studies of chiral fermions near the symmetry-breaking phase transition. In particular, our results for the critical exponents ν and ω and the anomalous dimension η_ϕ and $\eta_{\mathrm{L,R}}$ as summarized in Tabs. 3.2–3.3 can provide for first benchmarks for these new universality classes.

From our classification of all fermionic interaction terms compatible with the required symmetries, it is clear that the Higgs-like condensation channel is not the only possible channel. Aside from vectorlike channels, there are two further pseudoscalar channels, cf. Eq. (3.26), and further scalar and pseudoscalar channels in the flavor-singlet Fierz transforms (3.22)–(3.22). In fact, the present analysis is a restricted study of a particular condensation process. We expect that

the phase diagram of the general model is much more involved and might exhibit a variety of possible phases and corresponding transitions. This phase diagram is parameterized by up to six independent couplings being associated with the linearly independent fermionic interactions. The calculation of the true condensation channel for a given set of initial couplings remains a challenging problem. As such a problem of competing order parameters is well known also in other systems, e.g., in the Hubbard model [181–185], the present system can serve as a rich and controllable model system.

A special feature of our model arises in the symmetric regime: here, a fixed point within our truncation implies a sum rule for the anomalous dimensions, $\eta_\phi^* + \eta_{\mathrm{L}}^* + \eta_{\mathrm{R}}^* = 1 \equiv 4 - d$. This sum rule is relevant, since the underlying balancing between anomalous dimensions and dimensional power-counting scaling can be a decisive feature of many other models as well. Most prominently, the asymptotic-safety scenario in quantum gravity [186–194] as well as in extra-dimensional Yang-Mills theories [195] requires similar sum rules to be satisfied. In contrast to these latter models, the present model for $N_{\mathrm{L}} = 1$ can serve as a much simpler example for a test of this sum rule at a fixed point. A verification of this sum rule also by other nonperturbative tools can shed light on this important mechanism to generate RG fixed points.

This is another reason why we believe that the new universality classes defined by our models can serve as prototypes for studies of strongly-correlated chiral fermions in general and of nonperturbative features of standard-model-like chiral symmetry breaking in particular.

4 UV fixed-point structure of the Thirring model

Let us now turn our focus to the maximally symmetric case, that is to say, the theories invariant under *all* possible chiral transformations. In particular, the 3d Thirring as well as the 3d Nambu-Jona-Lasinio (NJL) model is of this class. As a first step, we classify all possible four-fermi interactions compatible with the continuous and discrete symmetries of these models and calculate the purely fermionic RG flow using a full basis of fermionic four-point functions in the pointlike limit. Our results show that the UV complete (asymptotically safe) Thirring model lies in a two-dimensional coupling plane which reduces to the conventional Thirring coupling only in the strict large-N_f limit. In addition to the Thirring universality class, which is characterized by one relevant direction (also at finite N_f), two further interacting fixed points occur which may define new universality classes of second-order phase transitions also involving parity-broken phases. The N_f dependence of the Thirring fixed point sheds further light on the existence of a critical flavor number N_f^cr above which chiral symmetry remains unbroken for arbitrary large coupling: Our findings suggest that the quantum phase transition at N_f^cr does not occur because of a drastic change of the UV fixed-point structure (with respect to N_f), but rather because of a competition between different condensation channels in the IR. However, a definite answer will require a direct investigation of the composite degrees of freedom. Within the functional RG, this can conveniently be studied by means of partial or dynamical bosonization; see Chap. 5.

4.1 Symmetries of the Thirring model

The bare action for the massless Thirring model in three Euclidean space-time dimensions reads

$$S_\mathrm{Thirring} = \int \mathrm{d}^3x \left[\bar\psi^a \mathrm{i}\partial\!\!\!/ \psi^a + \frac{\bar g}{2N_\mathrm{f}} \left(\bar\psi^a \gamma_\mu \psi^a\right)^2\right]. \tag{4.1}$$

Let us again work with a 4×4 *reducible* representation of the Dirac algebra

$$\{\gamma_\mu, \gamma_\nu\} = 2\delta_{\mu\nu}, \tag{4.2}$$

such that the index a in Eq. (4.1) runs over N_f distinct flavors of four-component Dirac fermions. We have seen in Chap. 3 that there are now *two* further 4×4 matrices, which anticommute with

all γ_μ as well as with each other; we will again label them γ_4 and γ_5,

$$\{\gamma_\mu, \gamma_4\} = \{\gamma_\mu, \gamma_5\} = \{\gamma_4, \gamma_5\} = 0. \tag{4.3}$$

The massless Lagrangian (4.1) is invariant under the axial transformations

$$\mathrm{U}_{\gamma_4}(1): \qquad \psi \mapsto \mathrm{e}^{\mathrm{i}\alpha\gamma_4}\,\psi, \qquad \bar\psi \mapsto \bar\psi\,\mathrm{e}^{\mathrm{i}\alpha\gamma_4}, \tag{4.4}$$

$$\mathrm{U}_{\gamma_5}(1): \qquad \psi \mapsto \mathrm{e}^{\mathrm{i}\beta\gamma_5}\,\psi, \qquad \bar\psi \mapsto \bar\psi\,\mathrm{e}^{\mathrm{i}\beta\gamma_5}, \tag{4.5}$$

as well as the vector transformations

$$\mathrm{U}_{\mathbb{1}}(1): \qquad \psi \mapsto \mathrm{e}^{\mathrm{i}\vartheta}\,\psi, \qquad \bar\psi \mapsto \bar\psi\,\mathrm{e}^{-\mathrm{i}\vartheta}, \tag{4.6}$$

$$\mathrm{U}_{\gamma_{45}}(1): \qquad \psi \mapsto \mathrm{e}^{\mathrm{i}\varphi\gamma_{45}}\,\psi, \qquad \bar\psi \mapsto \bar\psi\,\mathrm{e}^{-\mathrm{i}\varphi\gamma_{45}}, \tag{4.7}$$

where we have defined $\gamma_{45} \coloneqq \mathrm{i}\gamma_4\gamma_5$. For each flavor $a = 1, \ldots, N_\mathrm{f}$, the theory thus has a global U(2) symmetry with the Hermitian generators

$$\tau_\alpha = \mathbb{1}_4, \gamma_4, \gamma_5, \gamma_{45}, \qquad \alpha = 1, \ldots, 4. \tag{4.8}$$

This symmetry transformations together with flavor rotations form a larger symmetry of the classical massless Lagrangian, corresponding to the group $\mathrm{U}(2N_\mathrm{f})$ with the $(2N_\mathrm{f})^2$ generators

$$\tau_\alpha \otimes \lambda_\beta, \qquad \alpha = 1, \ldots, 4, \qquad \beta = 1, \ldots, {N_\mathrm{f}}^2. \tag{4.9}$$

Here, $\{\lambda_1, \ldots, \lambda_{{N_\mathrm{f}}^2-1}\}$ are the generalized $N_\mathrm{f} \times N_\mathrm{f}$ Gell-Mann matrices, and $\lambda_{{N_\mathrm{f}}^2} \coloneqq \mathbb{1}_{N_\mathrm{f}}$ is the unit matrix. The $\mathrm{U}(2N_\mathrm{f})$ symmetry can be made more obvious in terms of two-component (Weyl-like) fermions, which are eigenvectors of the projectors $P^{(45)}_{\mathrm{L/R}} = (1 \pm \gamma_{45})/2$. In the representation (3.2)–(3.3) the projectors read[a]

$$P^{(45)}_{\mathrm{L/R}} = \frac{1}{2}(1 \pm \gamma_{45}) = \frac{1}{2}\begin{pmatrix} \mathbb{1}_2 & (-\mathrm{i})\,\mathbb{1}_2 \\ \mathrm{i}\,\mathbb{1}_2 & \mathbb{1}_2 \end{pmatrix}, \tag{4.10}$$

and we may employ the decomposition

$$\psi^a = \frac{1}{\sqrt{2}}\begin{pmatrix} \chi^a + \chi^{a+N_\mathrm{f}} \\ \mathrm{i}\left(\chi^a - \chi^{a+N_\mathrm{f}}\right) \end{pmatrix}, \quad \bar\psi^a = \left(\bar\chi^a - \bar\chi^{a+N_\mathrm{f}}, \quad (-\mathrm{i})\left(\bar\chi^a + \bar\chi^{a+N_\mathrm{f}}\right)\right), \quad a = 1, \ldots, N_\mathrm{f}, \tag{4.11}$$

with the definition of the Dirac adjoint $\bar\chi$ chosen such that $\chi^\dagger \coloneqq \mathrm{i}\bar\chi\sigma_3$ in agreement with $\psi^\dagger \coloneqq \mathrm{i}\bar\psi\gamma_3$. In other words, we can trade the N_f flavors of four-component spinors ψ for $2N_\mathrm{f}$ flavors of two-component spinors χ. Therewith, the Thirring action (4.1) can be rewritten as

$$S_\mathrm{Thirring} = \int \mathrm{d}^3x \left[\bar\chi^i \mathrm{i}\partial_\mu\sigma_\mu\chi^i + \frac{\bar g}{2N_\mathrm{f}}\left(\bar\chi^i\sigma_\mu\chi^i\right)^2\right], \qquad i = 1, \ldots, 2N_\mathrm{f}, \tag{4.12}$$

[a] We note that one could choose more adapted representations in which $\gamma_{45} = \mathrm{diag}(\mathbb{1}_2, -\mathbb{1}_2)$ and thus the Weyl spinor χ^a (χ^{a+N_f}) is simply given by the upper (lower) two components of the Dirac spinor ψ^a. The "graphene representation" [26, 27] is of this type.

where we have introduced the collective index i, running over $2N_\mathrm{f}$ flavors. The Weyl formulation (4.12) corresponds to an irreducible representation of the Dirac algebra with gamma matrices $\gamma_\mu \equiv \sigma_\mu$. Here, the $\mathrm{U}(2N_\mathrm{f})$ symmetry is manifest,

$$\mathrm{U}(2N_\mathrm{f}): \qquad \chi^i \mapsto U^{ij}\chi^j \qquad \bar\chi^i \mapsto \bar\chi^j \left(U^\dagger\right)^{ji}, \qquad U \in \mathrm{U}(2N_\mathrm{f}). \tag{4.13}$$

In the ensuing chapter 5, we will exclusively be using this two-component language. However, the four-component formulation (4.1) shall prove instructive when it comes to discussing possible (dynamically generated) mass terms and their symmetries; throughout this chapter, we will therefore retain both representations. We note that what is commonly labeled "chiral" symmetry in the four-component reducible formulation is in fact just a part of the $\mathrm{U}(2N_\mathrm{f})$ flavor symmetry in the two-component irreducible language.

In the reducible formulation, discrete transformations can be implemented in various ways, cf. Sec. 3.1 and Ref. [63]. Let us define[b]

$$\mathcal{C}: \qquad \psi(x) \mapsto \left[\bar\psi(x) C_\xi\right]^\mathrm{T}, \qquad \bar\psi(x) \mapsto -\left[C_\xi^\dagger \psi(x)\right]^\mathrm{T}, \tag{4.14}$$

$$\mathcal{P}: \qquad \psi(x) \mapsto P_\zeta \psi(\hat x), \qquad \bar\psi(x) \mapsto \bar\psi(\hat x) P_\zeta^\dagger, \qquad \hat x \coloneqq (-x_1, x_2, x_3) \tag{4.15}$$

$$\mathcal{T}: \qquad \psi(x) \mapsto T_\eta \psi(x), \qquad \bar\psi(x) \mapsto \bar\psi(x) T_\eta^\dagger, \tag{4.16}$$

where the 4×4 matrices C_ξ, P_ζ, and T_η in the gamma matrix representation (3.2)–(3.3) are given by

$$C_\xi = \frac{1}{2}\left[(1+\xi)\gamma_2\gamma_4 + \mathrm{i}(1-\xi)\gamma_2\gamma_5\right], \tag{4.17}$$

$$P_\zeta = \frac{1}{2}\left[(1+\zeta)\gamma_1\gamma_4 + \mathrm{i}(1-\zeta)\gamma_1\gamma_5\right], \tag{4.18}$$

$$T_\eta = \frac{1}{2}\left[(1+\eta)\gamma_2\gamma_4 + \mathrm{i}(1-\xi)\gamma_2\gamma_5\right], \tag{4.19}$$

and depend on the pure phases ξ, ζ, η with $|\xi| = |\zeta| = |\eta| = 1$. However, for a $\mathrm{U}(2N_\mathrm{f})$-symmetric theory we can choose without loss of generality $\xi = \zeta = \eta = 1$, for instance. Any other definition of the discrete transformations can then be obtained by combining $\mathcal{C}$, $\mathcal{P}$, and $\mathcal{T}$ with a suitably chosen $\mathrm{U}(2N_\mathrm{f})$ rotation, see Eqs. (4.4)–(4.7). In other words, the distinction between the various discrete transformations in the preceding chapter 3 becomes redundant for a $\mathrm{U}(2N_\mathrm{f})$-symmetric theory. We note however, that it might become important once it comes to spontaneous breaking of one of the discrete symmetries; see below. On the classical level, the Thirring model is in any case invariant under any definition of $\mathcal{C}$, $\mathcal{P}$, and $\mathcal{T}$.

Let us now consider building blocks of the effective action, starting at the two-fermion level. There are, in fact, four possible mass terms $\bar\psi\tau_\alpha\psi$ with τ_α given in Eq. (4.8) and diagonal flavor structure. (We shall suppress the flavor index as long as it is not needed.) However, the term

[b] Note that in contrast to [134] we define $\mathcal{T}$ without reversing x_3, cf. Sec. 3.1.

$\bar{\psi}(\mathrm{i}m + m'\gamma_4)\psi$ transforms under $\psi \mapsto \mathrm{e}^{\mathrm{i}\alpha\gamma_4}\,\psi$ into a parity even mass term $\propto \bar{\psi}\psi$ if α is chosen to satisfy $2\alpha = \arctan(m'/m)$. The analogous statement holds for the mass term involving γ_5. More generally, any mass term can be transformed by a $\mathrm{U}(2N_\mathrm{f})$ rotation into[c]

$$\mathrm{i}\bar{m}_{\mathrm{f},\chi}\bar{\psi}^a\psi^a + \mathrm{i}\bar{m}_{\mathrm{f},\mathcal{P}}\bar{\psi}^a\gamma_{45}\psi^a = \mathrm{i}\bar{m}_{\mathrm{f},\chi}\left(\bar{\chi}^a\chi^a - \bar{\chi}^{a+N_\mathrm{f}}\chi^{a+N_\mathrm{f}}\right) + \mathrm{i}\bar{m}_{\mathrm{f},\mathcal{P}}\left(\bar{\chi}^a\chi^a + \bar{\chi}^{a+N_\mathrm{f}}\chi^{a+N_\mathrm{f}}\right), \quad (4.20)$$

where the right hand side holds for the irreducible representation with two-component Weyl fermions χ, $\bar{\chi}$. A dynamically generated mass $\bar{m}_{\mathrm{f},\chi} \neq 0$ spontaneously breaks the $\mathrm{U}(2N_\mathrm{f})$ symmetry according to the pattern

$$\mathrm{U}(2N_\mathrm{f}) \to \mathrm{U}_{\mathbb{1}+\gamma_{45}}(N_\mathrm{f}) \otimes \mathrm{U}_{\mathbb{1}-\gamma_{45}}(N_\mathrm{f}) \quad (4.21)$$

with the $\mathrm{U}(N_\mathrm{f})$ factors generated by $P^{(45)}_{\mathrm{L/R}} \otimes \lambda_\beta$ with $\beta = 1, \ldots, {N_\mathrm{f}}^2$, cf. Eqs. (4.9)–(4.10). However, it leaves the discrete space-time symmetries $\mathcal{C}$, $\mathcal{P}$, and $\mathcal{T}$ intact. By contrast, a nonvanishing mass $\bar{m}_{\mathrm{f},\mathcal{P}}$ does *not* break the $\mathrm{U}(2N_\mathrm{f})$ symmetry, since γ_{45} anticommutes with γ_4 and γ_5. However, as can be read off from Eqs. (4.14)–(4.16), such a mass term is odd under parity inversion and time reversal, since $\gamma_{45}P_\zeta = -P_\zeta\gamma_{45}$ and $(\mathrm{i}\gamma_{45})^* = -\mathrm{i}\gamma_{45}$, respectively. Because of $\{\gamma_{45}, C_\xi\} = 0$ and $(\gamma_{45})^\mathrm{T} = -\gamma_{45}$ it is even under charge conjugation. In fact, all this is well known from the analogous discussion in the context of QED_3 [43].

A complete basis of the 4×4 Dirac algebra can be given by the 16 matrices[d]

$$\{\gamma_A\}_{A=1,\ldots,16} = \{\mathbb{1}, \gamma_\mu, \gamma_{\mu\nu}, \mathrm{i}\gamma_\mu\gamma_4, \mathrm{i}\gamma_\mu\gamma_5, \gamma_4, \gamma_5, \gamma_{45}\}, \quad (4.22)$$

where we have introduced the generators of the Lorentz transformation of the four-component Dirac spinors $\gamma_{\mu\nu} \coloneqq \frac{\mathrm{i}}{2}[\gamma_\mu, \gamma_\nu]$. In Eq. (4.22), we only count those matrices $\gamma_{\mu\nu}$ with $\mu < \nu$. A bilinear $\bar{\psi}\gamma_A\psi$ is invariant under $\mathrm{U}(2N_\mathrm{f})$ transformations if and only if γ_A anticommutes with the generators of $\mathrm{U}_{\gamma_4}(1)$ and $\mathrm{U}_{\gamma_5}(1)$ while it commutes with the generators of $\mathrm{U}_{\mathbb{1}}(1)$ and $\mathrm{U}_{\gamma_{45}}(1)$. Obviously, this is only the case for $\bar{\psi}\gamma_\mu\psi$ and $\bar{\psi}\gamma_{45}\psi$. Imposing an invariance under $\mathrm{U}(2N_\mathrm{f})$ as well as $\mathcal{C}$, $\mathcal{P}$, and $\mathcal{T}$, there is thus no bilinear to zeroth derivative order. In particular, no mass term is permitted. To first order, only the standard kinetic term

$$\mathcal{L}_\mathrm{kin} = \mathrm{i}\bar{\psi}\partial\!\!\!/\psi \quad (4.23)$$

can appear. Consequently, on the level of four-fermion interactions, the Thirring interaction is not the only fermionic four-point function in the pointlike limit (i.e., with momentum independent

[c] Note that due to our chiral conventions a nonzero expectation value $\langle\bar{\psi}\psi\rangle$ or $\langle\bar{\psi}\gamma_{45}\psi\rangle$ is purely imaginary [155].

[d] We note that for a given representation the indicated set in Eq. (4.22) is not necessarily linearly independent. This is, for instance, the case for the "graphene representation" [26, 27], where $\gamma_{\mu\nu} = \epsilon_{\mu\nu\rho}\gamma_\rho$. However, it can be straightforwardly verified that the condition of linear independence is in fact fulfilled for our representation (3.2)–(3.3).

couplings) which is invariant under the present $\mathrm{U}(2N_\mathrm{f})$ flavor symmetry and the discrete space-time symmetries. In fact, the possible interactions are

$$(V)^2 \coloneqq \left(\bar\psi^a\gamma_\mu\psi^a\right)^2 \qquad \text{and} \qquad (P)^2 \coloneqq \left(\bar\psi^a\gamma_{45}\psi^a\right)^2, \tag{4.24}$$

as well as the two interaction terms with nonsinglet flavor structure

$$(S)^2 \coloneqq \left(\bar\psi^a\psi^b\right)^2 - \left(\bar\psi^a\gamma_4\psi^b\right)^2 - \left(\bar\psi^a\gamma_5\psi^b\right)^2 + \left(\bar\psi^a\gamma_{45}\psi^b\right)^2 \tag{4.25}$$

$$(A)^2 \coloneqq \left(\bar\psi^a\gamma_\mu\psi^b\right)^2 + \frac{1}{2}\left(\bar\psi^a\gamma_{\mu\nu}\psi^b\right)^2 - \left(\bar\psi^a\mathrm{i}\gamma_\mu\gamma_4\psi^b\right)^2 - \left(\bar\psi^a\mathrm{i}\gamma_\mu\gamma_5\psi^b\right)^2, \tag{4.26}$$

where we have defined $(\bar\psi^a\psi^b)^2 \equiv \bar\psi^a\psi^b\bar\psi^b\psi^a$, etc. This generalizes the discussion of [27] to larger flavor number $N_\mathrm{f} \geq 1$. With respect to Lorentz (chiral $\mathrm{U}(2N_\mathrm{f})$) transformations these interactions correspond to the vector (scalar), pseudoscalar (scalar), scalar/pseudoscalar (vector), and axial/vector (vector) condensation channel. [Properties given in order of Eqs. (4.24)–(4.26).] However, the four-fermi terms are not independent, but can be mapped onto each other by means of the Fierz identities. For instance, the scalar/pseudoscalar interaction in Eq. (4.25) and the axial/vector-type interaction in (4.26) can be written as a linear combination of the interaction terms in (4.24),

$$(S)^2 = -(V)^2 - (P)^2, \qquad (A)^2 = (V)^2 - 3(P)^2. \tag{4.27}$$

We give a derivation of the Fierz identities in App. A. Let us for a moment come back to the irreducible representation in terms of the Weyl spinors χ and $\bar\chi$. In this formulation the four-fermi interactions simply read

$$(V)^2 = \left(\bar\chi^i\sigma_\mu\chi^i\right)^2, \qquad (P)^2 = \left(\bar\chi^i\chi^i\right)^2, \tag{4.28}$$

$$(S)^2 = 2\left(\bar\chi^i\chi^j\right)^2, \qquad (A)^2 = 2\left(\bar\chi^i\sigma_\mu\chi^j\right)^2. \tag{4.29}$$

Again, we have made use of the collective indices $i, j = 1, \ldots, 2N_\mathrm{f}$. It is now obvious that firstly, these interactions are invariant under $\mathrm{U}(2N_\mathrm{f})$ and secondly, there exist no further independent invariant interactions than the four of these.

To summarize: In addition to the Thirring coupling $(V)^2$, a second pointlike linearly independent four-fermi coupling $(P)^2$ satisfies the symmetries of the Thirring model. In an RG analysis, it has to be included on the same fundamental level as the Thirring interaction.

4.2 Fermionic RG flow

As a first step, let us employ the most simple approximation of the effective action in terms of purely fermionic degrees of freedom with pointlike interactions,

$$\Gamma_k[\bar\psi,\psi] = \int \mathrm{d}^3x \left\{ Z_{\psi,k}\bar\psi^a\mathrm{i}\partial_\mu\gamma_\mu\psi^a + \frac{\tilde{\bar g}_k}{2N_\mathrm{f}}\left(\bar\psi^a\gamma_{45}\psi^a\right)^2 + \frac{\bar g_k}{2N_\mathrm{f}}\left(\bar\psi^a\gamma_\mu\psi^a\right)^2 \right\} \tag{4.30}$$

$$= \int \mathrm{d}^3x \left\{ Z_{\chi,k}\bar\chi^i\mathrm{i}\partial_\mu\sigma_\mu\chi^i + \frac{\tilde{\bar g}_k}{2N_\mathrm{f}}\left(\bar\chi^i\chi^i\right)^2 + \frac{\bar g_k}{2N_\mathrm{f}}\left(\bar\chi^i\sigma_\mu\chi^i\right)^2 \right\}, \tag{4.31}$$

corresponding to the next-to-leading order in the derivative expansion. In addition to the interaction terms discussed above, we have included a wave function renormalization $Z_{\psi,k} \equiv Z_{\chi,k}$. All parameters in the effective average action are understood to be scale dependent, indicated by the momentum-scale index k. The truncation (4.30) represents a full basis of fermionic four-point functions in the pointlike limit, which are compatible with the present chiral and discrete symmetries. Such a pointlike truncation can be a reasonable approximation in the chiral symmetric regime, as has been quantitatively confirmed for the zero-temperature chiral phase transition in many-flavor QCD_4 [78].

Inserting Eq. (4.30) into the Wetterich equation (2.21), we obtain the flow equations (i.e., beta functions) for the four-fermi couplings $\bar{g}_k$ and $\tilde{\bar{g}}_k$ and the wave function renormalization $Z_{\psi,k}$ via suitable projections onto the associated operators. In fact, this can straightforwardly be done for both the four-component as well as the two-component representation; of course, both approaches yield identical beta functions. In terms of the renormalized fields $\tilde{\psi} \coloneqq Z_{\psi,k}^{1/2}\psi_k$, $\tilde{\bar{\psi}} \coloneqq Z_{\psi,k}^{1/2}\bar{\psi}_k$ and dimensionless renormalized couplings

$$g \coloneqq Z_{\psi,k}^{-2}k^{d-2}\bar{g}_k, \qquad \tilde{g} \coloneqq Z_{\psi,k}^{-2}k^{d-2}\tilde{\bar{g}}_k, \tag{4.32}$$

we obtain the beta functions as

$$\partial_t\tilde{g} = (d-2+2\eta_\psi)\tilde{g} - 4v_d d_\gamma\, \ell_1^{(\mathrm{F})d}(0;\eta_\psi)\left(\frac{2N_\mathrm{f}-1}{2N_\mathrm{f}}\tilde{g}^2 - \frac{3}{2N_\mathrm{f}}\tilde{g}g - \frac{1}{N_\mathrm{f}}g^2\right), \tag{4.33}$$

$$\partial_t g = (d-2+2\eta_\psi)g + 4v_d d_\gamma\, \ell_1^{(\mathrm{F})d}(0;\eta_\psi)\left(\frac{1}{2N_\mathrm{f}}\tilde{g}g + \frac{2N_\mathrm{f}+1}{6N_\mathrm{f}}g^2\right), \tag{4.34}$$

with $v_d^{-1} \coloneqq 2^{d+1}\pi^{d/2}\Gamma(d/2) = 8\pi^2$ for $d = 3$ and $d_\gamma = 4$ is the number of components of the Dirac fermions ψ, $\bar{\psi}$. The definition of the threshold function $\ell_1^{(\mathrm{F})d}(\dots)$ as well as their explicit expressions for linear and sharp cutoff can be found in App. B. Within the present truncation of pointlike interactions, the anomalous dimension remains

$$\eta_\psi = -\partial_t \ln Z_{\psi,k} = 0. \tag{4.35}$$

This is a general feature of the pointlike approximation and remains true even if one includes higher fermion interactions $\propto (\bar{\psi}\gamma_A\psi)^n$ with $n \geq 3$. In fact, it is a direct consequence of the one-loop structure of the Wetterich equation (cf. also Sec. 2.2): if one allows for solely fermionic degrees of freedom any diagram contributing to $\Gamma_k^{(2)}$ is a tadpole and therefore momentum independent; it cannot contribute to the flow of $Z_{\psi,k}$. By another rescaling $g \mapsto g/(4v_d d_\gamma \ell_1^{(\mathrm{F})d})$ and $\tilde{g} \mapsto \tilde{g}/(4v_d d_\gamma \ell_1^{(\mathrm{F})d})$, the multiplicative regulator dependence drops out,

$$\partial_t\tilde{g} = \tilde{g} - \frac{2N_\mathrm{f}-1}{2N_\mathrm{f}}\tilde{g}^2 + \frac{3}{2N_\mathrm{f}}\tilde{g}g + \frac{1}{N_\mathrm{f}}g^2, \tag{4.36}$$

$$\partial_t g = g + \frac{1}{2N_\mathrm{f}}\tilde{g}g + \frac{2N_\mathrm{f}+1}{6N_\mathrm{f}}g^2, \tag{4.37}$$

where we have made use of Eq. (4.35) and specified to $d = 3$. For $N_\mathrm{f} = 1$, Eqs. (4.36)–(4.37) coincide with the result found via a perturbative RG approach in the context of interacting electrons on the honeycomb lattice [27].

4.3 Fixed points and critical exponents

From the coupling flows, it is straightforward to analyze the fixed-point structure in order to study possible asymptotically safe UV trajectories of the RG flow. For the present set of flow equations, a general property of the fixed points and their critical exponents can be proven: both beta functions are of the quadratic form

$$\beta_i(g_j) = g_i + g_k A_i^{kl} g_l, \tag{4.38}$$

with $\beta_i(g_j) \equiv \partial_t g_i$, $(g_i)_{i=1,2} \equiv (\tilde{g}, g)$, and matrices A_i^{kl} which are symmetric in the upper indices. Therewith, the corresponding stability matrix $B_i{}^j = \partial\beta_i/\partial g_j|_{g^*}$ at a fixed point g^* with $\beta_i(g^*) = 0$ reads

$$B_i{}^j = \delta_i{}^j + 2 g_k^* A_i^{kj}. \tag{4.39}$$

Hence, for every interacting fixed point $g^* \neq 0$ the fixed-point vector itself is an eigenvector of B with the critical exponent (including a minus sign) $\Theta = 1$,

$$B_i{}^j g_j^* = g_i^* + 2 g_k^* A_i^{kj} g_j^* = -g_i^*. \tag{4.40}$$

In the last step, we have made use of the fixed-point equation $\beta_i(g^*) = 0$. We conclude that every fixed point besides the Gaußian fixed point $g^* = 0$ has at least one relevant and thus IR repulsive direction. Each non-Gaußian fixed point is therefore a candidate for a possible UV completion, potentially defining an own universality class [196]. Moreover, for beta functions of the quadratic form (4.38), the straight line through an interacting fixed point g^* and the Gaußian fixed point defines an RG invariant subspace of theory space: Without loss of generality we may rotate our coordinate system such that the non-Gaußian fixed point is located on, for instance, the first axis with $g^* = (g_1^*, 0)$ and $g_1^* \neq 0$. In this basis, the fixed-point equation $\beta_2(g^*) = 0$ is satisfied, iff it is of the form

$$\beta_2(g_1, g_2) = g_2 + 2 g_1 A_2^{12} g_2 + g_2 A_2^{22} g_2 \qquad \Leftrightarrow \qquad A_2^{11} = 0. \tag{4.41}$$

Consequently, once we start the flow on the first axis with $g_2 = 0$, the coupling g_2 will never be generated during the RG procedure. The existence of an invariant subspace defined by the non-Gaußian fixed point is in fact a feature which holds for any system with polynomial beta functions; in particular, it remains true if one includes higher fermion interactions $\propto (\bar{\psi}\gamma_A\psi)^n$ with $n \geq 3$. For the Gaußian fixed point $g^* = 0$, the stability matrix is just the identity $B_i{}^j = \delta_i{}^j$,

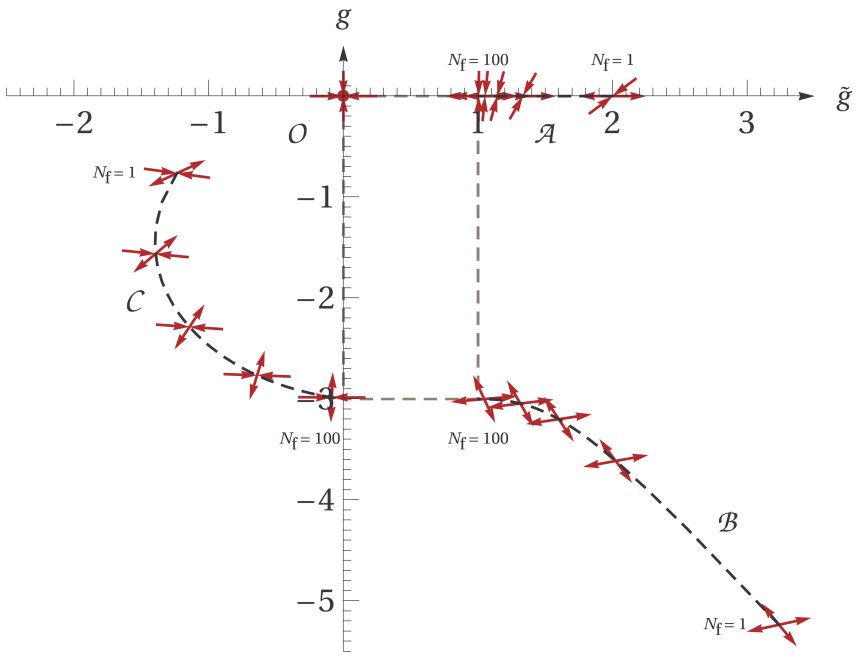

Figure 4.1 Positions of RG fixed points and (ir-)relevant directions for flavor numbers $N_f = 1, 2, 4, 10, 100$. For $N_f \to \infty$ the fixed points form the corners of a rectangle (gray dashed). Arrows denote the RG flow toward the IR. In agreement with Eq. (4.40), one relevant direction of every interacting fixed point points toward the Gaußian fixed point $\mathcal{O}$.

such that the Gaußian fixed point is infrared attractive in every direction with $\Theta = -1$, giving rise to only trivial theories at long ranges.

For fixed $g_{j\neq i}$, the beta function β_i corresponds graphically to a parabola, such that we expect for our truncation exactly $2^2 = 4$ (possibly complex or degenerate) solutions of the fixed-point equations. For any $N_f \in \mathbb{N}$, we find them to be real and nondegenerate; the explicit solutions in the basis $(\tilde{g}, g)$ for the Gaußian fixed point $\mathcal{O}$ and the three non-Gaußian fixed points $\mathcal{A}, \mathcal{B}, \mathcal{C}$ are

$$\mathcal{O}: \qquad (0,0)\,, \tag{4.42}$$

$$\mathcal{A}: \qquad \left(\frac{2N_f}{2N_f-1}, 0\right), \tag{4.43}$$

$$\mathcal{B}: \qquad \left(\frac{N_f\left(14-7N_f+2{N_f}^2+(1+2N_f)\sqrt{16+28N_f+{N_f}^2}\right)}{-5+8N_f+2{N_f}^2+4{N_f}^3}, -\frac{12{N_f}^2}{4+4N_f+4{N_f}^2-\sqrt{16+28N_f+{N_f}^2}}\right), \tag{4.44}$$

$$\mathcal{C}: \qquad \left(\frac{N_f\left(14-7N_f+2{N_f}^2-(1+2N_f)\sqrt{16+28N_f+{N_f}^2}\right)}{-5+8N_f+2{N_f}^2+4{N_f}^3}, -\frac{12{N_f}^2}{4+4N_f+4{N_f}^2+\sqrt{16+28N_f+{N_f}^2}}\right). \tag{4.45}$$

It is straightforward (though somewhat tedious) to derive the eigenvectors and eigenvalues of the stability matrix [and thus the critical exponents and the RG (ir-)relevant directions] analytically; but as the general formulas may not provide much physical insight, we present the results graphically: In Fig. 4.1, we plot the positions of the fixed points in theory space (spanned by the two couplings $\tilde{g}$ and g) together with the corresponding eigenvectors of the stability matrix $B_i{}^j$ for various flavor numbers N_f. In Fig. 4.2, the (nontrivial) critical exponents Θ for the interacting

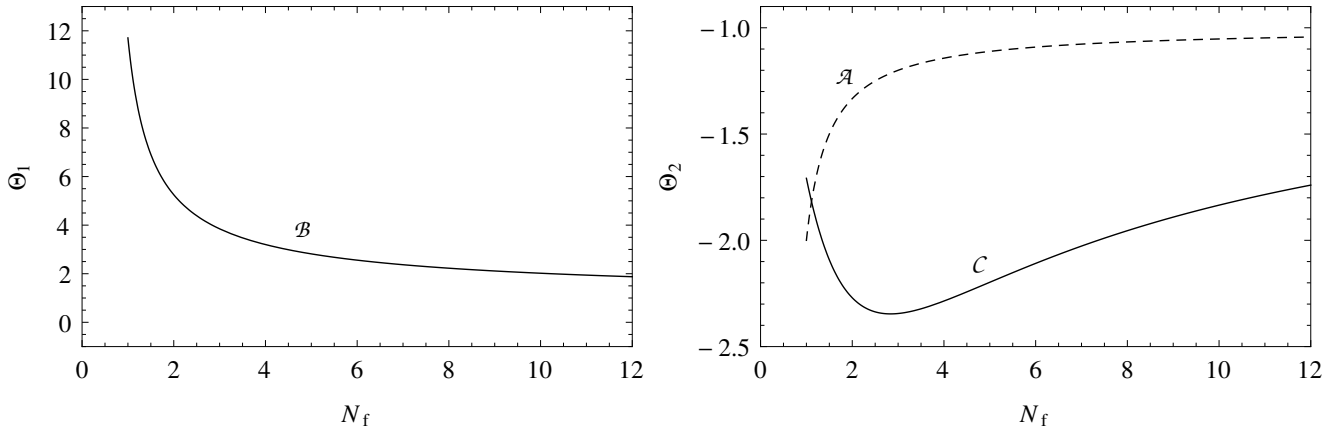

Figure 4.2 Critical exponents Θ as a function of flavor number N_f for the interacting fixed points $\mathcal{B}$ (left) and $\mathcal{A}$, $\mathcal{C}$ (right). The value of the respective other critical exponent is $\Theta_2 = 1$ ($\mathcal{B}$) and $\Theta_1 = 1$ ($\mathcal{A}$, $\mathcal{C}$) for all N_f.

fixed points are given as a function of N_f . For any N_f, fixed point $\mathcal{B}$ has two RG relevant directions with $\Theta_1 > \Theta_2 = 1$, whereas the interacting fixed points $\mathcal{A}$ and $\mathcal{C}$ have one relevant ($\Theta_1 = 1$) and one irrelevant direction ($\Theta_2 < 0$). As the number of relevant directions corresponds to the number of physical parameters to be fixed, theories emanating from $\mathcal{A}$ and $\mathcal{C}$ are fully determined, once the initial condition for this relevant direction is fixed. In the sense of dimensional transmutation, fixing this one parameter can be viewed as fixing a total scale for the system. Therefore, theories belonging to these universality classes defined by $\mathcal{A}$ and $\mathcal{C}$ are fully predictive, once a global scale is fixed. Theories emanating from $\mathcal{B}$ are fixed by a mass scale and one further parameter, e.g., a dimensionless coupling ratio, whereas $\mathcal{O}$ does not support an interacting system at long ranges.

At this point, let us already stress that no interacting fixed point is on the pure Thirring axis ($\tilde{g} = 0$) for any finite N_f. In fact, as discussed below, we associate the Thirring universality class with fixed point $\mathcal{C}$ which approaches the pure Thirring coupling only in the asymptotic limit $N_\mathrm{f} \to \infty$. For any finite N_f, the renormalized UV trajectory of the Thirring model will have to pass through the full two-dimensional coupling plane, even though the long-range physics does depend only on one physical parameter (e.g., the value of the Thirring coupling at a certain scale).

4.4 Prospects for long-range physics

A technical means for the discussion of long-range phases are the separatrices, i.e., those RG trajectories that interpolate between two fixed points. They subdivide the theory space into separate flow regions, providing a classification which can potentially be related to spontaneous symmetry breaking in the long-range limit. Let us emphasize at this point, that the purely fermionic truncation is not sufficient for a complete discussion of long-range physics which is expected to be dominated by composite bosonic degrees of freedom such as condensates and

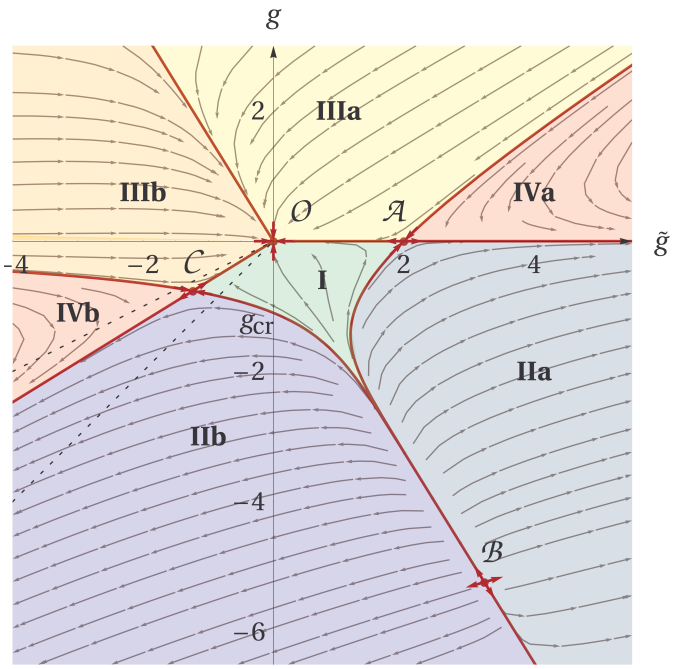

Figure 4.3 Classification of Thirring-like four-fermi theories determined by the fixed-point positions and the corresponding RG trajectories (arrows denote the flow toward the IR) for $N_f = 1$. Red lines depict separatrices that interpolate between fixed points and separate different regions. The vertical axis $\tilde{g} = 0$ corresponds to models with a pure Thirring coupling. The dashed lines ($g = \tilde{g}/2$ and $g = \tilde{g}$, resp.) mark two different definitions of the 3d NJL model, see text.

excitations on top of condensates. Based on the classification given in this section, the IR regime will be studied in detail in the subsequent chapter 5.

Let us start with a closer look at the one-flavor case $N_f = 1$. Differences occurring for larger N_f will be stressed below. The separatrices subdivide the theory space into distinct sections defined by their IR and UV behavior; in Fig. 4.3, we plot the RG flow using Eqs. (4.36)–(4.37). A classification of RG trajectories is listed in Tab. 4.1. The IR behavior of the theories in the regions I, IIIa and IIIb is governed by the Gaußian fixed point $\mathcal{O}$. In these regions, both couplings $\tilde{g}$ and g are irrelevant, leading to noninteracting theories in the IR. The regions IIa and IVa are characterized by an irrelevant Thirring coupling g, $\lim_{k\to 0} g = 0$, but diverging pseudoscalar coupling $\tilde{g}$. We thus expect that the bosonic channel $(P) \propto \bar{\psi}^a \gamma_{45} \psi^a$ becomes critical at a sufficiently large $\tilde{g}$, dynamically generating a parity breaking mass term $\propto \bar{m}_{f,\mathcal{P}} \langle \bar{\psi} \gamma_{45} \psi \rangle$. If so, the fixed point $\mathcal{A}$ governs the spontaneous breaking of parity, potentially being associated with a second-order phase transition. In fact, since in the two-component representation $(P)^2 = (\bar{\psi}\gamma_{45}\psi)^2 = (\bar{\chi}^i \chi^i)^2$ with $i = 1, 2$, the fixed point $\mathcal{A}$ defines the universality class of the three-dimensional $\mathbb{Z}_2$-symmetric Gross-Neveu model, the critical behavior of which is well known [99–101, 103–107].

By contrast, both $\tilde{g}$ and g diverge in the regions IIb and IVb in the infrared limit. To interpret

Table 4.1 Classification of all RG trajectories, cf. Fig. 4.3. Whereas the fixed-point and UV/IR classification holds for all N_f, the IR symmetry breaking pattern determining the universality class may change for larger N_f.

Type	UV behavior $\lim_{k\to\Lambda}(\tilde{g}, g)$	IR behavior $\lim_{k\to 0}(\tilde{g}, g)$	Universality class for $N_\mathrm{f} = 1$
I	$\mathcal{B}$	$\mathcal{O}$	noninteracting
IIa	$\mathcal{B}$	$(\infty, 0)$	parity breaking
IIb	$\mathcal{B}$	$\mathcal{C}\cdot\infty$	chirality breaking
IIIa	$(-\mathcal{C})\cdot\infty$	$\mathcal{O}$	noninteracting
IIIb	$(-\infty, 0)$	$\mathcal{O}$	noninteracting
IVa	$(-\mathcal{C})\cdot\infty$	$(\infty, 0)$	parity breaking
IVb	$(-\infty, 0)$	$\mathcal{C}\cdot\infty$	chirality breaking
I-IIa separatrix	$\mathcal{B}$	$\mathcal{A}$	interacting, symmetric
I-IIb separatrix	$\mathcal{B}$	$\mathcal{C}$	interacting, symmetric
I-IIIa separatrix	$\mathcal{A}$	$\mathcal{O}$	noninteracting
I-IIIb separatrix	$\mathcal{C}$	$\mathcal{O}$	noninteracting
IIa-IIb separatrix	$\mathcal{B}$	$\mathcal{B}\cdot\infty$	?
IIa-IVa separatrix	$\mathcal{A}$	$(\infty, 0)$	parity breaking
IIb-IVb separatrix	$\mathcal{C}$	$\mathcal{C}\cdot\infty$	chirality breaking
IIIa-IIIb separatrix	$(-\mathcal{B})\cdot\infty$	$\mathcal{O}$	noninteracting
IIIa-IVa separatrix	$(-\mathcal{C})\cdot\infty$	$\mathcal{A}$	interacting, symmetric
IIIb-IVb separatrix	$(-\infty, 0)$	$\mathcal{C}$	interacting, symmetric

this behavior, let us rewrite the interaction terms by means of the Fierz identities (4.27) as

$$\frac{\tilde{g}}{2N_\mathrm{f}}(P)^2 + \frac{g}{2N_\mathrm{f}}(V)^2 = \frac{2g-\tilde{g}}{4N_\mathrm{f}}\left(\bar{\psi}\gamma_\mu\psi\right)^2 + \frac{-\tilde{g}}{4N_\mathrm{f}}\left[\left(\bar{\psi}\psi\right)^2 - \left(\bar{\psi}\gamma_4\psi\right)^2 - \left(\bar{\psi}\gamma_5\psi\right)^2\right], \tag{4.46}$$

cf. Eqs. (4.24)–(4.26) and App. A. The interaction then simply is a linear combination of the Thirring interaction with coupling $2g - \tilde{g}$ and a Nambu-Jona-Lasinio (NJL)-type [93] interaction with coupling $-\tilde{g}$. Along the straight line through $\mathcal{O}$ and $\mathcal{C}$ which may govern the IR behavior of the trajectories IIb and IVb for $N_\mathrm{f} = 1$ the NJL-type interaction in fact dominates, $|\tilde{g}|/|2g - \tilde{g}| \approx 4.24 \gg 1$. To illustrate this, we have also plotted in Fig. 4.3 the line of vanishing Thirring interaction $2g - \tilde{g} = 0$ in the Fierz-transformed form (upper dashed line). This resulting NJL-type line is fairly close to the separatrix through $\mathcal{O}$ and $\mathcal{C}$ (red line). We thus expect that at a large coupling on this separatrix the NJL-type channel eventually becomes critical, inducing a symmetry-broken state with mass term

$$\bar{m}_{\mathrm{f},\chi}\langle\bar{\psi}\psi\rangle \neq 0.$$

This is equivalent to saying that $\langle\bar{\psi}\gamma_4\psi\rangle \neq 0$ or $\langle\bar{\psi}\gamma_5\psi\rangle \neq 0$ is expected to be favored in this state. For $N_\mathrm{f} = 1$, we therefore identify the fixed point $\mathcal{C}$ with the critical point governing the phase transition into the chiral symmetry-broken phase for all theories of the regions IIb and IVb, in agreement with [27]. This is precisely the behavior which is expected in the $N_\mathrm{f} = 1$ Thirring model, hence we associate all trajectories emanating from $\mathcal{C}$ with UV complete fully renormalized versions of the 3d $N_\mathrm{f} = 1$ Thirring model.

This discussion may be extended to larger flavor number $N_\mathrm{f} > 1$. However, the naive generalization of the second term with coupling $-\tilde{g}$ in Eq. (4.46) is not invariant under U($2N_\mathrm{f}$). For $N_\mathrm{f} > 1$, the invariant NJL-type interaction is given by $(S)^2 = (\bar{\psi}^a\psi^b)^2 - (\bar{\psi}^a\gamma_4\psi^b)^2 - (\bar{\psi}^a\gamma_5\psi^b)^2 + (\bar{\psi}^a\gamma_{45}\psi^b)^2$ and we employ the slightly different Fierz decomposition

$$\begin{aligned}\frac{\tilde{g}}{2N_\mathrm{f}}(P)^2 + \frac{g}{2N_\mathrm{f}}(V)^2 = \frac{g-\tilde{g}}{2N_\mathrm{f}}\left(\bar{\psi}^a\gamma_\mu\psi^a\right)^2 \\ + \frac{-\tilde{g}}{2N_\mathrm{f}}\left[\left(\bar{\psi}^a\psi^b\right)^2 - \left(\bar{\psi}^a\gamma_4\psi^b\right)^2 - \left(\bar{\psi}^a\gamma_5\psi^b\right)^2 + \left(\bar{\psi}^a\gamma_{45}\psi^b\right)^2\right], \qquad (4.47)\end{aligned}$$

which for $N_\mathrm{f} \to 1$ does not coincide with Eq. (4.46). We illustrate the difference in Fig. 4.3, where we have also depicted the line of vanishing Thirring interaction $g - \tilde{g} = 0$ in the decomposition (4.47) (lower dashed line). In fact, both dashed lines are in the attractive domain of fixed point $\mathcal{C}$ and we therefore expect that the distinction between the two definitions of the one-flavor NJL interaction is unimportant for the critical behavior. In Fig. 4.4, we show how the positions of the fixed points and the separatrices behave for an increasing flavor number. For $N_\mathrm{f} \to \infty$ region I turns into a rectangle with the vertices $(\tilde{g}, g) = (0, 0)$ and $(1, -3)$, cf. also Fig. 4.1. The Thirring fixed point $\mathcal{C}$ hence moves to $(0, -3)$ and becomes a pure Thirring coupling. Thus, for increasing N_f, the IR attractive line $\mathcal{OC}$ does no longer coincide with the NJL-type line (dashed line in Fig. 4.3) but approaches the Thirring axis $\tilde{g} = 0$. In fact, e.g., for $N_\mathrm{f} \simeq 10$ the ratio of the NJL-type versus the Thirring coupling in Eq. (4.47) along the separatrix $\mathcal{OC}$ is $|\tilde{g}|/|g| \approx 0.23 \ll 1$.

Along this line of coupling values, we expect the flow to be dominated no longer by the NJL-type channel but now by the vector channel $(V) \propto \bar{\psi}^a\gamma_\mu\psi^a$, which agrees precisely with the dominant bosonic degree of freedom in a large-N_f analysis [60–64]. As there is no chiral symmetry breaking at large N_f, it is natural to expect a quantum phase transition to occur for increasing N_f while the line $\mathcal{OC}$ undergoes a transition from the NJL-regime $\tilde{g} \approx g$ to the large-N_f regime where $\tilde{g} = 0$. Put differently, once the number of fermion flavors is larger than a critical value N_f^cr, the expected large-N_f-dominant vector channel inhibits χSB also in the limit of infinite Thirring coupling. Unfortunately, a more quantitative picture of this quantum phase transition is difficult to obtain in the purely fermionic language. A quantitative RG analysis requires the inclusion of dynamical chiral (i.e., NJL-type) and vector bosonic degrees of freedom in order to study the interplay of these competing orders as a function of N_f; see Chap. 5.

For the remainder of this section, we shall be satisfied with a simple estimate of the transition region. As a rough criterion, let us determine the flavor number where the separatrix $\mathcal{OC}$ is

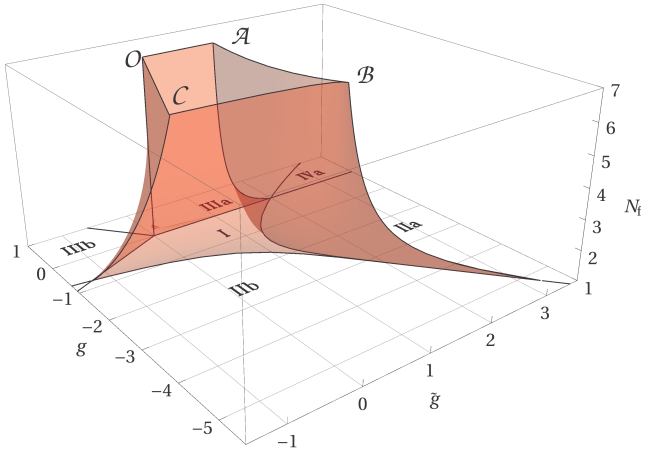

Figure 4.4 Fixed-point positions and separatrices in the $(g, \tilde{g})$ coupling plane as a function of flavor number for $1 \leq N_f \leq 7$. The horizontal slice at $N_f = 1$ is equivalent to Fig. 4.3. For larger N_f the IR attractive line $\mathcal{OC}$ approaches the Thirring axis $\tilde{g} = 0$, where the vector channel is expected to dominate toward the IR, inhibiting chiral symmetry breaking.

half way in-between the NJL model ($\tilde{g}/g = 1$) on the one hand and the pure Thirring coupling ($\tilde{g}/g = 0$) on the other hand. This value of N_f follows from

$$\left.\frac{\tilde{g}}{g}\right|_{\mathcal{C}} \approx \frac{1}{2} \tag{4.48}$$

and is given by $N_f \approx 4$. We stress that this number should not be viewed as a direct estimate of N_f^{cr}, as the onset of true critical behavior can easily provide further correction factors of order $\mathcal{O}(1)$.

It is instructive to compare our results with those obtained by other methods such as Monte Carlo simulations or truncated Dyson-Schwinger equations (DSE). A variety of studies have computed the modulus of the critical Thirring coupling which is necessarily required for chiral symmetry breaking (but not sufficient beyond the critical flavor number). Two cautionary remarks are in order: First of all, these critical couplings similarly as the fixed-point values are not universal, such that the choice of the regularization scheme can have a strong quantitative influence on the estimated values. Second, most other studies have defined the microscopic Thirring model exactly on the Thirring axis $\tilde{g} = 0$; in principle, the full coupling plane has to be considered such that the critical coupling on the axis may be different (larger in modulus) from a corresponding estimate directly at the fixed point.

To circumvent the second caveat, we also consider the coupling on the Thirring axis $\tilde{g} = 0$ with an initial value of the coupling g above the separatrix which interpolates between the fixed points $\mathcal{B}$ and $\mathcal{C}$. Then the theory is in the region I or IIIa, depending on the sign of g, such that the RG flow drives the couplings to the free theory at Gaußian fixed point $\mathcal{O}$. Therefore, the absolute value of the g coordinate of the intersection point of this separatrix with the Thirring axis provides a lower bound for the absolute value of the critical coupling g_{cr} at which the χSB phase transition occurs, cf. Fig. 4.3. We compare this lower bound for different regulator functions

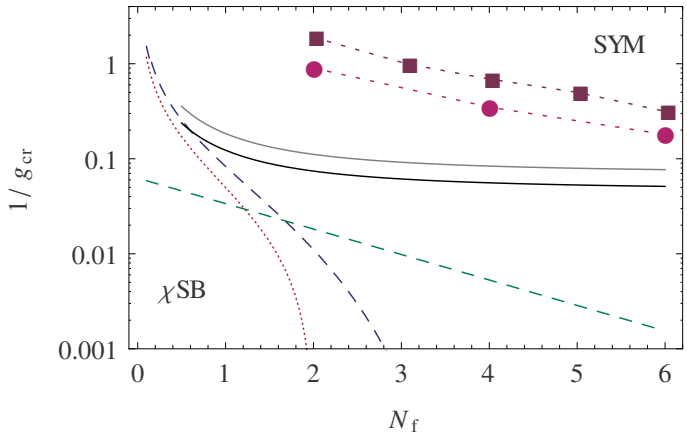

Figure 4.5 Comparison of nonuniversal critical Thirring couplings from different methods. Solid lines display the critical couplings from this work taken as the g coordinate of the intersection point of the separatrix $\mathcal{B}C$ with the Thirring axis $\tilde{g} = 0$ for the sharp (gray) or the linear regulator (black). Upper right: "bare" lattice results (purple with squares [69–72], magenta with circles [68]). Lower left: DSE approaches (green [64], blue [65, 66]) and $1/N_\mathrm{f}$ study (red [67]).

R_k with the values of the critical coupling obtained by Monte Carlo simulations [68–72], different sequences of truncated DSE approaches [64–66], and the $1/N_\mathrm{f}$ study [67]. In Fig. 4.5, we plot this inverse coupling $1/g_\mathrm{cr}$ for a varying number of flavors $0 < N_\mathrm{f} \leq 6$. In one of the Monte Carlo studies [72], the lattice coupling g has been "renormalized" in order to ensure transversity of the vector field propagator. In that sense we compare in Fig. 4.5 to the "bare" lattice values. For the sharp cutoff as well as for the linear cutoff our results for $1/g_\mathrm{cr}$ lie above the values obtained by DSE approaches but below the values from lattice-regularized Monte Carlo simulations. Note that similar to the lattice and one of the DSE results, we do not observe a sharp decay of the inverse critical coupling. This behavior would indicate a sharp growth of g_cr above a certain number of flavors, corresponding to a critical flavor number in the infinite coupling limit. Instead, we observe a rather smooth dependence on N_f as on the lattice for $N_\mathrm{f} \lesssim 6$, which is compatible with our expectation that the quantum phase transition toward the chiral symmetric phase occurs because of competing large-N_f degrees of freedom and not because of a change in the UV critical structure.

4.5 Conclusions

In this chapter, we have investigated 3d relativistic fermion models in a theory space defined by chiral and a set of discrete symmetries and pointlike interactions. Even though the construction of these models has been inspired by the uniquely fixed 2d Thirring model, the corresponding 3d symmetries involving a reducible four-component Dirac spinor representation enlarge the minimal coupling space and give room for a larger fixed-point structure and thus for different microscopic realizations of such fermion models.

We have classified all pointlike interactions satisfying the symmetry constraints and determined their RG flow in a systematic next-to-leading order derivative expansion. The fact that leading-order and next-to-leading order results are identical as the anomalous dimension remains zero can be interpreted as a signature for the convergence of the expansion, as long as no further composite channels develop a strong RG flow.

The resulting flow equations for the two independent fermionic couplings generate a fixed-point structure of one trivial Gaußian and three interacting fixed points $\mathcal{A}$, $\mathcal{B}$, $\mathcal{C}$ which can be classified by their critical exponents. We associate all RG trajectories emanating from the fixed point $\mathcal{C}$ with fully renormalized UV complete versions of the 3d Thirring; as this fixed point has one RG relevant direction, fixing one physical scale suffices to obtain a fully IR predictive quantum field theory in the Thirring universality class. Moreover, our results show that the Thirring model and the NJL model in three dimensions are in fact in the same universality class, which is governed by the Thirring fixed point $\mathcal{C}$. However, this statement ultimately only holds for our specific regularization scheme.

Fixed point $\mathcal{A}$ which, incidentally, lives in an RG invariant submanifold of theory space (defined by $g = 0$) is also characterized by only one RG relevant direction. From the nature of the scalar channel associated with this coupling direction, we conjecture that this fixed point can be related to a critical point of a second-order phase transition to a phase with broken parity, defining the universality class of the 3d Gross-Neveu model [99–101,103–107]. The third interacting fixed point $\mathcal{B}$ has two relevant directions; depending on the initial conditions, theories emanating from this fixed point can flow to the Thirring phase as well as to the parity-broken or symmetric phases.

Unfortunately, our purely fermionic RG analysis does so far not permit us to reliably run toward or into the symmetry-broken phases. Such a quantitative description is required in order to analyze the true IR behavior of the Thirring phase. From the structure of the fermionic flow, in particular, from the behavior of the separatrix $\mathcal{OC}$, we conjecture that the long-range dynamics is characterized by a competition between NJL-type chiral condensation channels on the one hand and large-N_f-type vector bosons on the other hand. As the vector-boson fluctuations generically inhibit chiral symmetry breaking, we expect the occurrence of a quantum phase transition of the Thirring model at a critical flavor number N_f^cr, separating a broken phase for small N_f from a disordered phase for large N_f. Our very rough estimate of the transition region in any case is compatible with the findings from lattice simulations indicating that $N_\mathrm{f}^\mathrm{cr} \simeq 6.6$ [72].

Our results on the position of the Thirring fixed point $\mathcal{C}$ being actually away from the pure Thirring axis $\tilde{g} = 0$ for any finite N_f provokes an important comment: Both lattice simulations as well as DSE studies build on a microscopic definition of the 3d Thirring model which is fixed only with the Thirring coupling, i.e., by a pure bare Thirring-like action. Our fixed-point results indeed provide a fundamental justification for this, as the Thirring fixed point indeed is characterized by only one relevant direction. As long as the microscopic actions chosen in other formulations

are in a sufficiently attractive domain of the Thirring fixed point, universality guarantees that the long-range physics is indeed purely governed by the Thirring fixed point. We expect this to hold also for the determination of the critical flavor number (there is no universality for quantities such as the scheme-dependent critical coupling, see Fig. 4.5). Nevertheless, one caveat should be emphasized: this conclusion about universality only holds as long as the microscopic bare actions indeed are in the attractive domain of the Thirring fixed point. For instance, if by accident a lattice formulation turned out to be influenced by fixed point $\mathcal{B}$, the simulation would simply describe a model different from the Thirring model potentially exhibiting a different quantum phase transition as a function of $N_{\mathrm{f}}^{\mathrm{cr}}$. As the fixed-point positions are not universal, our results are unfortunately not directly transferable to the lattice theory space. However, provided that the fixed-point structure is qualitatively similar, our results can be taken as a support for the implicit assumption that the lattice simulations have indeed been performed in the real Thirring universality class.

Given the importance of the quantitative value of the critical flavor number $N_{\mathrm{f}}^{\mathrm{cr}}$ of the Thirring model in the light of condensed-matter applications, the natural next step of our studies is the inclusion of composite degrees of freedom in order to study the competition among the various bosonic channels. Within the functional RG, this can conveniently be investigated by means of partial or dynamical bosonization [116, 161, 197]. As the problem of competing order is a paradigmatic one in (quantum) critical phenomena and statistical physics [198, 199], we consider the relativistic 3d Thirring model as an ideal test case.

5 Long-range dynamics of the Thirring model and the critical flavor number

The discussion of the UV fixed-point structure of the Thirring model in the preceding chapter suggests that a quantum phase transition at a critical flavor number $N_{\mathrm{f}}^{\mathrm{cr}}$, separating a broken phase for small N_{f} from a disordered phase for large N_{f}, might occur due to a competition between a NJL-type chiral condensation channel on the one hand and large-N_{f}-type vector bosons on the other hand. In order to investigate this IR competition on a quantitative level, it is necessary to allow for composite bosonic fields in the effective action. This allows to reliably investigate the IR behavior of the Thirring universality class; in particular, to predict the values of the universal critical exponents associated with a possible chiral symmetry breaking phase transition as a function of N_{f}.

5.1 Condensation channels and Fierz basis

Consider the general fermionic Lagrangian compatible with $\mathrm{U}(2N_{\mathrm{f}})$ chiral as well as $\mathcal{C}$, $\mathcal{P}$, and $\mathcal{T}$ discrete symmetry,

$$\mathcal{L} = \bar{\psi}^a \mathrm{i}\partial\!\!\!/ \psi^a + \frac{\bar{g}_1}{2N_{\mathrm{f}}}(V)^2 + \frac{\bar{g}_2}{2N_{\mathrm{f}}}(S)^2 + \frac{\bar{g}_3}{2N_{\mathrm{f}}}(P)^2 + \frac{\bar{g}_4}{2N_{\mathrm{f}}}(A)^2, \tag{5.1}$$

with the flavor singlet channels

$$(V)^2 \coloneqq \left(\bar{\psi}^a \gamma_\mu \psi^a\right)^2, \qquad (P)^2 \coloneqq \left(\bar{\psi}^a \gamma_{45} \psi^a\right)^2, \tag{5.2}$$

and the flavor nonsinglet channels

$$(S)^2 \coloneqq \left(\bar{\psi}^a \psi^b\right)^2 - \left(\bar{\psi}^a \gamma_4 \psi^b\right)^2 - \left(\bar{\psi}^a \gamma_5 \psi^b\right)^2 + \left(\bar{\psi}^a \gamma_{45} \psi^b\right)^2, \tag{5.3}$$

$$(A)^2 \coloneqq \left(\bar{\psi}^a \gamma_\mu \psi^b\right)^2 + \frac{1}{2}\left(\bar{\psi}^a \gamma_{\mu\nu} \psi^b\right)^2 - \left(\bar{\psi}^a \mathrm{i}\gamma_\mu \gamma_4 \psi^b\right)^2 - \left(\bar{\psi}^a \mathrm{i}\gamma_\mu \gamma_5 \psi^b\right)^2. \tag{5.4}$$

By means of the Fierz identities (cf. App. A),

$$(V)^2 + (S)^2 + (P)^2 = 0, \qquad -4(V)^2 - 3(S)^2 + (A)^2 = 0, \tag{5.5}$$

any two four-fermi terms can be rewritten as a linear combination of the remaining two. Put differently, by adding a linear combination of Eqs. (5.5) with coefficients $\alpha_i \in \mathbb{R}$ to the Lagrangian (5.1),

$$\begin{aligned}\mathcal{L} = \bar{\psi}^a \mathrm{i}\partial\!\!\!/ \psi^a &+ \frac{1}{2N_\mathrm{f}}(\bar{g}_1 + \alpha_1 - 4\alpha_2)(V)^2 + \frac{1}{2N_\mathrm{f}}(\bar{g}_2 + \alpha_1 - 3\alpha_2)(S)^2 \\ &+ \frac{1}{2N_\mathrm{f}}(\bar{g}_3 + \alpha_1)(P)^2 + \frac{1}{2N_\mathrm{f}}(\bar{g}_4 + \alpha_2)(A)^2,\end{aligned} \tag{5.6}$$

the α_i are redundant parameters, i.e., in a full computation of the functional integral any physical quantity has to be independent of α_i. Nonetheless, this no longer necessarily remains true once approximations are employed. This is in particular the case for mean-field theory, where this so-called "Fierz ambiguity" has a sizable influence on the results, limiting its quantitative reliability [200]. The ambiguity is absent in the purely fermionic renormalization group equations of Chap. 4. The RG equations in a partially bosonized setting also can overcome the Fierz ambiguity if the four-fermi terms are dynamically bosonized, see below [201].

The couplings $\bar{g}$ and $\tilde{\bar{g}}$ from Chapter 4 are recovered for the choice $\alpha_1 = -\bar{g}_2 - 3\bar{g}_4$ and $\alpha_2 = -\bar{g}_4$ and the definition

$$\bar{g} \coloneqq \bar{g}_1 - \bar{g}_2 + \bar{g}_4, \tag{5.7}$$

$$\tilde{\bar{g}} \coloneqq -\bar{g}_2 + \bar{g}_3 - 3\bar{g}_4. \tag{5.8}$$

By contrast, if we choose $\alpha_1 = -\bar{g}_3$ and $\alpha_2 = -\bar{g}_4$ the Lagrangian reads

$$\mathcal{L} = \bar{\psi}^a \mathrm{i}\partial\!\!\!/ \psi^a - \frac{\bar{g}_V}{2N_\mathrm{f}}\left(\bar{\psi}^a \gamma_\mu \psi^a\right)^2 + \frac{\bar{g}_\phi}{4N_\mathrm{f}}\left[\left(\bar{\psi}^a \psi^b\right)^2 - \left(\bar{\psi}^a \gamma_4 \psi^b\right)^2 - \left(\bar{\psi}^a \gamma_5 \psi^b\right)^2 + \left(\bar{\psi}^a \gamma_{45} \psi^b\right)^2\right], \tag{5.9}$$

where we have defined the new couplings

$$\bar{g}_V \coloneqq -\bar{g}_1 + \bar{g}_3 - 4\bar{g}_4 = \tilde{\bar{g}} - \bar{g}, \tag{5.10}$$

$$\bar{g}_\phi \coloneqq 2(\bar{g}_2 - \bar{g}_3 + 3\bar{g}_4) = -2\tilde{\bar{g}}. \tag{5.11}$$

The latter form is convenient in order to investigate the competition between the vector $(V)^2$ and NJL-type $(S)^2$ channel for $N_\mathrm{f} \geq 2$. For $N_\mathrm{f} = 1$ one might however choose yet another basis [cf. Eqs. (4.46)–(4.47)],

$$\mathcal{L} = \bar{\psi} \mathrm{i}\partial\!\!\!/ \psi + \frac{2\bar{g}_1 - \bar{g}_3 + 3\bar{g}_4}{4}\left(\bar{\psi}\gamma_\mu\psi\right)^2 + \frac{2\bar{g}_2 - \bar{g}_3 + 3\bar{g}_4}{4}\left[\left(\bar{\psi}\psi\right)^2 - \left(\bar{\psi}\gamma_4\psi\right)^2 - \left(\bar{\psi}\gamma_5\psi\right)^2\right]. \tag{5.12}$$

We have seen in Sec. 4.1 that the theory (5.9) can equivalently be described using an irreducible representation by an action consisting of $2N_\mathrm{f}$ flavors of two-component Weyl spinors $\bar{\chi}$, χ [cf. Eq. (4.11)],

$$S = \int_x \bar{\chi}^i \mathrm{i}\partial\!\!\!/ \chi^i - \frac{\bar{g}_V}{2N_\mathrm{f}}\left(\bar{\chi}^i \sigma_\mu \chi^i\right)^2 + \frac{\bar{g}_\phi}{2N_\mathrm{f}}\left(\bar{\chi}^i \chi^j\right)^2, \qquad i,j = 1,\ldots,2N_\mathrm{f}, \tag{5.13}$$

where we have introduced the collective indices i, j, running over $2N_\mathrm{f}$ flavors. It is this representation in which the $\mathrm{U}(2N_\mathrm{f})$ symmetry is manifest,

$$\mathrm{U}(2N_\mathrm{f}): \qquad \chi^i \mapsto U^{ij}\chi^j \qquad \bar\chi^i \mapsto \bar\chi^j \left(U^\dagger\right)^{ji}, \qquad U \in \mathrm{U}(2N_\mathrm{f}). \tag{5.14}$$

In the following, we use this formulation, allowing us to very conveniently introduce collective low-energy degrees of freedom.

5.2 Low-energy degrees of freedom

The partition function[a] of the theory defined by (5.13),

$$Z = \int \mathcal{D}\bar\chi\mathcal{D}\chi \exp(-S), \tag{5.15}$$

is in fact equivalent to the partition function of the "mesonic" theory of a $(2N_\mathrm{f}) \times (2N_\mathrm{f})$ scalar matrix field ϕ^{ij} and a vector field V_μ, coupling via a Yukawa-type interaction to the fermions,

$$Z = \mathcal{N}\int \mathcal{D}\chi\mathcal{D}\bar\chi\mathcal{D}\phi\mathcal{D}V \exp\left[-\left(\bar\chi^i \mathrm{i}\partial\!\!\!/\chi^i + \frac{1}{2}\bar m_\phi^2\phi^{ij}\phi^{ji} + \frac{1}{2}\bar m_V^2 V_\mu^2 - \bar h_V V_\mu \bar\chi^i\sigma_\mu\chi^i + \mathrm{i}\bar h_\phi\bar\chi^i\phi^{ij}\chi^j\right)\right], \tag{5.16}$$

where $i, j = 1, \ldots, 2N_\mathrm{f}$. The equivalence can be seen by multiplying Eq. (5.15) with appropriate Gaußian (Hubbard-Stratonovich) factors,

$$1 = \mathcal{N}\int \mathcal{D}\phi \, \exp\left[-\frac{1}{2}\left(\bar m_\phi\phi^{ij} + \mathrm{i}\frac{\bar h_\phi}{\bar m_\phi}\bar\chi^j\chi^i\right)\left(\bar m_\phi\phi^{ji} + \mathrm{i}\frac{\bar h_\phi}{\bar m_\phi}\bar\chi^i\chi^j\right)\right], \tag{5.17}$$

$$1 = \mathcal{N}\int \mathcal{D}V \, \exp\left[-\frac{1}{2}\left(\bar m_V V_\mu - \frac{\bar h_V}{\bar m_V}\bar\chi^i\sigma_\mu\chi^i\right)^2\right], \tag{5.18}$$

with some normalization constants $\mathcal{N}$, not affecting any expectation values. The scalar matrix field is Hermitian, $\phi^\dagger = \phi$, and the vector field V is real. The four-fermi terms in Eq. (5.15) are then precisely canceled if the constraints

$$\frac{\bar h_\phi^2}{2\bar m_\phi^2} = \frac{\bar g_\phi}{2N_\mathrm{f}}, \qquad\qquad \frac{\bar h_V^2}{2\bar m_V^2} = \frac{\bar g_V}{2N_\mathrm{f}}, \tag{5.19}$$

are imposed at the microscopic scale. From Eqs. (5.17)–(5.18) we can read off the properties of the boson fields under chiral transformations,

$$\mathrm{U}(2N_\mathrm{f}): \qquad \phi^{ij} \mapsto U^{ik}\phi^{kl}\left(U^\dagger\right)^{lj}, \qquad V_\mu \mapsto V_\mu, \qquad U \in \mathrm{U}(2N_\mathrm{f}). \tag{5.20}$$

The scalar matrix ϕ may be decomposed into a traceless part and its trace [202]

$$\Phi^{ij} \coloneqq \phi^{ij} - \frac{\delta^{ij}}{2N_\mathrm{f}}\operatorname{Tr}\phi, \qquad\qquad \varphi \coloneqq \operatorname{Tr}\phi. \tag{5.21}$$

[a] For simplicity we suppress here the source terms $\bar\eta\chi - \bar\chi\eta$.

The φ field is parity odd and can be attributed to the parity breaking channel $(P) \sim \bar{\psi}^a \gamma_{45} \psi^a = \bar{\chi}^i \chi^i$. By contrast, a vacuum expectation value of the traceless part Φ corresponds to the dynamical breakdown of chiral symmetry,

$$\langle \Phi^{ij} \rangle \neq 0 \qquad \Leftrightarrow \qquad \langle \bar{\psi}^a \psi^a \rangle = \langle \bar{\chi}^a \chi^a - \bar{\chi}^{a+N_\mathrm{f}} \chi^{a+N_\mathrm{f}} \rangle \neq 0, \qquad a = 1, \ldots, N_\mathrm{f}, \tag{5.22}$$

with the breaking pattern [cf. Eq. (4.21)]

$$\mathrm{U}(2N_\mathrm{f}) \to \mathrm{U}\left(N_\mathrm{f}\right) \otimes \mathrm{U}\left(N_\mathrm{f}\right). \tag{5.23}$$

We can trade the $(2N_\mathrm{f}) \times (2N_\mathrm{f})$ Hermitian traceless matrix Φ for its independent components Φ_α,

$$\Phi^{ij} = \sqrt{2} \Phi_\alpha (t_\alpha)^{ij}, \qquad i, j = 1, \ldots, 2N_\mathrm{f}, \qquad \alpha = 1, \ldots, (2N_\mathrm{f})^2 - 1, \tag{5.24}$$

where the t_α are the generators of $\mathrm{SU}(2N_\mathrm{f})$ in the fundamental representation, normalized so that $\mathrm{Tr}(t_\alpha t_\beta) = \delta_{\alpha\beta}/2$.

In the one-flavor case $N_\mathrm{f} = 1$ this formulation is equivalent to a partial bosonization of the Fierz basis in the four-spinor representation (5.12): the Hubbard-Stratonovich transformation leads to the equivalent Yukawa-type theory with three scalar modes $(\sigma, \tau, \pi) \sim (\bar{\psi}\psi, \bar{\psi}\gamma_4\psi, \bar{\psi}\gamma_5\psi)$ and a vector mode $V_\mu \sim \bar{\psi}\gamma_\mu\psi$ with Lagrangian density

$$\mathcal{L} = \bar{\psi} \mathrm{i} \partial\!\!\!/ \psi + \frac{1}{2} \bar{m}_\sigma^2 (\sigma^2 + \tau^2 + \pi^2) + \mathrm{i} \bar{h}_\sigma \bar{\psi} \left(\sigma + \mathrm{i}\gamma_4 \tau + \mathrm{i}\gamma_5 \pi\right) \psi - \bar{h}_V V_\mu \bar{\psi} \gamma_\mu \psi. \tag{5.25}$$

From the discussion of the fermionic RG flow in Chap. 4 one would predict that the long-range dynamics of this system is dominated by the scalar NJL-type channel. For large enough coupling $\bar{h}_\sigma^2 / \bar{m}_\sigma^2$ we thus expect the scalar mode to acquire a nonvanishing vacuum expectation value (VEV), e.g., in the σ direction, and the spectrum in the broken phase consists of two massless Goldstone modes, e.g., τ and π, and a massive radial mode σ. The corresponding critical behavior is an interesting problem by itself [95]; however, we will in the following focus on the case $N_\mathrm{f} > 1$ where a true competition between the two channels (V) and (S) is expected.

In contrast to the purely fermionic formulation of Chap. 4, the bosonized formulation presented here is well suitable to quantitatively describe the spontaneous breaking of chiral symmetry. Loosely speaking, the bosonic fields ϕ^{ij} and V_μ parametrize the possible formation of bound states of the fermionic fields $\sim \bar{\chi}^i \chi^j$ and $\sim \bar{\chi}^a \sigma_\mu \chi^i$, respectively. The corresponding critical phenomena of such a strongly-correlated system require nonperturbative approximation schemes. The functional renormalization group formulated in terms of the Wetterich equation is such an appropriate tool and has already shown its quantitative reliability in other $(2+1)$-dimensional fermion systems, see e.g., [105, 106]. In the effective action we then have to take into account also higher boson-boson interactions, e.g.,

$$\left(\mathrm{Tr}\, \Phi^2\right)^2 = \left(\Phi_\alpha \Phi_\alpha\right)^2, \qquad \mathrm{Tr}\, \Phi^4 = \frac{1}{2N_\mathrm{f}} \left(\Phi_\alpha \Phi_\alpha\right)^2 + 2 d_{\alpha\beta\epsilon} d_{\gamma\delta\epsilon} \Phi_\alpha \Phi_\beta \Phi_\gamma \Phi_\delta, \tag{5.26}$$

where the $d_{\alpha\beta\gamma}$'s are the structure constants for the group $\mathrm{SU}(2N_\mathrm{f})$. For $N_\mathrm{f} = 1$ the $d_{\alpha\beta\gamma}$'s vanish. Of course, the clever way of computing the flow equations would be to use this representation with independent components Φ_α of the traceless matrix Φ^{ij}. For $N_\mathrm{f} > 1$ however, this implies the decomposition of a product of two vertices, each involving two $d_{\alpha\beta\gamma}$'s, into a sum over single vertices, each term involving just two $d_{\alpha\beta\gamma}$'s. Unfortunately, we are not aware of such a decomposition; in what follows, we will therefore stick to the representation (5.16) with scalar matrix field ϕ^{ij} having arbitrary trace. We expand the effective average action Γ_k in powers of the gradient and truncate the series after the second order. Moreover, we simplify the discussion by considering interactions only up to fourth order in the fields. Our ansatz for the effective action then reads

$$\begin{aligned}\Gamma_k = \int_x \Big[& Z_{\chi,k}\bar{\chi}^i \mathrm{i}\partial\!\!\!/\chi^i + \frac{Z_{\phi,k}}{2}\partial_\mu\phi^{ij}\partial_\mu\phi^{ji} + U_k(\phi) + \frac{Z_{V,k}}{4}V_{\mu\nu}V_{\mu\nu} + \frac{\bar{A}_{V,k}}{2}(\partial_\mu V_\mu)^2 + \frac{\bar{m}^2_{V,k}}{2}V_\mu V_\mu \\ & + \frac{\bar{\zeta}_k}{6}V_\mu V_\mu \partial_\nu V_\nu + \frac{\bar{\mu}_k}{8}\left(V_\mu V_\mu\right)^2 + \frac{\bar{\nu}_k}{4}V_\mu V_\mu \phi^{ij}\phi^{ji} - \bar{h}_{V,k}V_\mu \bar{\chi}^i\gamma_\mu\chi^i + \mathrm{i}\bar{h}_{\phi,k}\bar{\chi}^i\phi^{ij}\chi^j \\ & - \frac{\bar{g}_{V,k}}{2N_\mathrm{f}}\left(\bar{\chi}^i\sigma_\mu\chi^i\right)^2 + \frac{\bar{g}_{\phi,k}}{2N_\mathrm{f}}\left(\bar{\chi}^i\chi^j\right)^2\Big],\end{aligned} \tag{5.27}$$

where $V_{\mu\nu} \coloneqq \partial_\mu V_\nu - \partial_\nu V_\mu$ and $i, j = 1, \ldots, 2N_\mathrm{f}$. $U_k(\phi)$ describes an effective potential in the scalar sector. All couplings in the effective action are understood to be scale-dependent, indicated by the index k. At a fixed scale, say, at the UV cutoff $k = \Lambda$, we can remove the four-fermi interactions by means of the Hubbard-Stratonovich transformation. This no longer necessarily remains true below this scale, since typically new four-fermi interactions will be generated by the flow. However, those can dynamically be reabsorbed into the bosonic sector, if we allow for suitably defined scale-dependent field transformations and adjust the fermion-boson couplings correspondingly [161]. In this approach bosonization thus takes place at each renormalization group step instead of just initially. We will start computing the RG flow in Sec. 5.4 for fixed-field variables. As a next step we will then incorporate dynamically bosonized fields in Sec. 5.5. For the results presented we will furthermore omit all momentum-dependent terms in the vector channel, i.e., we will consider the pointlike limit

$$Z_{V,k} \to 0, \qquad \bar{A}_{V,k} \to 0, \qquad \bar{\zeta}_k \to 0. \tag{5.28}$$

The beta functions will however be computed for general $Z_{V,k}, \bar{A}_{V,k} \geq 0$ (but $\bar{\zeta}_k = 0$).

5.3 Scalar mass spectrum

For the effective action being invariant under $\mathrm{U}(2N_\mathrm{f})$ rotations, the effective potential $U_k(\phi)$ necessarily has to be a pure function of $\mathrm{U}(2N_\mathrm{f})$-invariant quantities. One can, e.g., diagonalize

the scalar matrix field by a U($2N_\mathrm{f}$) rotation [cf. Eq. (5.20)],

$$\phi \mapsto U\phi U^\dagger = \begin{pmatrix} \widehat{m}_1 & 0 & \dots & 0 \\ 0 & \widehat{m}_2 & \dots & 0 \\ \vdots & & \ddots & \vdots \\ 0 & 0 & \dots & \widehat{m}_{2N_\mathrm{f}} \end{pmatrix}, \tag{5.29}$$

with real eigenvalues $\widehat{m}_i$. In a quartic approximation $U_k(\phi)$ is then parametrized in terms of the two invariants ρ and τ,

$$\rho = \frac{1}{2}\operatorname{Tr}\phi^2 = \frac{1}{2}\sum_i \widehat{m}_i^2, \tag{5.30}$$

$$\tau = \frac{1}{2}\operatorname{Tr}\left(\frac{1}{2}\phi^2 - \frac{\rho}{2N_\mathrm{f}}\right)^2 = \frac{1}{8}\sum_i \widehat{m}_i^4 - \frac{1}{2}\left(\frac{\sum_i \widehat{m}_i}{4N_\mathrm{f}}\right)^2, \tag{5.31}$$

that is to say, we neglect the dependence on (suitably defined [165]) additional higher order invariants constructed from $\tilde{\tau}_n \sim \operatorname{Tr}(\phi^2/2 - \rho/2N_\mathrm{f})^n$ for $n \geq 3$. We expand the scalar potential about its k-dependent minimum $(\rho_{0,k}, \tau_{0,k})$. In the symmetric (SYM) regime the potential is minimal at the origin $(\rho_{0,k}, \tau_{0,k}) = (0,0)$, whereas in the chiral symmetry breaking (χSB) regime we allow for a nonvanishing VEV which we assume to be acquired along the ρ-direction, i.e., $\rho_{0,k} > 0$ and $\tau_{0,k} = 0$:

$$U_k(\rho,\tau) = \begin{cases} \bar{m}_{\phi,k}^2\rho + \frac{\bar{\lambda}_{1,k}}{2}\rho^2 + \bar{\lambda}_{2,k}\tau, & \text{SYM regime,} \\ \frac{\bar{\lambda}_{1,k}}{2}\left(\rho - \rho_{0,k}\right)^2 + \bar{\lambda}_{2,k}\tau, & \chi\text{SB regime.} \end{cases} \tag{5.32}$$

If the potential solely depends on ρ and τ, it is sufficient to evaluate its flow equation in a two-dimensional subspace of all possible scalar configurations. We consider the traceless class

$$(\phi^{ij}) =: \widehat{m}\,\mathrm{diag}(\epsilon, \underbrace{+1,\dots,+1}_{N_\mathrm{f}-1 \text{ times}}, -\epsilon, \underbrace{-1,\dots,-1}_{N_\mathrm{f}-1 \text{ times}}) \qquad \text{where } \epsilon \geq 1,\ \widehat{m} \in \mathbb{R}, \tag{5.33}$$

valid for $N_\mathrm{f} > 1$. In fact, for any ρ and τ with $\tau/\rho^2 < (N_\mathrm{f}-1)/4N_\mathrm{f}$ we find parameters $\widehat{m}$ and ϵ according to

$$\widehat{m}^2 = \frac{\rho}{N_\mathrm{f}}\left(1 - \sqrt{\frac{4N_\mathrm{f}}{N_\mathrm{f}-1}\frac{\tau}{\rho^2}}\right), \qquad \epsilon^2 = 1 + N_\mathrm{f}\left(\frac{1}{1 - \sqrt{\frac{4N_\mathrm{f}}{N_\mathrm{f}-1}\frac{\tau}{\rho^2}}} - 1\right). \tag{5.34}$$

If the flow eventually chooses a vacuum configuration with $\epsilon = 1$ and $\widehat{m} > 0$, the chiral symmetry is spontaneously broken while parity symmetry remains preserved,

$$\left(\phi_0^{ij}\right) = \frac{\rho_0}{N_\mathrm{f}}\begin{pmatrix} \mathbb{1} & 0 \\ 0 & -\mathbb{1} \end{pmatrix} \neq 0 \qquad \Leftrightarrow \qquad \langle \bar{\chi}^a\chi^a - \bar{\chi}^{a+N_\mathrm{f}}\chi^{a+N_\mathrm{f}}\rangle = \langle \bar{\psi}^a\psi^a\rangle \neq 0. \tag{5.35}$$

Table 5.1 Spectrum of the scalar mass matrix $\delta^2 U_k/\delta\phi\delta\phi$ for $N_\mathrm{f} > 1$. Primes denote partial derivatives with respect to ρ, $U_k^{(n)} \equiv \partial^n U_k/\partial\rho^n$, and $U_{k,\tau} \equiv \partial U_k/\partial\tau$. For $\widehat{m} \equiv \widehat{m}(\rho,\tau)$ and $\epsilon \equiv \epsilon(\rho,\tau)$ see Eqs. (5.34).

Eigenvalue	Degeneracy
$U_k' + \frac{\widehat{m}^2}{2} U_{k,\tau}\left[3\epsilon^2 - 1 + \frac{1-\epsilon^2}{N_\mathrm{f}}\right]$	1
$U_k' + \frac{\widehat{m}^2}{4N_\mathrm{f}}\Big\{4N_\mathrm{f}(N_\mathrm{f}-1)U_k'' + (4-N_\mathrm{f})U_{k,\tau} + [4N_\mathrm{f}U_k'' + (3N_\mathrm{f}-4)U_{k,\tau}]\,\epsilon^2$ $\pm\Big[(4N_\mathrm{f}(N_\mathrm{f}-1)U_k'' + (N_\mathrm{f}+2)U_{k,\tau})^2$ $+2\big(16{N_\mathrm{f}}^2(N_\mathrm{f}-1)U_k''^2 - 4N_\mathrm{f}(N_\mathrm{f}+2)(3N_\mathrm{f}-2)U_k''U_{k,\tau}$ $-(3{N_\mathrm{f}}^2 - 4N_\mathrm{f} + 4)U_{k,\tau}^2\big)\epsilon^2 + (4N_\mathrm{f}U_k'' + (3N_\mathrm{f}-2)U_{k,\tau})^2\,\epsilon^4\Big]^{1/2}\Big\}$	$1+1$
$U_k' + \frac{\widehat{m}^2}{2} U_{k,\tau}\frac{1-N_\mathrm{f}}{N_\mathrm{f}}(1-\epsilon^2)$	2
$U_k' + \frac{\widehat{m}^2}{2} U_{k,\tau}\left[\epsilon^2 \pm \epsilon + \frac{1-\epsilon^2}{N_\mathrm{f}}\right]$	$4(N_\mathrm{f}-1) + 4(N_\mathrm{f}-1)$
$U_k' + \frac{\widehat{m}^2}{2} U_{k,\tau}\left[2 + \frac{1-\epsilon^2}{N_\mathrm{f}}\right]$	$2{N_\mathrm{f}}^2 - 4N_\mathrm{f} + 1$
$U_k' + \frac{\widehat{m}^2}{2} U_{k,\tau}\frac{1-\epsilon^2}{N_\mathrm{f}}$	$2\,(N_\mathrm{f}-1)^2$

For simplicity, we assume in the following that $\partial^2 U_k/\partial\tau^2 = \partial^2 U_k/\partial\rho\partial\tau = 0$, which holds in the case of the quartic approximation (5.32). The spectrum of the scalar mass matrix $\delta^2 U_k/\delta\phi\delta\phi$ for $N_\mathrm{f} > 1$ is given in Tab. 5.1.

For a vacuum configuration with $\epsilon = 1$ we have $\tau_{0,k} = 0$. In the SYM regime $\rho_{0,k} = 0$ all modes are degenerate and have mass $\bar{m}_\phi^2 = \partial U_k/\partial\rho|_{(\rho,\tau)=(0,0)}$. In the χSB regime with $\rho_{0,k} > 0$ and $\partial U_k/\partial\rho|_{(\rho,\tau)=(\rho_{0,k},0)} = 0$ we find $2{N_\mathrm{f}}^2$ massless scalar modes corresponding exactly to the number of broken generators in the symmetry breaking pattern

$$\mathrm{U}(2N_\mathrm{f}) \to \mathrm{U}\,(N_\mathrm{f}) \otimes \mathrm{U}\,(N_\mathrm{f})\,, \tag{5.36}$$

in accordance with Goldstone's theorem. Additionally, we obtain one massive radial mode with $\bar{m}_\rho^2 = 2\rho_{0,k}\partial^2 U_k/\partial\rho^2$ and $2{N_\mathrm{f}}^2 - 1$ massive modes in τ direction with $\bar{m}_\tau^2 = (\rho_{0,k}/N_\mathrm{f})\partial U_k/\partial\tau$.

5.4 Partially bosonized RG flow

We fix the standard RG invariance of field rescalings by defining the renormalized fields as

$$\tilde{\phi}^{ij} \coloneqq Z_{\phi,k}^{1/2}\phi^{ij}, \qquad \tilde{\chi}^i \coloneqq Z_{\chi,k}^{1/2}\chi^i, \tag{5.37}$$

$$\tilde{V}_\mu \coloneqq Z_{V,k}^{1/2}V_\mu, \qquad \tilde{\bar{\chi}}^i \coloneqq Z_{\chi,k}^{1/2}\bar{\chi}^i. \tag{5.38}$$

The dimensionless effective potential for space-time dimension d then reads

$$u(\tilde{\rho},\tilde{\tau}) \coloneqq k^{-d}U_k(Z_{\phi,k}^{-1}k^{d-2}\tilde{\rho}, Z_{\phi,k}^{-2}k^{2(d-2)}\tilde{\tau}), \tag{5.39}$$

where $\tilde{\rho} \coloneqq Z_{\phi,k} k^{2-d} \rho$ and $\tilde{\tau} \coloneqq Z_{\phi,k}^2 k^{2(2-d)} \tau$, and the dimensionless renormalized couplings are

$$A_{V,k} \coloneqq Z_V^{-1} \bar{A}_{V,k}, \qquad \mu \coloneqq Z_{V,k}^{-2} k^{d-4} \bar{\mu}_k, \qquad h_\phi^2 \coloneqq Z_{\phi,k}^{-1} Z_{\psi,k}^{-2} k^{d-4} \bar{h}_{\phi,k}^2, \tag{5.40}$$

$$m_V^2 \coloneqq Z_{V,k}^{-1} k^{-2} \bar{m}_{V,k}^2, \qquad \nu \coloneqq Z_{\phi,k}^{-1} Z_{V,k}^{-1} k^{d-4} \bar{\nu}_k, \qquad h_V^2 \coloneqq Z_{V,k}^{-1} Z_{\psi,k}^{-2} k^{d-4} \bar{h}_{V,k}^2. \tag{5.41}$$

By evaluating the Wetterich equation (2.21) for a constant field configuration (5.33), we gain the flow of the dimensionless scalar potential

$$\begin{aligned} \partial_t u = {} & -du + (d - 2 + \eta_\phi)\tilde{\rho} u' + (2d - 4 + 2\eta_\phi)\tilde{\tau} u_{,\tilde{\tau}} + 2v_d \sum_{i=1}^{2N_\mathrm{f}} \ell_0^{(\mathrm{B})d}(m_i^2; \eta_\phi) \\ & + 2v_d d\, \ell_0^{(\mathrm{B})d}(m_V^2 + \nu\tilde{\rho}; \eta_V) - 4v_d d_\gamma \left[(N_\mathrm{f} - 1)\, \ell_0^{(\mathrm{F})d}(\widetilde{m}^2 h_\phi^2; \eta_\psi) + \ell_0^{(\mathrm{F})d}(\widetilde{m}^2 \epsilon^2 h_\phi^2; \eta_\psi) \right] \end{aligned} \tag{5.42}$$

with $u \equiv u(\tilde{\rho}, \tilde{\tau})$, $u' \equiv \partial u / \partial \tilde{\rho}$, $u_{,\tilde{\tau}} \equiv \partial u / \partial \tilde{\tau}$ and $\widetilde{m}^2 \coloneqq Z_{\phi,k} k^{2-d} \widehat{m}^2$. The dimensionless scalar masses $m_i^2 \equiv m_i^2(\tilde{\rho}, \tilde{\tau})$ are given in Tab. 5.1. We have further defined the anomalous dimensions

$$\eta_{\phi/\psi/V} = -\partial_t \ln Z_{\phi/\psi/V,k}. \tag{5.43}$$

The threshold functions $\ell_n^{(\mathrm{B/F})}(\omega; \eta)$ are listed in App. B. We have again abbreviated $v_d^{-1} = 2^{d+1} \pi^{d/2} \Gamma(d/2) = 8\pi^2$ and have introduced the dimensionless RG time $t \coloneqq \ln(k/\Lambda)$. As discussed above, we use an irreducible representation of the Dirac algebra and thus the dimension of the gamma matrices is $d_\gamma = 2$. By suitable differentiation of Eq. (5.42) we obtain the flow of the scalar couplings. In the SYM regime,

$$\partial_t m_\phi^2 = \partial_t u' \Big|_{(\tilde{\rho},\tilde{\tau})=(0,0)}, \qquad \partial_t \lambda_1 = \partial_t u'' \Big|_{(\tilde{\rho},\tilde{\tau})=(0,0)}, \qquad \partial_t \lambda_2 = \partial_t u_{,\tilde{\tau}} \Big|_{(\tilde{\rho},\tilde{\tau})=(0,0)}, \tag{5.44}$$

whereas in the χSB regime,

$$\partial_t \kappa = -\frac{1}{\lambda_1} \partial_t u' \Big|_{(\tilde{\rho},\tilde{\tau})=(\kappa,0)}, \qquad \partial_t \lambda_1 = \partial_t u'' \Big|_{(\tilde{\rho},\tilde{\tau})=(\kappa,0)}, \qquad \partial_t \lambda_2 = \partial_t u_{,\tilde{\tau}} \Big|_{(\tilde{\rho},\tilde{\tau})=(\kappa,0)}, \tag{5.45}$$

with the dimensionless VEV $\kappa \coloneqq Z_{\phi,k} k^{2-d} \rho_{0,k}$ and $u^{(n)} \equiv \partial^n u / \partial \tilde{\rho}^n$ and $u_{,\tilde{\tau}} \equiv \partial u / \partial \tilde{\tau}$.

Similarly, the flow equations for all other couplings present in the effective action are straightforwardly obtained by suitable projections of the Wetterich equation (2.21). We have seen in Sec. 2.2 that this amounts to a summation of all possible 1-loop diagrams where the vertices are given by full (though truncated) average vertex functions and the inner lines correspond to the full average propagators. While possibly somewhat tedious to evaluate by hand, this procedure can quite easily be automated. In fact, since recently the very useful Mathematica package DoFun [203] is available, of which we have tremendously benefitted from when reviewing our calculations.

The beta function for the vector mass reads

$$\begin{aligned} \partial_t m_V^2 = {} & (-2 + \eta_V) m_V^2 - 2v_d (d+2)\, \ell_1^{(\mathrm{B})d}(m_V^2 + \nu\kappa; \eta_V)\mu \\ & - 2v_d \left[2{N_\mathrm{f}}^2\, \ell_1^{(\mathrm{B})d}(u'; \eta_\phi) + \left(2{N_\mathrm{f}}^2 - 1\right) \ell_1^{(\mathrm{B})d}(u' + \tfrac{\kappa}{N_\mathrm{f}} u_{,\tilde{\tau}}; \eta_\phi) + \ell_1^{(\mathrm{B})d}(u' + 2\kappa u''; \eta_\phi) \right] \nu \\ & + \frac{8v_d (d-2) d_\gamma N_\mathrm{f}}{d}\, \ell_1^{(\mathrm{F})d}(\tfrac{\kappa}{N_\mathrm{f}} h_\phi^2; \eta_\psi)\, h_V^2 + \frac{16 v_d d_\gamma}{d} \kappa\, \ell_2^{(\mathrm{F})d}(\tfrac{\kappa}{N_\mathrm{f}} h_\phi^2; \eta_\psi)\, h_\phi^2 h_V^2, \end{aligned} \tag{5.46}$$

with the derivatives of the potential $u^{(n)}$ and $u_{,\tilde{\tau}}$ being evaluated at the minimum $(\tilde{\rho},\tilde{\tau})=(\kappa,0)$. In the symmetric regime we have of course $\kappa=0$. For the vector-vector interaction μ and the vector-scalar interaction ν we get

$$\begin{aligned}
\partial_t\mu &= (d-4+2\eta_V)\mu \\
&\quad + \frac{2v_d(d^2+10d+12)}{d+2}\ell_2^{(\mathrm{B})d}(m_V^2+\nu\kappa;\eta_V)\mu^2 \\
&\quad + 2v_d\left[2{N_\mathrm{f}}^2\,\ell_2^{(\mathrm{B})d}(u';\eta_\phi)+\left(2{N_\mathrm{f}}^2-1\right)\ell_2^{(\mathrm{B})d}(u'+\tfrac{\kappa}{N_\mathrm{f}}u_{,\tilde{\tau}};\eta_\phi)+\ell_2^{(\mathrm{B})d}(u'+2\kappa u'';\eta_\phi)\right]\nu^2 \\
&\quad + \frac{16v_d(d-2)(4-d)d_\gamma N_\mathrm{f}}{d(d+2)}\,\ell_2^{(\mathrm{F})d}(\tfrac{\kappa}{N_\mathrm{f}}h_\phi^2;\eta_\psi)\,h_V^4+\frac{128v_d(4-d)d_\gamma}{d(d+2)}\kappa\,\ell_3^{(\mathrm{F})d}(\tfrac{\kappa}{N_\mathrm{f}}h_\phi^2;\eta_\psi)\,h_\phi^2h_V^4 \\
&\quad - \frac{384v_dd_\gamma}{d(d+2)N_\mathrm{f}}\kappa^2\,\ell_4^{(\mathrm{F})d}(\tfrac{\kappa}{N_\mathrm{f}}h_\phi^2;\eta_\psi)\,h_\phi^4h_V^4, \qquad (5.47)\\
\partial_t\nu &= (d-4+\eta_\phi+\eta_V)\nu+2(d+2)v_d\,\ell_2^{(\mathrm{B})d}(m_V^2+\nu\kappa;\eta_V)\mu\nu \\
&\quad + v_d\Bigg\{\left(\frac{2{N_\mathrm{f}}^2+1}{{N_\mathrm{f}}^2}u''+\frac{2{N_\mathrm{f}}^2-1}{2{N_\mathrm{f}}^3}u_{,\tilde{\tau}}\right)\left[2{N_\mathrm{f}}^2\,\ell_2^{(\mathrm{B})d}(u';\eta_\phi)+\left(2{N_\mathrm{f}}^2-1\right)\ell_2^{(\mathrm{B})d}(u'+\tfrac{\kappa}{N_\mathrm{f}}u_{,\tilde{\tau}};\eta_\phi)\right. \\
&\qquad \left.+\,\ell_2^{(\mathrm{B})d}(u'+2\kappa u'';\eta_\phi)\right]+\frac{1}{N_\mathrm{f}}u_{,\tilde{\tau}}\,\ell_2^{(\mathrm{B})d}(u'+\tfrac{\kappa}{N_\mathrm{f}}u_{,\tilde{\tau}};\eta_\phi)\Bigg\}\nu \\
&\quad + \frac{2v_d}{{N_\mathrm{f}}^2}\Bigg[2{N_\mathrm{f}}^2\,\ell_{1,1}^{(\mathrm{BB})d}(u',m_V^2+\nu\kappa;\eta_\phi,\eta_V)+\left(2{N_\mathrm{f}}^2-1\right)\ell_{1,1}^{(\mathrm{BB})d}(u'+\tfrac{\kappa}{N_\mathrm{f}}u_{,\tilde{\tau}},m_V^2+\nu\kappa;\eta_\phi,\eta_V) \\
&\qquad +\,\ell_{1,1}^{(\mathrm{BB})d}(u'+2\kappa u'',m_V^2+\nu\kappa;\eta_\phi,\eta_V)\Bigg]\nu^2+\frac{8v_d(4-d)d_\gamma}{d}\,\ell_2^{(\mathrm{F})d}(\tfrac{\kappa}{N_\mathrm{f}}h_\phi^2;\eta_\psi)\,h_V^2h_\phi^2 \\
&\quad - \frac{96v_dd_\gamma}{dN_\mathrm{f}}\kappa\,\ell_3^{(\mathrm{F})d}(\tfrac{\kappa}{N_\mathrm{f}}h_\phi^2;\eta_\psi)\,h_V^2h_\phi^4-\frac{32v_d(4-d)d_\gamma}{d{N_\mathrm{f}}^2}\kappa^2\,\ell_4^{(\mathrm{F})d}(\tfrac{\kappa}{N_\mathrm{f}}h_\phi^2;\eta_\psi)\,h_V^2h_\phi^6. \qquad (5.48)
\end{aligned}$$

In the symmetric regime the flow of the Yukawa coupling h_ϕ is unambiguous. In the broken regime however the diverse scalar modes in general can develop different couplings. We will focus on the Goldstone-mode coupling to the fermions, which is expected to give the dominant contribution for aspects of criticality. However, this Goldstone-mode projection may introduce artifacts deeply in the broken regime, see below. The flow equation reads

$$\begin{aligned}
\partial_t h_\phi^2 &= (d-4+\eta_\phi+2\eta_\psi)h_\phi^2 \\
&\quad + \frac{4v_d}{N_\mathrm{f}}\left[\ell_{1,1}^{(\mathrm{FB})d}(\tfrac{\kappa}{N_\mathrm{f}}h_\phi^2,u'+\tfrac{\kappa}{N_\mathrm{f}}u_{,\tilde{\tau}};\eta_\psi,\eta_\phi)-\ell_{1,1}^{(\mathrm{FB})d}(\tfrac{\kappa}{N_\mathrm{f}}h_\phi^2,u'+2\kappa u'';\eta_\psi,\eta_\phi)\right]h_\phi^4 \\
&\quad + \frac{8v_d}{{N_\mathrm{f}}^2}\kappa\Big[2{N_\mathrm{f}}^2u''\,\ell_{1,2}^{(\mathrm{FB})d}(\tfrac{\kappa}{N_\mathrm{f}}h_\phi^2,u';\eta_\psi,\eta_\phi) \\
&\qquad +\left((2{N_\mathrm{f}}^2-1)u_{,\tilde{\tau}}+2(N_\mathrm{f}-1)u''\right)\ell_{1,1,1}^{(\mathrm{FBB})d}(\tfrac{\kappa}{N_\mathrm{f}}h_\phi^2,u',u'+\tfrac{\kappa}{N_\mathrm{f}}u_{,\tilde{\tau}};\eta_\psi,\eta_\phi) \\
&\qquad +\left(2u''+u_{,\tilde{\tau}}\right)\ell_{1,1,1}^{(\mathrm{FBB})d}(\tfrac{\kappa}{N_\mathrm{f}}h_\phi^2,u',u'+2\kappa u'';\eta_\psi,\eta_\phi)\Big]\,h_\phi^4 \\
&\quad - 8v_d d\,\ell_{1,1}^{(\mathrm{FB})d}(\tfrac{\kappa}{N_\mathrm{f}}h_\phi^2,m_V^2+\nu\kappa;\eta_\psi,\eta_V)\,h_\phi^2h_V^2. \qquad (5.49)
\end{aligned}$$

For the flow of the fermion-vector coupling we find

$$\begin{aligned}
\partial_t h_V^2 = {}& (d-4+\eta_V+2\eta_\psi)h_V^2 \\
& - \frac{4v_d(d-2)}{dN_\mathrm{f}}\Big[2{N_\mathrm{f}}^2\,\ell_{1,1}^{(\mathrm{FB})d}(\tfrac{\kappa}{N_\mathrm{f}}h_\phi^2,u';\eta_\psi,\eta_\phi)+\big(2{N_\mathrm{f}}^2-1\big)\,\ell_{1,1}^{(\mathrm{FB})d}(\tfrac{\kappa}{N_\mathrm{f}}h_\phi^2,u'+\tfrac{\kappa}{N_\mathrm{f}}u_{,\tilde\tau};\eta_\psi,\eta_\phi) \\
& \qquad + \ell_{1,1}^{(\mathrm{FB})d}(\tfrac{\kappa}{N_\mathrm{f}}h_\phi^2,u'+2\kappa u'';\eta_\psi,\eta_\phi)\Big]h_\phi^2 h_V^2 \\
& - \frac{8v_d}{d{N_\mathrm{f}}^2}\kappa\Big[2{N_\mathrm{f}}^2\,\ell_{2,1}^{(\mathrm{FB})d}(\tfrac{\kappa}{N_\mathrm{f}}h_\phi^2,u';\eta_\psi,\eta_\phi)+\big(2{N_\mathrm{f}}^2-1\big)\,\ell_{2,1}^{(\mathrm{FB})d}(\tfrac{\kappa}{N_\mathrm{f}}h_\phi^2,u'+\tfrac{\kappa}{N_\mathrm{f}}u_{,\tilde\tau};\eta_\psi,\eta_\phi) \\
& \qquad + \ell_{2,1}^{(\mathrm{FB})d}(\tfrac{\kappa}{N_\mathrm{f}}h_\phi^2,u'+2\kappa u'';\eta_\psi,\eta_\phi)\Big]h_\phi^4 h_V^2 \\
& - \frac{8v_d(d-2)^2}{d}\,\ell_{1,1}^{(\mathrm{FB})d}(\tfrac{\kappa}{N_\mathrm{f}}h_\phi^2,m_V^2+\nu\kappa;\eta_\psi,\eta_V)\,h_V^4 \\
& - \frac{16v_d(d-2)}{dN_\mathrm{f}}\kappa\,\ell_{2,1}^{(\mathrm{FB})d}(\tfrac{2}{n}\kappa h_\phi^2,m_V^2+\nu\kappa;\eta_\psi,\eta_V)\,h_\phi^2 h_V^4,
\end{aligned} \tag{5.50}$$

and the anomalous dimensions read

$$\begin{aligned}
\eta_\phi = {}& \frac{8v_d d_\gamma}{d}\,m_4^{(\mathrm{F})d}(\tfrac{\kappa}{N_\mathrm{f}}h_\phi^2;\eta_\psi)\,h_\phi^2+\frac{8v_d d_\gamma}{dN_\mathrm{f}}\kappa\,m_2^{(\mathrm{F})d}(\tfrac{\kappa}{N_\mathrm{f}}h_\phi^2;\eta_\psi)\,h_\phi^4 \\
& + \frac{16v_d}{d{N_\mathrm{f}}^2}\kappa\left[{N_\mathrm{f}}^2u''^2+(N_\mathrm{f}-1)u_{,\tilde\tau}{}^2\right]m_{2,2}^{(\mathrm{B})d}(u',u'+2\kappa u'';\eta_\phi),
\end{aligned} \tag{5.51}$$

$$\begin{aligned}
\eta_\psi = {}& \frac{4v_d}{dN_\mathrm{f}}\Big[2{N_\mathrm{f}}^2\,m_{1,2}^{(\mathrm{FB})d}(\tfrac{\kappa}{N_\mathrm{f}}h_\phi^2,u';\eta_\psi,\eta_\phi)+\big(2{N_\mathrm{f}}^2-1\big)\,m_{1,2}^{(\mathrm{FB})d}(\tfrac{\kappa}{N_\mathrm{f}}h_\phi^2,u'+\tfrac{\kappa}{N_\mathrm{f}}u_{,\tilde\tau};\eta_\psi,\eta_\phi) \\
& \qquad + m_{1,2}^{(\mathrm{FB})d}(\tfrac{\kappa}{N_\mathrm{f}}h_\phi^2,u'+2\kappa u'';\eta_\psi,\eta_\phi)\Big]h_\phi^2-8v_d m_{1,2}^{(\mathrm{FB})d}(\tfrac{\kappa}{N_\mathrm{f}}h_\phi^2,m_V^2+\nu\kappa;\eta_\psi,\eta_V)\,h_V^2,
\end{aligned} \tag{5.52}$$

$$\eta_V = \frac{16v_d(d-2)d_\gamma N_\mathrm{f}}{d}\,m_4^{(\mathrm{F})d}(\tfrac{\kappa}{N_\mathrm{f}}h_\phi^2;\eta_\psi)\,h_V^2+16v_d d_\gamma\kappa\,m_2^{(\mathrm{F})d}(\tfrac{\kappa}{N_\mathrm{f}}h_\phi^2;\eta_\psi)\,h_\phi^2 h_V^2. \tag{5.53}$$

Within our truncation we find that the flows of the two possible vector-field kinetic terms are in fact equivalent, i.e., $\partial_t\bar{A}_k=\partial_t Z_{V,k}$. The vector propagator thus is diagonal, $G^{(V)}_{\mu\nu,k}=\delta_{\mu\nu}/(Z_{V,k}p^2+\bar{m}^2_{V,k})$. The definitions of the threshold functions $\ell_{\dots}^{(\mathrm{B/F})d}(\dots)$ and $m_{\dots}^{(\mathrm{B/F})d}(\dots)$ are listed in App. B, together with their explicit forms for linear and sharp regulator. The flow equations have been independently verified for the symmetric regime in local potential approximation with the DoFun package [203].

As is the case in the fermionic formulation, we expect for large enough flavor number N_f the flow to be dominated by the vector channel. Whether for large coupling the V field then can develop a finite vacuum expectation value is an interesting question on its own right: e.g., (2+1)-dimensional models exhibiting spontaneous breaking of Lorentz symmetry have been investigated in [204–208]. By contrast, one could suspect that the vector mass eventually flows to zero, triggering a close resemblance of the strongly coupled Thirring model for large flavor number to a U(1) gauge theory. This is in fact the prediction of the large-N_f studies [62,209]. In any case, we are mainly interested in a possible scalar condensation corresponding to chiral symmetry breaking and thus leave this issue for future studies. As long as the vector mass m_V^2 does not become too small it is then

sufficient to consider the pointlike approximation in the vector channel, $Z_{V,k} \to 0$ corresponding to $m_V^2 \to \infty$. Therewith, the beta functions no longer depend on h_V^2 and m_V^2 separately but only on the ratio $g_V = N_\mathrm{f} h_V^2/m_V^2$, reflecting the RG invariance of fields rescalings. In the remaining flow equations the vector anomalous dimension η_V completely drops out. The flow of $Z_{\psi,k}$ given by Eq. (5.52) is driven by a competition between a positive scalar loop term $\propto h_\phi^2$ and a negative vector loop term $\propto h_V^2$. In the pointlike approximation in the vector sector $m_V^2 \to \infty$ and hence the vector loop term vanishes. For reasons of consistency, we will therefore suppress also the scalar loop term in Eq. (5.52), i.e., we treat the fermionic sector in the leading-order derivative approximation $\eta_\psi \equiv 0$. This is compatible with the observation that the flow of the fermionic wave function renormalization in 3d fermion systems at criticality is usually very small [103, 105–107, 131, 180]. As we shall see in Sec. 5.5, this assumption is exactly fulfilled for large number of fermion flavors $N_\mathrm{f} \to \infty$, where the fixed-point equations can be solved analytically; in fact, this is the known result of the $1/N_\mathrm{f}$ expansion [61]. In comparison, the scalar anomalous dimension is nonvanishing in this limit, and we thus expect the flow of $Z_{\phi,k}$ to be crucial also for finite N_f. We note that also in the chiral scalar-fermion system of Chap. 3 we observed that a nonvanishing $\eta_\phi \sim \mathcal{O}(1)$ is essential in order to find the correct critical behavior.

In the following, we will omit the vector-vector interaction μ and the vector-scalar interaction ν for simplicity. In this section, we settle for discussing the UV structure only and compare it with our previous results in the fermionic language. For a full analysis of the IR properties we refer to the discussion of the dynamically bosonized RG flow in Sec. 5.5. For the search of a fixed point, we hence end up with a system of six coupled nonlinear equations for the five couplings in the SYM regime $(m_\phi^2, \lambda_1, \lambda_2, h_\phi^2, N_\mathrm{f} h_V^2/m_V^2)$ and the anomalous dimension η_ϕ. In the large-N_f limit the fixed-point structure can be mapped out analytically and we discover precisely the know structure from Chap. 4: the Thirring universality class is governed by a UV fixed point having one IR relevant direction with critical exponent $\Theta = 1$. It is located in the pure fermion-vector sector, i.e., $N_\mathrm{f} h_\phi^{*2}/m_\phi^{*2} = 0$ and $N_\mathrm{f} h_V^{*2}/m_V^{*2} > 0$. Moreover, the fixed-point position exactly coincides with the Thirring fixed point in the fermionic RG of Chap. 4,

$$N_\mathrm{f} \frac{h_\phi^{*2}}{m_\phi^{*2}} = -2\tilde{g}^* = 0, \qquad N_\mathrm{f} \frac{h_V^{*2}}{m_V^{*2}} = \tilde{g}^* - g^* = \frac{3\pi^2}{2\,\ell_1^{(\mathrm{F})}(0)}, \qquad N_\mathrm{f} \to \infty. \tag{5.54}$$

For finite N_f we discover deviations from the fermionic fixed-point structure, see Fig. 5.1. Besides the Thirring fixed point with one RG relevant direction we find two other interacting fixed points with two or more relevant directions. For $N_\mathrm{f} < 4$ they are located in the pure fermion-scalar sector $h_V^2/m_V^2 = 0$ and the pure fermion-vector sector $h_\phi^2/m_\phi^2 = 0$, respectively. Since $\partial_t h_\phi^2 \propto \mathcal{O}(h_\phi^2)$ and $\partial_t h_V^2 \propto \mathcal{O}(h_V^2)$ both sectors are in fact invariant under RG transformations. The Thirring fixed point, which for $N_\mathrm{f} < 4$ is located in the "full" theory $h_\phi^2/m_\phi^2 > 0$ and $h_V^2/m_V^2 > 0$, hits the fixed point in the fermion-vector sector once $N_\mathrm{f} \to 4$. The fixed-point position as a function of N_f is therefore nonanalytic at $N_\mathrm{f} = 4$. For $N_\mathrm{f} > 4$ the Thirring fixed-point stays in the fermion-vector

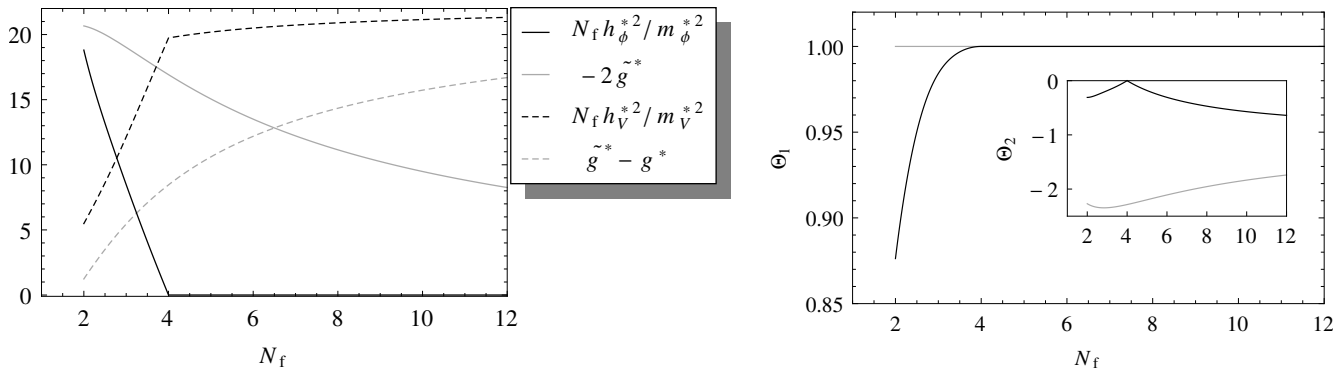

Figure 5.1 Left: nonuniversal UV fixed-point values for the bosonic (black) and fermionic RG flow (gray, cf. Chap. 4) for the optimized regulator. In the bosonic language already for $N_f \geq 4$ the fixed point is located in the pure fermion-vector sector, while in the fermionic language this is the case only for large N_f. Fermionic and bosonic descriptions coincide for $N_f \to \infty$. Right: largest critical exponent Θ_1 and subleading exponent Θ_2 (inset).

subspace $h_\phi^2/m_\phi^2 = 0$, coinciding with the fermionic-RG fixed point for $N_f \to \infty$. In Fig. 5.1 we have plotted the critical exponents for the RG relevant (Θ_1) and the RG irrelevant direction (Θ_2), showing good agreement in the former case while in the latter case, in particular for small N_f, large deviations occur.

To summarize: Despite quantitative disagreements, we find a consistent qualitative behavior. For small $N_f \sim \mathcal{O}(1)$ the flow is dominated by a strong fermion-scalar coupling $N_f h_\phi^2/m_\phi^2 \sim -2\tilde{g}$, whereas for large $N_f \gg 1$ the scalar sector decouples and only the fermion-vector interactions $N_f h_V^2/m_V^2 \sim -g$ matter. We want to emphasize the fact that fixed-point positions itself are in general nonuniversal quantities. It can nevertheless be shown that the bosonic flow in the pointlike limit $Z_{\phi,k} \to 0$ boils down to the fermionic flow with fully equivalent fixed-point structure, if one takes newly generated four-fermi interactions into account [201]. By contrast, here we bosonized only at the fixed scale $k = \Lambda$ and the deviations between bosonic and fermionic flows are in part related to that shortcoming. On the other hand, the formulation developed here allows for a specific momentum dependence in the 4-fermi couplings $\sim \bar{h}_{\phi,k}^2/(Z_{\phi,k}p^2 + \bar{m}_{\phi,k}^2)$. Once the scalar mass becomes small, e.g., before the flow eventually enters the χSB regime, a purely pointlike description is insufficient and only the bosonic language yields reliable results. We will bring together the advantages of both approaches in the following section 5.5 by dynamically bosonizing the four-fermi interaction at each scale $k \leq \Lambda$.

5.5 Dynamically bosonized RG flow

Although the bosonic partition function (5.16) is fully equivalent to the original fermion theory (5.13), the corresponding leading-order truncations of the effective action are not. The reason is that the four-fermi couplings, though absent in the bare action, are again generated by the box

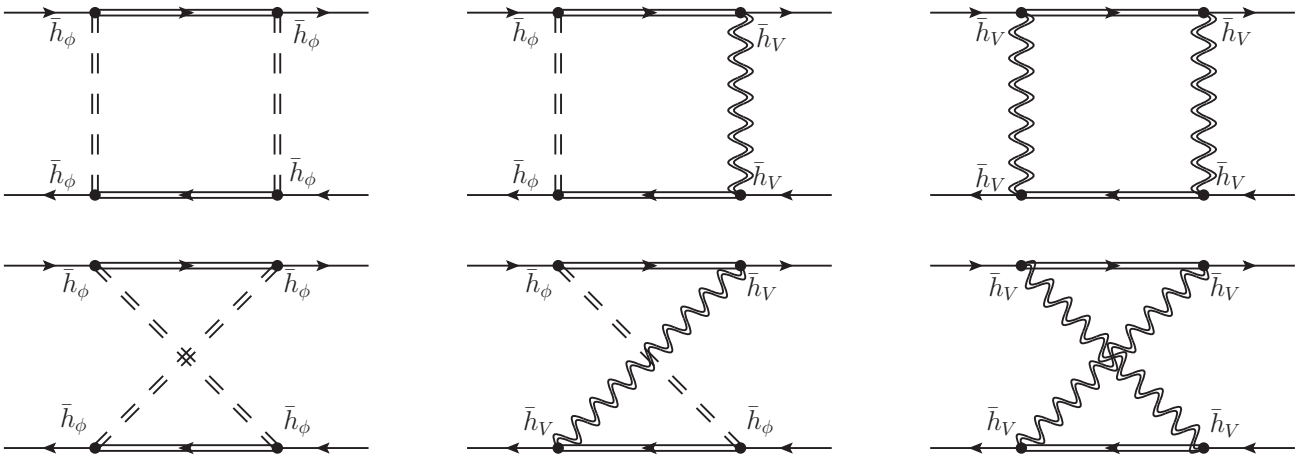

Figure 5.2 Box diagrams contributing to the flow of g_ϕ and g_V. Solid lines are fermions, dashed lines are scalar fields, and wiggly lines vector fields. Doubled inner lines denote full propagators $G_k = (\Gamma^{(2)}_{k,0} + R_k)^{-1}$.

diagrams displayed in Fig. 5.2. However, an inclusion of $\bar{g}_{\phi,k}$ and $\bar{g}_{V,k}$ in the truncation (5.27) does not seem very appealing. On the one hand, the flow equations would be of considerable higher complexity; on the other hand we would have to deal with the redundancy corresponding to the Hubbard-Stratonovich transformation. Instead, we will follow the approach proposed in [161]. The idea is to perform a Hubbard-Stratonovich transformation at *each* RG step, such that all newly generated 4-fermi interactions are again bosonized. The bosonic fields then necessarily become scale dependent. As we shall see in the following, the four-fermi couplings $\bar{g}_{\phi,k}$ and $\bar{g}_{V,k}$ then in fact vanish at all scales, if we use the following field redefinitions

$$\phi^{ij}_{k-dk} = \phi^{ij}_k - \mathrm{i}(\bar{\chi}^j\chi^i)\delta\omega_{\phi,k}, \qquad \partial_k\phi^{ij}_k = \mathrm{i}(\bar{\chi}^j\chi^i)\partial_k\omega_{\phi,k}, \qquad \phi_\Lambda \equiv \phi, \tag{5.55}$$

$$V_{\mu,k-dk} = V_{\mu,k} + (\bar{\chi}^i\sigma_\mu\chi^i)\delta\omega_{V,k}, \qquad \partial_k V_{\mu,k} = -(\bar{\chi}^i\sigma_\mu\chi^i)\partial_k\omega_{V,k}, \qquad V_\Lambda \equiv V, \tag{5.56}$$

with to be determined functions $\omega_{\phi/V,k}$. Note that we keep the fermion fields fixed. For scale-dependent bosonic fields the flow equation for the effective average action is modified,

$$\partial_k\Gamma_k[\phi_k, V_k] = \partial_k\Gamma_k[\phi_k, V_k, \chi]\big|_{\phi_k,V_k} + \int \frac{\delta\Gamma_k[\phi_k,V_k]}{\delta\phi^{ij}_k}\partial_k\phi^{ij}_k + \int \frac{\delta\Gamma_k[\phi_k,V_k]}{\delta V_{\mu,k}}\partial_k V_{\mu,k} \tag{5.57}$$

$$= \frac{1}{2}\,\mathrm{STr}\,\frac{\partial_k R_k}{\Gamma^{(2)}_k[\phi_k,V_k] + R_k} + \mathrm{i}\int \frac{\delta\Gamma_k[\phi_k,V_k]}{\delta\phi^{ij}_k}(\bar{\chi}^j\chi^i)\partial_k\omega_{\phi,k} - \int \frac{\delta\Gamma_k[\phi_k,V_k]}{\delta V_{\mu,k}}(\bar{\chi}^i\sigma_\mu\chi^i)\partial_k\omega_{V,k}, \tag{5.58}$$

where the first term is evaluated for fixed fields and hence leads to the standard flow of Γ_k with ϕ_Λ and V_Λ replaced by ϕ_k and V_k, respectively [161]. We suppressed the dependence of Γ_k on the fermion fields $\bar{\chi}$ and χ for simplicity. Projecting onto the boson couplings we find the beta

functions

$$\partial_t u = \partial_t u\big|_{\phi_k,V_k}, \qquad \partial_t m_V^2 = \partial_t m_V^2\big|_{\phi_k,V_k}, \qquad \partial_t h_\phi^2 = \partial_t h_\phi^2\big|_{\phi_k,V_k} + u'\partial_t\omega_{\phi,k}, \tag{5.59}$$

$$\partial_t \mu^2 = \partial_t \mu^2\big|_{\phi_k,V_k}, \qquad \partial_t \nu^2 = \partial_t \nu^2\big|_{\phi_k,V_k}, \qquad \partial_t h_V^2 = \partial_t h_V^2\big|_{\phi_k,V_k} + m_V^2\partial_t\omega_{V,k}, \tag{5.60}$$

i.e., the scale-dependent bosonization changes only the flow of h_ϕ^2 and h_V^2 and leaves the other beta functions in the bosonic sector invariant. For the four-fermi couplings we obtain

$$\partial_t g_\phi = \partial_t g_\phi\big|_{\phi_k,V_k} - h_\phi\partial_t\omega_{\phi,k}, \qquad \partial_t g_V = \partial_t g_V\big|_{\phi_k,V_k} - h_V\partial_t\omega_{V,k}. \tag{5.61}$$

Choosing

$$\partial_t\omega_{\phi,k} \equiv \frac{\beta_{g_\phi}}{h_\phi}, \qquad \partial_t\omega_{V,k} \equiv \frac{\beta_{g_V}}{h_V}, \qquad \text{where} \qquad \beta_{g_\phi} \coloneqq \partial_t g_\phi\big|_{\phi_k,V_k}, \qquad \beta_{g_V} \coloneqq \partial_t g_V\big|_{\phi_k,V_k}, \tag{5.62}$$

establishes that $g_{V,k}$ and $g_{\phi,k}$ vanish at all scales, if absent at the UV scale $k = \Lambda$. The beta functions β_{g_ϕ} and β_{g_V} are straightforwardly obtained by suitable projections of the box diagrams in Fig. 5.2,

$$\begin{aligned}
\beta_{g_{\phi/V}} = {} & 4v_d a^{(1)}_{\phi/V}\Big[2{N_\mathrm{f}}^2\,\ell^{(\mathrm{FB})d}_{1,2}(\tfrac{\kappa}{N_\mathrm{f}}h_\phi^2, u'; \eta_\psi, \eta_\phi) + \big(2{N_\mathrm{f}}^2 - 1\big)\,\ell^{(\mathrm{FB})d}_{1,2}(\tfrac{\kappa}{N_\mathrm{f}}h_\phi^2, u' + \tfrac{\kappa}{N_\mathrm{f}}u_{,\tilde\tau}; \eta_\psi, \eta_\phi) \\
& + \ell^{(\mathrm{FB})d}_{1,2}(\tfrac{\kappa}{N_\mathrm{f}}h_\phi^2, u' + 2\kappa u''; \eta_\psi, \eta_\phi)\Big]h_\phi^4 + 4v_d a^{(2)}_{\phi/V}\,\ell^{(\mathrm{FB})d}_{1,2}(\tfrac{\kappa}{N_\mathrm{f}}h_\phi^2, m_V^2 + \nu\kappa; \eta_\psi, \eta_V)h_V^4, \\
& + 4v_d a^{(3)}_{\phi/V}\Big[2{N_\mathrm{f}}^2\,\ell^{(\mathrm{FBB})d}_{1,1,1}(\tfrac{\kappa}{N_\mathrm{f}}h_\phi^2, u', m_V^2; \eta_\psi, \eta_\phi) \\
& + \big(2{N_\mathrm{f}}^2 - 1\big)\,\ell^{(\mathrm{FBB})d}_{1,1,1}(\tfrac{\kappa}{N_\mathrm{f}}h_\phi^2, u' + \tfrac{\kappa}{N_\mathrm{f}}u_{,\tilde\tau}, m_V^2; \eta_\psi, \eta_\phi) \\
& + \ell^{(\mathrm{FBB})d}_{1,1,1}(\tfrac{\kappa}{N_\mathrm{f}}h_\phi^2, u' + 2\kappa u'', m_V^2; \eta_\psi, \eta_\phi)\Big]h_\phi^2 h_V^2
\end{aligned} \tag{5.63}$$

with to be determined (possibly N_f-dependent) constants $a^{(i)}_{\phi/V}$. In the χSB regime the fermions couple also to the expectation value κ and there are more terms $\sim \kappa\,\ell^{(\mathrm{FB})d}_{2,2}(\kappa h_\phi^2/N_\mathrm{f}, \dots)\,h^4_{\phi/V}h_\phi^2$. They are suppressed for small $\kappa \ll 1$ and bounded from above for large $\kappa \gg 1$ since $\kappa\,\ell^{(\mathrm{FB})d}_{2,2}(\dots) \sim \kappa/(1+\kappa h_\phi/N_\mathrm{f})\cdot\ell^{(\mathrm{FB})d}_{1,2}(\dots)$ and we therefore expect that they change the flow only slightly. For simplicity, we will omit them in the following. Instead of evaluating the diagrams in Fig. 5.2 explicitly, we can determine the $a^{(i)}_{\phi/V}$ by taking advantage of the fact [161,201] that the dynamically bosonized flow in the pointlike limit $Z_{V,k} \to 0$ and $Z_{\phi,k} \to 0$ exactly coincides with the fermionic flow computed in Chap. 4,

$$\partial_t\left(N_\mathrm{f}\frac{h_\phi^2}{m_\phi^2}\right) \equiv -2\partial_t\tilde g\big|_{\phi_k,V_k}, \qquad \partial_t\left(N_\mathrm{f}\frac{h_V^2}{m_V^2}\right) \equiv \partial_t(\tilde g - g)\big|_{\phi_k,V_k}. \tag{5.64}$$

Therewith, the $a^{(i)}_{\phi/V}$ are uniquely fixed. This also establishes an exact mapping of the fermionic fixed-point structure computed in Chap. 4 onto the bosonized language in the pointlike limit. Beyond the pointlike approximation, the bosonized RG permits to reliably run toward and into the χSB regime, allowing us to predict the desired IR values of, for instance, fermion mass or order parameter as a function of N_f.

5.6 UV structure and fixed points

In the limit of infinite flavor number $N_\mathrm{f} \to \infty$, the flow equations simplify considerably. For the dynamically bosonized flow in the symmetric regime we have

$$\partial_t \left(\frac{m_\phi^2}{{N_\mathrm{f}}^2}\right) = (-2+\eta_\phi)\left(\frac{m_\phi^2}{{N_\mathrm{f}}^2}\right), \tag{5.65}$$

$$\partial_t m_V^2 = (-2+\eta_V) m_V^2 + \frac{2}{3\pi^2}\,\ell_1^{(\mathrm{F})}(0;\eta_\psi)\,\left(N_\mathrm{f} h_V^2\right), \tag{5.66}$$

$$\partial_t \left(N_\mathrm{f}\lambda_1\right) = (-1+2\eta_\phi)\left(N_\mathrm{f}\lambda_1\right) - \frac{1}{\pi^2}\,\ell_2^{(\mathrm{F})}(0;\eta_\psi)\,h_\phi^4, \tag{5.67}$$

$$\partial_t \lambda_2 = (-1+2\eta_\phi)\lambda_2 - \frac{2}{\pi^2}\,\ell_2^{(\mathrm{F})}(0;\eta_\psi)\,h_\phi^4, \tag{5.68}$$

$$\partial_t \left(N_\mathrm{f}\mu\right) = (-1+2\eta_V)\left(N_\mathrm{f}\mu\right) + \frac{4}{15\pi^2}\,\ell_2^{(\mathrm{F})}(0;\eta_\psi)\,\left(N_\mathrm{f} h_V^2\right)^2, \tag{5.69}$$

$$\partial_t \left(N_\mathrm{f}\nu\right) = (-1+\eta_\phi+\eta_V)\left(N_\mathrm{f}\nu\right) + \frac{2}{3\pi^2}\,\ell_2^{(\mathrm{F})}(0;\eta_\psi)\,\left(N_\mathrm{f} h_V^2\right) h_\phi^2, \tag{5.70}$$

$$\partial_t h_\phi^2 = (-1+\eta_\phi+2\eta_\psi) h_\phi^2 - \frac{4}{\pi^2}\left(\frac{m_\phi^2}{{N_\mathrm{f}}^2}\right)\ell_{1,2}^{(\mathrm{FB})}(0,m_V^2;\eta_\psi,\eta_V)\left(N_\mathrm{f} h_V^2\right)^2, \tag{5.71}$$

$$\partial_t \left(N_\mathrm{f} h_V^2\right) = (-1+\eta_V+2\eta_\psi)\left(N_\mathrm{f} h_V^2\right), \tag{5.72}$$

$$\eta_\phi = \frac{2}{3\pi^2}\,m_4^{(\mathrm{F})}(0;\eta_\psi)\,h_\phi^2, \tag{5.73}$$

$$\eta_V = \frac{4}{3\pi^2}\,m_4^{(\mathrm{F})}(0;\eta_\psi)\,\left(N_\mathrm{f} h_V^2\right), \tag{5.74}$$

$$\eta_\psi = 0, \tag{5.75}$$

where we have multiplied the flow equations with suitable factors of N_f in order to simplify the large-N_f counting of orders. Hence, in this limit the fermion wave function renormalization does not flow, $\eta_\psi = -\partial_t \ln Z_{\psi,k} \equiv 0$, whereas the flow of the bosonic wave function renormalizations is nonzero. Let us search for fixed points: assuming a fixed-point value $m_\phi^{*2} \neq 0$ we obtain from Eq. (5.65) for the scalar anomalous dimension at the fixed point $\eta_\phi^* = 2$, and Eq. (5.72) gives for an interacting fixed point with $h_V^{*2} \neq 0$ for the vector anomalous dimension $\eta_V^* = 1$. In fact, this is the known large-N_f result [61]. With these values of the anomalous dimensions, the full set of fixed-point values can be computed analytically, see Tab. 5.2. At this point, it may be worthwhile to make a few comments.

For taking the limit $N_\mathrm{f} \to \infty$ we have implicitly assumed a specific N_f-scaling of the couplings, defining the respective 't Hooft coupling. This may be justified retrospectively: since all couplings have finite (in particular nonzero) fixed-point values the large-N_f limit is well-defined. For the original four-fermion couplings $g_\phi = N_\mathrm{f} h_\phi^2/m_\phi^2$ and $g_V = N_\mathrm{f} h_V^2/m_V^2$ this implies the large-N_f scaling $g_\phi = \mathcal{O}(1/N_\mathrm{f})$ and $g_V = \mathcal{O}(1)$, already known from the fermionic flow, cf. Eq. (4.45). In fact, the fixed-point positions of g_ϕ and g_V for the dynamically bosonized flow in the large-N_f limit and fermionic flow exactly coincide, provided the same cutoff is employed. We note, however, that the equivalence in general does not hold for the flow beyond the fixed-point regime, since kinetic terms

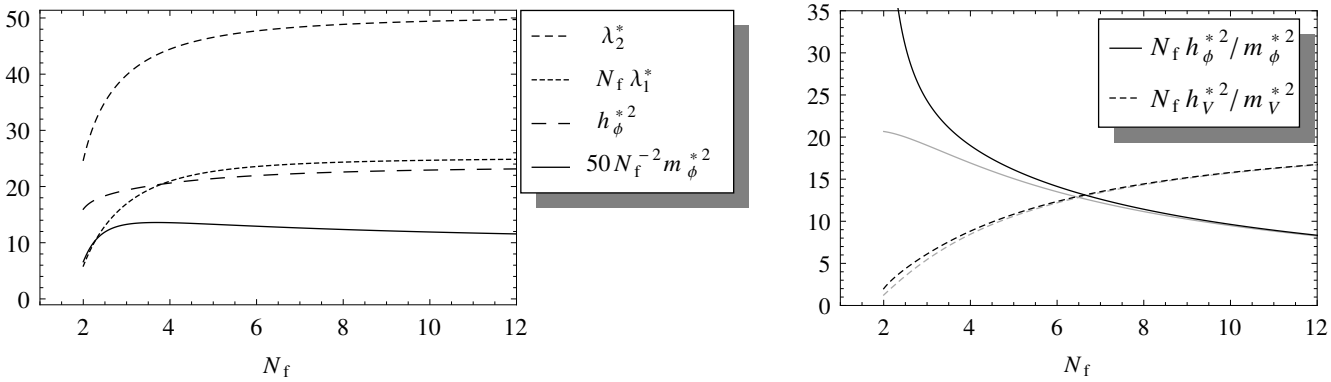

Figure 5.3 Left: nonuniversal UV fixed-point values of dynamically bosonized RG flow for the optimized regulator. The couplings have been multiplied with suitable N_f factors; for better visibility, the scalar mass has been multiplied with an additional factor 50. Right: Comparison of dynamically bosonized RG (black) with fermionic RG (gray).

of the bosonic fields are generated during the flow according to their finite anomalous dimensions. For instance, the large anomalous dimension $\eta_\phi^* = 2$ indicates a rapid generation of the scalar kinetic term.

Consider the second contribution to the beta function of the scalar-fermion coupling h_ϕ^2 in Eq. (5.71), being proportional to m_ϕ^2. This is exactly the contribution from the diagrams in Fig. 5.2, i.e., the large-N_f reminiscence of the scale-dependent Hubbard-Stratonovich transformation. Without this contribution, the large-N_f fixed-point equations cannot be solved with finite couplings. In other words, dynamical bosonization is crucial to find the correct large-N_f behavior in the scalar sector. We have already seen an indication for this in Sec. 5.4, where the scalar sector completely decoupled for $N_\mathrm{f} \geq 4$.

For the given set of integer anomalous dimensions, the large-N_f fixed-point values for the vector-vector coupling μ and the vector-scalar coupling ν are in fact negative. We attribute this to the fact that we neglected the momentum-dependent contribution $\propto \bar{\zeta}_k$ in Eq. (5.27) as well as higher order terms in the effective potential. In any case, in the large-N_f limit μ and ν do not feed back into the flow of the remaining couplings. For consistency, we again evaluate in what follows the flow equations for a pointlike current-current interaction, $Z_{V,k} \to 0$, and neglect the vector-vector selfinteractions μ and vector-scalar interactions ν, analogous to Sec. 5.4. This is expected to be a reasonable approximation as long as the vector mass m_V^2 does not become too small.

Beyond the large-N_f limit, we evaluate the fixed-point equations numerically, both for the optimized and sharp cutoff. Again, we recover the known UV structure: there is one interacting Thirring fixed point for all $1 < N_\mathrm{f} \leq \infty$, having only one IR relevant direction. [Recall that the case $N_\mathrm{f} = 1$ has been explicitly excluded in the derivation of our bosonic flow equations, cf. Eq. (5.33).] For small N_f it is located close to the pure scalar channel subspace, whereas for $N_\mathrm{f} \to \infty$ the scalar-fermion coupling becomes negligible. The fixed-point position in this limit in

Table 5.2 Left: nonuniversal fixed-point couplings for optimized regulator and various flavor numbers N_f. Right: universal quantities: correlation length exponent ν, subleading exponent ω, and anomalous dimension η_ϕ. Rough error estimates by comparison to sharp cutoff results. For $N_\mathrm{f} \gtrsim 6$ we do not expect chiral symmetry breaking due to vector channel domination, indicated by the gray font of the corresponding critical exponents; see Sec. 5.7.

N_f	$m_\phi^2/{N_\mathrm{f}}^2$	$N_\mathrm{f}\lambda_1$	λ_2	h_ϕ^{*2}	$N_\mathrm{f}h_V^{*2}/m_V^{*2}$	ν	ω	η_ϕ^*
2	0.132	5.85	24.68	15.96	1.99	2.36(?)	1.02(21)	1.35(66)
3	0.265	16.94	39.84	19.36	6.11	1.215(22)	1.49(21)	1.64(26)
4	0.271	20.95	44.45	20.61	8.83	1.0839(52)	1.65(12)	1.74(17)
5	0.266	22.70	46.55	21.41	10.83	1.0428(78)	1.744(72)	1.81(11)
6	0.259	23.56	47.70	21.95	12.35	1.0255(63)	1.797(41)	1.853(83)
8	0.247	24.34	48.86	22.59	14.44	1.0118(33)	1.837(15)	1.907(45)
10	0.238	24.68	49.42	22.93	15.79	1.0066(17)	1.790(35)	1.936(27)
12	0.231	24.85	49.73	23.14	16.74	1.0041(9)	1.715(43)	1.954(17)
25	0.209	25.16	50.33	23.54	19.39	1.0006(1)	1.423(1)	1.988(2)
100	0.187	25.26	50.52	23.68	21.45	1.0000(1)	1.126(1)	1.999(1)
∞	$\frac{8}{45}$	$\frac{64\pi^2}{25}$	$\frac{128\pi^2}{25}$	$\frac{12\pi^2}{5}$	$\frac{9\pi^2}{4}$	1	1	2

fact exactly coincides with the fermionic fixed point. For small N_f we find deviations from the fermionic UV structure. They are fully related to the fact that in the bosonized flow we allow for a possible momentum dependence in the scalar channel, which is in particular important once the scalar coupling becomes long range, i.e., if $\bar{m}_\phi^2$ is small. In other words, the bosons dynamically become fluctuating relevant degrees of freedom. We depicted the fixed-point positions for the optimized regulator in Fig. 5.3, together with the corresponding values for the fermionic flow compiled from Chap. 4 for comparison. Explicit values are given in Tab. 5.2. If (for instance, if N_f small) the fixed point corresponds to a (for instance, chiral symmetry breaking) second-order phase transition, the critical behavior is uniquely determined by the fixed-point regime, where the flow can be linearized. The scaling of the correlation length in the vicinity of the critical point is

$$\xi = \bar{m}_{\phi,\mathrm{R}}^{-1} \propto |\delta g|^{-\nu} \left(1 + b_\pm |\delta g|^{\omega\nu} + \dots\right), \tag{5.76}$$

with $\delta g \coloneqq g_\Lambda - g_\mathrm{cr}$ measuring the distance from criticality ("reduced temperature") and the renormalized scalar mass $\bar{m}_{\phi,\mathrm{R}}^2 = \lim_{k\to 0} m_\phi^2 k^2$. By again denoting the smallest eigenvalue (being negative) of the stability matrix $\partial\beta_i/\partial g_j|_{g^*}$ with $-\Theta_1 < 0$ and the second smallest eigenvalue (being positive) with $-\Theta_2 > 0$ we have

$$\nu = 1/\Theta_1 > 0, \qquad \text{and} \qquad \omega = -\Theta_2 > 0, \tag{5.77}$$

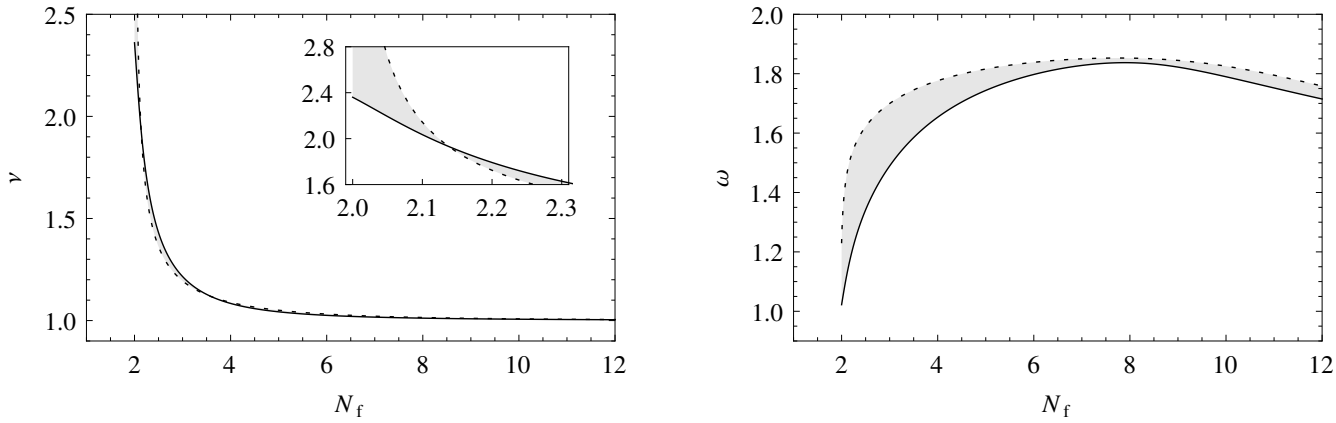

Figure 5.4 Left: correlation length exponent ν, extracted from the linearized flow in the fixed-point regime with optimized regulator (solid) and sharp regulator (dashed). The difference (gray shaded) serves as rough error estimate. The critical exponent is to a large extent independent of the regulator, while the uncertainty increases for $N_\mathrm{f} \searrow 2$, as shown in the inset. For increasing N_f it approaches rapidly the fermionic result $1/\Theta_1 = 1$. Right: corrections-to-scaling exponent ω.

see Sec. 2.3. At the critical point $\delta g = 0$, where the correlation length diverges, the asymptotic behavior of the scalar two-point function is determined by the anomalous dimension $\eta_\phi^* = \eta_\phi(g^*)$ as

$$\langle \varphi(x)\varphi(0)\rangle \propto \frac{1}{|x|^{d-2+\eta_\phi^*}}. \tag{5.78}$$

The critical exponents extracted from the flow in the fixed-point regime are shown in Figs. 5.4 and 5.5. We expect the values obtained with the optimized regulator to be our most accurate ones and use the difference to the sharp-cutoff results as a rough estimate on the truncation-induced error, cf. Sec. 2.2. We find that the correlation-length exponent is to a large extent regulator-independent, $\Delta\nu/\nu \lesssim 1\ldots2\%$ for $N_\mathrm{f} > 2$. As expected, slightly larger deviations between optimized and sharp cutoff occur for the anomalous dimension and the corrections-to-scaling exponent, $\Delta\eta_\phi/\eta_\phi, \Delta\omega/\omega \lesssim 10\ldots15\%$. Explicit values are again given in Tab. 5.2. This hierarchy of accuracy is well-known from RG studies of scalar models based on the derivative expansion [89, 171].

5.7 IR behavior and N_f-controlled quantum phase transition

If we start the flow for small N_f with initial UV couplings close to the fixed point, we find that the scalar mass eventually vanishes at some scale k^*, indicating the spontaneous breakdown of chiral symmetry. In the following, we will refer to k^* as "χSB scale". Continuing the flow for $k < k^*$ in the χSB regime the fermions become massive with renormalized mass $\bar{m}^2_{\mathrm{R,f}} = {N_\mathrm{f}}^{-1}\kappa h^2 k^2$ and the scalar sector consists of one radial mode with renormalized mass $\bar{m}^2_{\mathrm{R},\rho} = 2\kappa\lambda_1 k^2$, $2{N_\mathrm{f}}^2 - 1$ massive modes with $\bar{m}^2_{\mathrm{R},\tau} = {N_\mathrm{f}}^{-1}\kappa\lambda_2 k^2$, and $2{N_\mathrm{f}}^2$ massless Goldstone modes. In the broken regime with

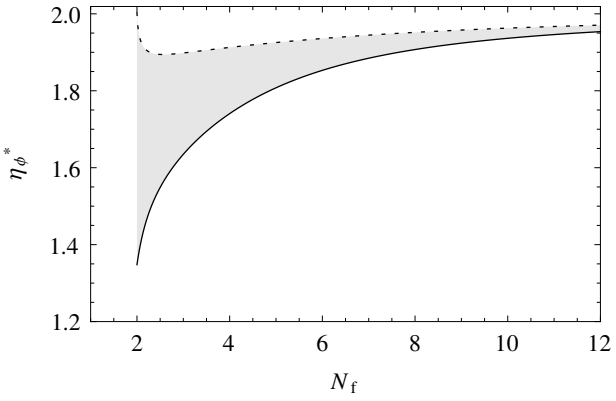

Figure 5.5 Anomalous dimension η_ϕ at the fixed point, with optimized regulator (solid) and sharp regulator (dashed).

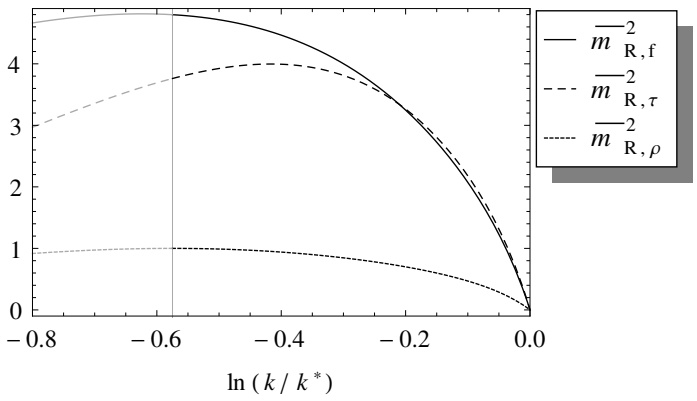

Figure 5.6 RG evolution of renormalized masses in χSB regime for $k < k^*$ and $N_\mathrm{f} = 2$. We stop the flow when the radial mass $\bar{m}^2_{\mathrm{R},\rho}$ approaches its maximum (vertical line).

a finite VEV κ the various scalar modes can in principle acquire different couplings during the flow. For instance, we would expect that the Goldstone modes eventually decouple in the deep IR, such that the flow freezes out, i.e., it is only given by the dimensional contributions in the beta functions. However, our ansatz (5.32) does not take this into account, but rather assumes the same coupling between massive and massless modes among themselves and massive modes to the VEV. In fact, we find that the dimensionless parameters run into an attractive IR fixed point, such that the dimensionful masses run into a maximum and eventually decrease again for small $k \ll k^*$, see Fig. 5.6. This effect is a well-known drawback of our polynomial expansion of the effective potential and has been attempted to circumvent by an adapted choice of coordinates [210]. Since we are mainly interested in the qualitative features of the theory, we simply stop the flow when it enters the IR fixed-point regime, indicated by a maximum of the masses. For our quantitative results, we use the maximum of the radial mass $\bar{m}^2_{\mathrm{R},\rho}$; however, our results to a large extent do not depend on this choice. We note that the critical behavior in terms of the exponents ν and η_ϕ^* remains, of course, unaffected by this, since it is solely determined by the UV structure of the theory.

Once the physical scale has been set, for instance, by measuring the value of the radial mass $\bar{m}^2_{\mathrm{R},\rho}$, we can compare the dynamically generated masses among different N_f. As a function of N_f, we show in Fig. 5.7 the renormalized fermion mass $\bar{m}^2_{\mathrm{R},\mathrm{f}}$ and scalar mass $\bar{m}^2_{\mathrm{R},\tau}$ in units of the radial mass $\bar{m}^2_{\mathrm{R},\rho}$. For increasing flavor number we observe that both $\bar{m}^2_{\mathrm{R},\mathrm{f}}$ and $\bar{m}^2_{\mathrm{R},\tau}$ decrease (apart from some interesting nonmonotonic behavior of the fermion mass for $N_\mathrm{f} \sim 3$) and eventually vanish for some critical flavor number $N_\mathrm{f} \nearrow N_\mathrm{f}^\mathrm{cr}$. Directly at $N_\mathrm{f} = N_\mathrm{f}^\mathrm{cr}$ we find that the vector-fermion coupling $N_\mathrm{f} h_V^2/m_V^2$ diverges at the same time as the scalar mass $m^2_{\phi,k}$ approaches zero, i.e., at the χSB scale k^*. We expect that this divergence is an artifact of our truncation which will be stabilized by higher terms in the vector sector [for instance, the terms $\propto \bar{\mu}_k$, $\bar{\nu}_k$, $\bar{\zeta}_k$ in Eq. (5.27)].

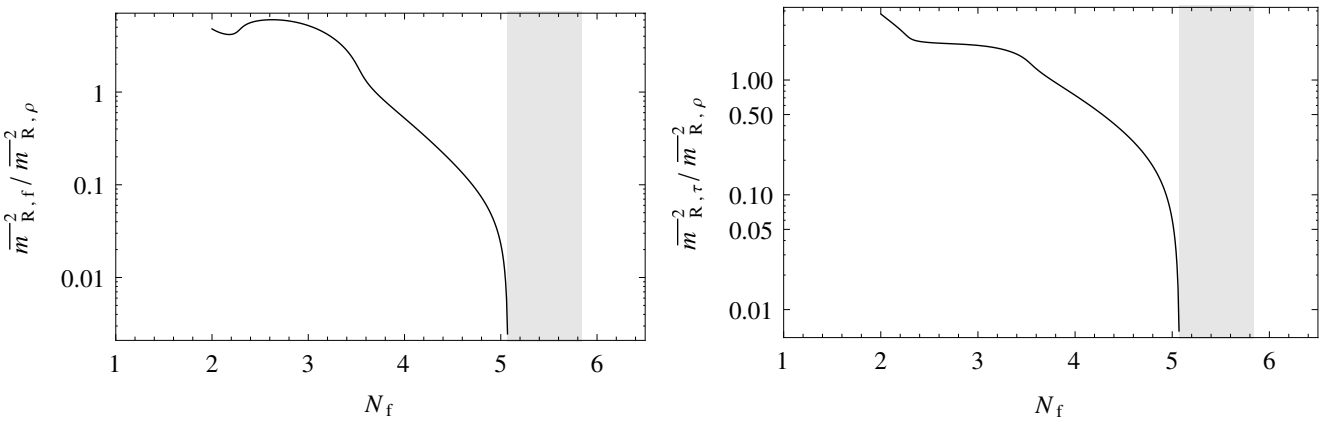

Figure 5.7 Logarithmic plot of dynamically generated fermion mass $\bar{m}^2_{\mathrm{R,f}}$ (left) and scalar mass $\bar{m}^2_{\mathrm{R},\tau}$ (right) in units of the radial mass $\bar{m}^2_{\mathrm{R},\rho}$. Gray shaded area: estimates for critical flavor number $N_\mathrm{f}^\mathrm{cr} \simeq 5.1$ (optimized cutoff) and 5.8 (sharp cutoff).

Here, we interpret the divergence as an indication for a "vector-boson-dominance" in the IR, inhibiting χSB. If the divergence was real, the model would exhibit dynamical Lorentz symmetry breaking [204–208]. For larger $N_\mathrm{f} > N_\mathrm{f}^\mathrm{cr}$ we observe the divergence already at higher scales $k > k^*$, inhibiting the flow to enter the χSB regime. The value of N_f^cr can thus be computed in two ways: on the one hand, coming from small flavor number, we observe a sharp decrease of the logarithm of the fermion mass once $N_\mathrm{f} \nearrow N_\mathrm{f}^\mathrm{cr}$. On the other hand, we look for the largest N_f below which the vector-fermion coupling h_V^2/m_V^2 remains finite for all scales in the interval $k \in [k^*, \Lambda]$. For the optimized cutoff we find $N_\mathrm{f}^\mathrm{cr} \simeq 5.07$ with the former method and $N_\mathrm{f}^\mathrm{cr} \simeq 5.1$ with the latter. For the sharp cutoff our truncation unfortunately does not allow to enter the χSB regime: we find $\lambda_{1,k^*} < 0$ at the χSB scale, indicating the requirement of higher terms in the polynomial expansion of the effective potential (5.32). We interpret this observation in the sense of optimization: for a nonoptimized regulator (as is the sharp cutoff) compared to optimized flows a higher order of the expansion is needed to achieve similar predictive power. Nonetheless, also in the sharp-cutoff scheme, we can determine the flavor number above which the vector-fermion coupling diverges before $m_{\phi,k} \to 0$. There, we find $N_\mathrm{f}^\mathrm{cr} \simeq 5.8$. Identifying the cutoff dependence with a rough error estimate yields our result for the critical flavor number

$$N_\mathrm{f}^\mathrm{cr} \simeq 5.1(7). \tag{5.79}$$

In the fermionic RG, we have shown that the "pure" Thirring model, defined by a microscopic action including only current-current interaction, is in the universality class defined by the interacting Thirring fixed point with one IR relevant coupling. Of course, this statement ultimately only holds for our specific regularization scheme, since fixed point positions itself are nonuniversal. In the bosonized formulation developed here we can check the universality class of the "pure"

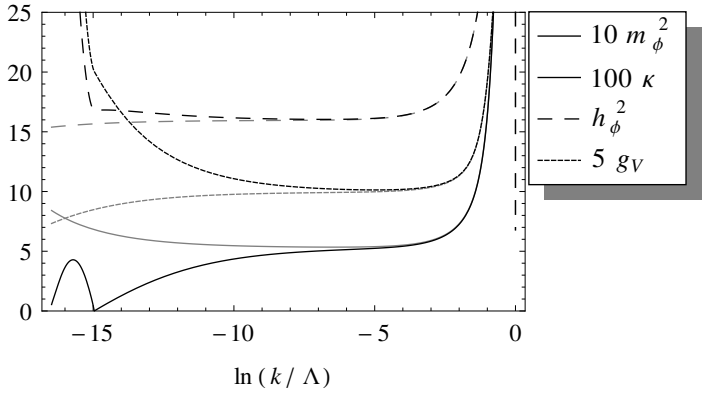

Figure 5.8 RG evolution of dimensionless couplings for the "pure" Thirring model with $N_\mathrm{f} = 2$ and initial couplings $m^2_{\phi,\Lambda} = 10^6$, $\lambda_{i,\Lambda} = 0$, $h^2_{\phi,\Lambda} = 0$, and two different $g_{V,\Lambda} = N_\mathrm{f} h^2_{V,\Lambda}/m^2_{V,\Lambda}$ just above (black) and below (gray) g_cr. For $\ln(k/\Lambda) \simeq -5$ the flow approaches the UV fixed-point regime. The black solid line corresponds to m^2_ϕ above and to κ below the χSB scale $\ln(k^*/\Lambda) \simeq -15$.

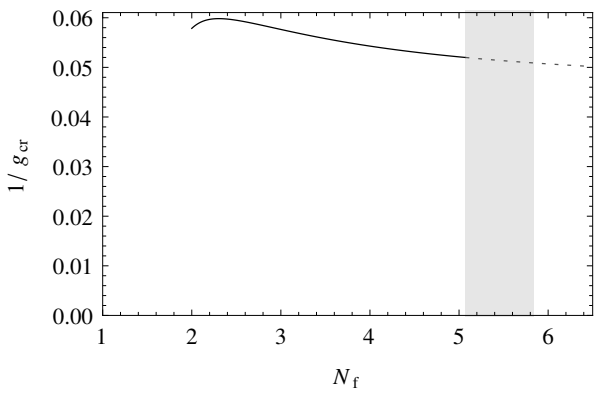

Figure 5.9 Critical coupling $1/g_\mathrm{cr}$ for the "pure" Thirring model with initially decoupled scalar sector as a function of N_f. For $N_\mathrm{f} \gtrsim 6$ (gray area) we do not expect chiral symmetry breaking (dashed line).

Thirring model by starting the flow with initial couplings

$$Z_\phi^{-1} \propto m^2_{\phi,\Lambda} \gg 1, \qquad \lambda_{i,\Lambda} \ll 1 \quad (i = 1, 2), \qquad h^2_{\phi,\Lambda} \ll 1, \tag{5.80}$$

i.e., with a decoupled scalar sector. In our explicit computations we use $Z_{\phi,\Lambda} = 10^{-6}$, $m_{\phi,\Lambda} = 10^6$, $\lambda_{i,\Lambda} = 0$, $h^2_{\phi,\Lambda} = 0$. However, universality guarantees that our results are independent of the exact values for the initial couplings, a fact which we have also explicitly verified. Fig. 5.8 shows for $N_\mathrm{f} = 2$ the RG evolution of the dimensionless couplings for two different initial values of the vector-fermion coupling $g_V = N_\mathrm{f} h_V^2/m_V^2$ just above and below the critical value g_cr. Though we start with a decoupled scalar sector, the scalar couplings are again generated by the RG flow, as already known from the purely fermionic RG. Furthermore, we find for initial couplings close to criticality that the flow runs into the fixed-point regime, which is exactly given by the Thirring fixed-point couplings in Tab. 5.2, cf. Fig. 5.8. Thus, the critical behavior of a conventionally defined "pure" Thirring model without scalar channel in the bare action is indeed given by the universality class of our Thirring fixed point. For completeness, we show in Fig. 5.9 the critical coupling g_cr for which the flow approaches the Thirring fixed point as a function of N_f, to be compared with previous results in Fig. 4.5. Again, we do not find a sharp decrease of $1/g_\mathrm{cr}$ as $N_\mathrm{f} \nearrow N_\mathrm{f}^\mathrm{cr}$, since the critical flavor number does not occur because of a change in the UV structure, but rather due to a competition between the vector and scalar channel. Since the Thirring fixed point is present for all N_f, we can still determine a "would-be" critical coupling g_cr even for $N_\mathrm{f} > N_\mathrm{f}^\mathrm{cr}$ (dashed line in Fig. 5.9). In other words, the critical coupling (for any N_f) is given by the intersection point of the separatrix with the Thirring axis, cf. Fig. 4.3.

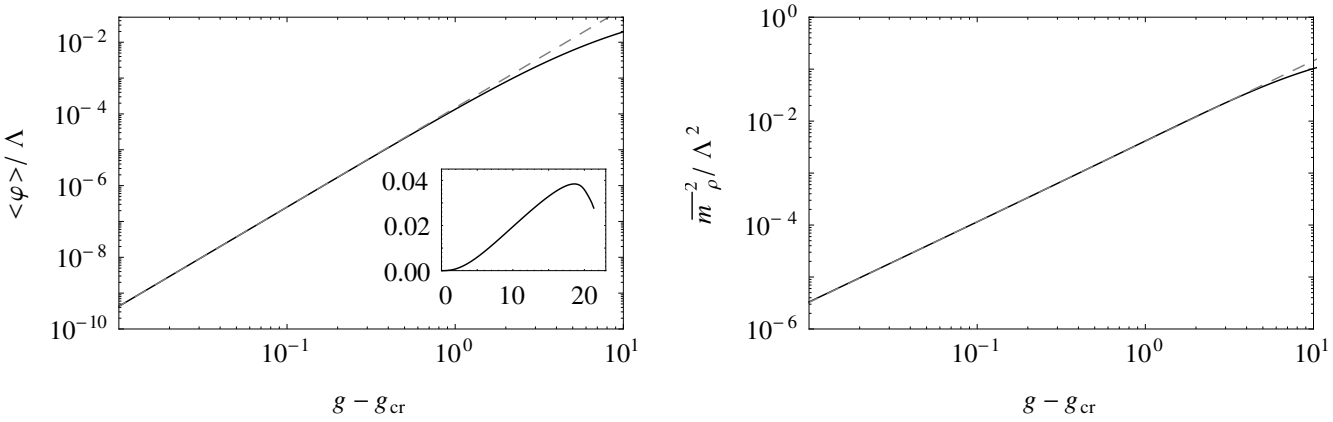

Figure 5.10 Critical behavior of "pure" Thirring model with $N_{\mathrm{f}} = 2$: order parameter $\langle\varphi\rangle \propto |\delta g|^{\beta}$ (left) and inverse susceptibility $\chi^{-1} = \bar{m}_{\rho}^{2} \propto |\delta g|^{\gamma}$ (right) on log-log plot, showing the expected power law. The slope of the regression line (gray dashed) is $\beta = 2.769$ and $\gamma = 1.553$, respectively. Left inset: for very large coupling on the pure Thirring axis the order parameter decreases again, see Sec. 5.8.

In order to establish the connection between the negative eigenvalues of the stability matrix Θ_I and the critical exponents in Eq. (5.77) we have assumed that the propagator has a scaling form, from which one infers the hyperscaling relations (see Sec. 2.3)

$$\beta = \frac{\nu}{2}(d - 2 + \eta_{\phi}^{*}), \qquad \gamma = \nu(2 - \eta_{\phi}^{*}). \tag{5.81}$$

The hyperscaling assumption can in fact explicitly be verified by computing directly the critical behavior of the order parameter $\langle\varphi\rangle \propto |\delta g|^{\beta}$, inverse susceptibility (unrenormalized mass) $\chi^{-1} = \bar{m}_{\rho}^{2} \propto |\delta g|^{\gamma}$, and inverse correlation length (renormalized mass) $\xi^{-1} = \bar{m}_{\mathrm{R},\rho} \propto |\delta g|^{\nu}$. As a function of the distance to criticality, we indeed find that the expected linear behavior on a log-log plot is excellently fulfilled; see Fig. 5.10 for the case of the "pure" Thirring model (initially decoupled scalar sector) and $N_{\mathrm{f}} = 2$. The slopes of the regression lines for initial couplings on the pure Thirring axis are (for $N_{\mathrm{f}} = 2$)

$$\beta = 2.769, \qquad \gamma = 1.553, \qquad \nu = 2.364, \tag{5.82}$$

whereas if we start the flow at the Thirring fixed point, we obtain

$$\beta = 2.771, \qquad \gamma = 1.539, \qquad \nu = 2.361. \tag{5.83}$$

The values should be compared with the critical exponents obtained from the linearized flow in the Thirring fixed-point regime (see Tab. 5.2), together with the hyperscaling assumption:

$$\frac{\nu}{2}(d - 2 + \eta_{\phi}) = 2.771, \qquad \nu\,(2 - \eta_{\phi}) = 1.539, \qquad \nu = 2.360, \tag{5.84}$$

in excellent agreement with Eqs. (5.83). However, hyperscaling is to a large extent also fulfilled for the conventionally defined "pure" Thirring model, cf. Eqs. (5.82) with (5.84). We attribute the

small (but significant) deviations for the latter to the presence of other fixed points: in particular the critical behavior could be influenced by fixed point $\mathcal{B}$ (in the nomenclature of Chap. 4), which (at least in the pointlike limit, see Fig. 4.3) is located in the broader vicinity of the pure Thirring axis and potentially describes a different universality class. We will further elaborate on this aspect in the following section, see also Fig. 5.12.

5.8 Comparison with previous studies

Let us compare our results with those previously obtained by means of other analytical or numerical methods. In the large-N_f expansion, renormalizability of the "pure" 3d Thirring model with only current-current interaction $\propto g_V(\bar\psi\gamma_\mu\psi)^2$ (i.e., without scalar channel) has been shown to hold if and only if a regularization scheme is employed in which the vector field propagator remains purely transverse on the quantum level, defining an interacting UV fixed point [60–63, 211]. In Ref. [61] it is found to leading order in $1/N_\mathrm{f}$ (in terms of our notation)

$$\partial_t g_V = g_V\left(1-\frac{g_V}{g_V^*}\right), \qquad \eta_V = \frac{g_V}{g_V^*}, \qquad \eta_\psi = \mathcal{O}(1/N_\mathrm{f}), \tag{5.85}$$

which is exactly the large-N_f behavior of our flow equations (5.65)–(5.75): if the fixed point corresponds to a second-order phase transition, the corresponding correlation-length exponent is $\nu = 1/\Theta = 1$ where $\Theta = -\partial\beta/\partial g_V|_{g_V^*}$ and the vector field anomalous dimension is $\eta_V(g_V^*) = 1$.

However, we should be cautious: Yang [211] claims that the partially bosonized Thirring model is equivalent to (a gauge-fixed version of) a U(1) gauge theory, in which the mass of the vector boson is generated by the Higgs mechanism. Insisting on the gauge symmetry, it is therewith argued that the coupling g_V *cannot* be renormalized. Consequently, the beta function is vanishing for any value of g_V and there is no fixed point condition [62, 69].

The formulation of the Thirring model as a gauge theory is at the basis of the analytical studies [63–66], which attempt to solve the Dyson-Schwinger equations (DSE) by setting the full vector propagator to its large-N_f form, and the full vertex to the bare vertex (known as ladder approximation). All such studies claim the existence of a nontrivial solution corresponding to chiral symmetry breaking for small values of $N_\mathrm{f} < N_\mathrm{f}^\mathrm{cr}$. However, their predictions for the value of N_f^cr and the critical behavior of fermion mass and chiral order parameter differ significantly: Ref. [63] reports $N_\mathrm{f}^\mathrm{cr} \simeq 3.24$. Hong and Park [64] claim that symmetry breaking should persist for any value of N_f, i.e., $N_\mathrm{f}^\mathrm{cr} = \infty$. In Ref. [65] an essentially singular behavior close to $N_\mathrm{f}^\mathrm{cr} \simeq 4.32$ is found,

$$\bar m_{\mathrm{R,f}} \propto \Lambda \exp\left(-\frac{2\pi}{\sqrt{N_\mathrm{f}^\mathrm{cr}/N_\mathrm{f}-1}}\right), \qquad \text{for } N_\mathrm{f} < N_\mathrm{f}^\mathrm{cr}, \tag{5.86}$$

that is to say, a phase transition of *infinite* order. Such an essential scaling law has been found in a number of gauge theories, such as quenched QED_4 [74, 212, 213] and QED_3 with N_f fermion

flavors [47–49, 56, 59], as well as many-flavor QCD_4 [74–78, 85–87]. In this context, the scaling law is often referred to as Miransky scaling; the scenario has also been termed (pseudo-)conformal phase transition [74]. Essential scaling has also been found in two-dimensional statistical systems, such as the XY model, where the scenario is called Kosterlitz-Thouless phase transition [214–217]. As has been pointed out recently [218], the general mechanism being responsible for essential scaling is the merger of two RG fixed points and their subsequent disappearance into the complex plane, or a running off of a fixed point to zero or infinite coupling. By contrast, we find that the UV Thirring fixed point persists for any N_f, with no hint of essential scaling.

By constructing an effective potential for the chiral order parameter $\langle\varphi\rangle$, up to the leading order of $1/N_\mathrm{f}$ expansion, Kondo [67] reports a *second-order* phase transition,

$$\langle\varphi\rangle \propto \left(\frac{N_\mathrm{f}^\mathrm{cr}}{N_\mathrm{f}} - 1\right)^b, \qquad \text{for } N_\mathrm{f} < N_\mathrm{f}^\mathrm{cr}, \tag{5.87}$$

where for $d = 3$ the critical exponent is given by $b = 1$ and $N_\mathrm{f}^\mathrm{cr} = 2$. We have been motivated by these consideration to attempt a fit to our results for order parameter and fermion mass. In Fig. 5.11, we depict $\langle\varphi\rangle/\bar{m}_{\mathrm{R},\rho}$ versus the combination $(N_\mathrm{f}^\mathrm{cr}/N_\mathrm{f}) - 1$ in a log-log plot. In fact, the behavior is very well compatible with a power-law scaling corresponding to a second-order phase transition at N_f^cr. However, the linear fit (gray line) gives $b = 0.44$ in qualitative, but not quantitative agreement with the Kondo scenario [67]. We note that for a quantum phase transition at N_f^cr occurring due to competing condensation channels, the corresponding critical exponents not necessarily have to coincide with those determining the phase transition with the coupling as control parameter. In particular, we do not expect that $\beta|_{N_\mathrm{f}^\mathrm{cr}}$ and b coincide. In any case, a fit to an essential scaling behavior analogous to (5.86) both for order parameter and fermion mass is much less successful and is not supported by our results.

Chiral symmetry breaking in the "pure" 3d Thirring model has also been investigated on the lattice [68–73]. One extensive study [72] finds $N_\mathrm{f}^\mathrm{cr} = 6.6(1)$, the bare value of which we consider as still consistent with our result, see below. Moreover, the study also attempts to predict the critical behavior close to the phase transition, both for fixed $N_\mathrm{f} < N_\mathrm{f}^\mathrm{cr}$ as a function of the bare coupling g and for fixed $g > g_\mathrm{cr}$ as a function of N_f. In the latter case, the data is fitted to an equation of state of the form

$$m = A\left[(N_\mathrm{f} - N_\mathrm{f}^\mathrm{cr}) + CL^{-\frac{1}{\nu}}\right]\langle\bar{\psi}\psi\rangle^p + B\langle\bar{\psi}\psi\rangle^\delta, \tag{5.88}$$

with m being the bare fermion mass (explicit symmetry-breaking parameter), L the linear extent of the system, and A, B, C some constants. Close to criticality in the chiral ($m \to 0$) and thermodynamic ($L \to \infty$) limit, Eq. (5.88) in fact reduces to the Kondo-formula (5.87) upon identification of $b \equiv 1/(\delta - p)$ and $\langle\varphi\rangle \propto \langle\bar{\psi}\psi\rangle$. It is interesting to notice that the fit reported in [72] yields $1/(\delta - p) = 0.37$, which could be considered as roughly compatible with our result $b = 0.44$.

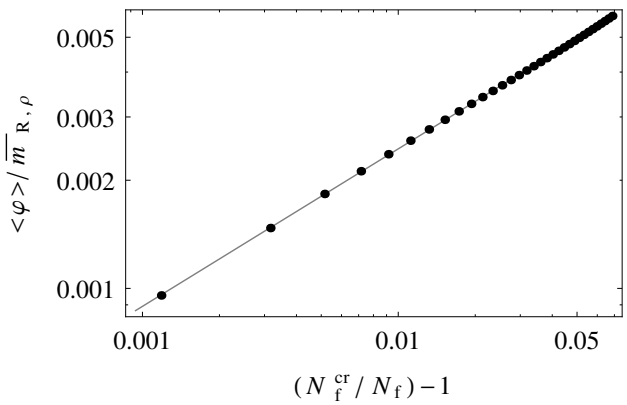

Figure 5.11 Order parameter (black dots) vs. $N_\mathrm{f}^\mathrm{cr}/N_\mathrm{f} - 1$ in log-log plot, showing very good compatibility to power-law scaling behavior $\langle\varphi\rangle \propto (N_\mathrm{f}^\mathrm{cr}/N_\mathrm{f} - 1)^b$. The slope of the regression line (gray) is $b = 0.44$.

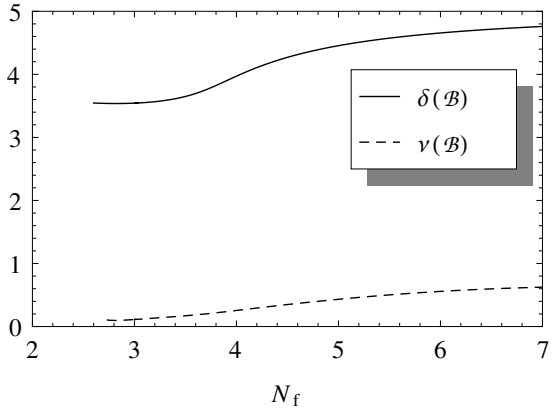

Figure 5.12 Critical exponents δ and ν for a theory defined at the fixed point $\mathcal{B}$ (nomenclature of Chap. 4) with more than one RG relevant direction; to be compared with Fig. 5 of Ref. [72].

However, striking discrepancies occur, when one compares the critical behavior for fixed $N_\mathrm{f} < N_\mathrm{f}^\mathrm{cr}$ with the bare coupling as control parameter. In particular, in the sequence of studies [69–72] it is found that the exponent δ lies between $\delta \approx 2.8$ ($N_\mathrm{f} = 2$) and $\delta \approx 5.8$ ($N_\mathrm{f} = 6$), i.e., most notably, δ *increases* with N_f. The result for $N_\mathrm{f} = 2$ has been confirmed in a particular interesting very recent work [73], where the same lattice action has been employed directly in the massless-fermion limit with manifest U(1)⊗U(1) chiral symmetry. The resulting anomalous dimension reads $\eta_\phi = 0.65(1)$, which (under the hyperscaling assumption) is equivalent to $\delta = (5 - \eta_\phi)/(1 + \eta_\phi) = 2.64(2)$. By contrast, we find (cf. Tab. 5.2) $\delta \approx 1.5$ ($N_\mathrm{f} = 2$) and $\delta \approx 1.1$ ($N_\mathrm{f} = 6$), that is to say, δ *decreases* with N_f and the values lie well below the lattice predictions[b].

The lattice simulations build on a microscopic definition of the Thirring model which is fixed by a bare action including only the Thirring-like current-current interaction. It is therefore *a priori* not necessarily clear, whether the critical behavior in the lattice models is in fact given by the Thirring fixed point, cf. our discussion in Sec. 4.5. Our analysis in the preceding section 5.6 supports this (cf. Fig. 5.8); nonetheless, since fixed-point positions are scheme-dependent, our results may not be directly transferable to the lattice theory. In particular, we have seen in Chap. 4, that a microscopic formulation, being fixed on the Thirring axis, could, for instance, be influenced by the fixed point $\mathcal{B}$ (in the nomenclature of Chap. 4), which has more than one RG relevant direction. In order to get a glimpse of how such a situation could change the corresponding critical behavior we compute in the dynamically bosonized formulation the critical exponents associated with fixed

[b] As a side remark we note that the DSE studies [65, 66] point to $\delta = 2$ ($N_\mathrm{f} < N_\mathrm{f}^\mathrm{cr}$) and $\delta = 1$ ($N_\mathrm{f} = N_\mathrm{f}^\mathrm{cr}$). (This fact has been argued in Ref. [72].) While it is appealing to conclude consistency with our findings at the Thirring fixed point (at least to some extent), we refrain from doing so, since the nature of the transition reported in the these studies substantially differs from ours; see Eq. (5.86) above.

point $\mathcal{B}$. We emphasize however that a theory defined at $\mathcal{B}$ in any case cannot be fixed by just one bare parameter. Naively using the hyperscaling relation[c] $\delta(\mathcal{B}) = [5 - \eta_\phi(\mathcal{B})]/[1 + \eta_\phi(\mathcal{B})]$ we can relate the critical exponent $\delta(\mathcal{B})$ to the anomalous dimension $\eta_\phi(\mathcal{B})$ at $\mathcal{B}$, see Fig. 5.12. The values for $\delta(\mathcal{B})$ lie well above those for the Thirring fixed point. Most notably, $\delta(\mathcal{B})$ in fact now *increases* with N_f, in qualitative (but not quantitative) consistency with the behavior shown in Fig. 5 of [72]. For comparison, we also depict the correlation length exponent $\nu = 1/\Theta_1$, associated with the largest negative eigenvalue of the stability matrix, i.e., the strongest RG relevant direction. It should be interesting to further elucidate whether this scenario could account for the discrepancy between our findings at the Thirring fixed point and the lattice results.

However, we would like to propose yet another way out of this contradiction: the exact same lattice action employed in the studies quoted above has also been used in simulations of the chiral $\mathrm{U}(1) \otimes \mathrm{U}(1)$ Gross-Neveu (GN) model in three dimensions [97], yielding $\nu = 0.88(8)$ and $\eta_\phi = 0.46(11)$, probably consistent with the lattice Thirring results $\nu = 0.85(1)$, $\eta_\phi = 0.65(1)$ [73] and $\nu = 0.71(4)$, $\eta_\phi = 0.60(2)$ [69] for $N_\mathrm{f} = 2$. In fact, the symmetry breaking pattern of the lattice Thirring model is [70]

$$\mathrm{U}(N_\mathrm{stagg}) \otimes \mathrm{U}(N_\mathrm{stagg}) \to \mathrm{U}(N_\mathrm{stagg}), \tag{5.89}$$

where N_stagg is the number of staggered fermion flavors and the number of continuum four-component fermions is $N_\mathrm{f} = 2N_\mathrm{stagg}$ [110]. It is an open question whether the breaking pattern of the continuum Thirring model,

$$\mathrm{U}(2N_\mathrm{f}) \to \mathrm{U}(N_\mathrm{f}) \otimes \mathrm{U}(N_\mathrm{f}), \tag{5.90}$$

is restored in the continuum limit of the lattice Thirring model; see [69, 70] for a discussion. This scenario could be checked by a careful analysis of the low-energy spectrum in the broken phase: the number of Goldstone modes for the breaking pattern (5.89) would be $N_\mathrm{stagg}^2 = {N_\mathrm{f}}^2/4$, whereas for (5.90) one expects $2{N_\mathrm{f}}^2$ massless modes. Unfortunately, we do not know of any such study so far. If the continuum Thirring pattern (5.90) is not restored in the simulations, then the lattice Thirring result could possibly describe the chiral GN universality class with breaking pattern (5.89). We have been motivated by these consideration to compare the lattice results also to our findings for the chiral GN model considered in Chap. 3. There, we have found, for instance, $\delta_{\chi\mathrm{GN}} = 2.58(9)$ for the left-right symmetric $\mathrm{U}(1) \otimes \mathrm{U}(1)$ model; see Tab. 3.2. Interestingly enough, we observe that our chiral GN findings are in fact well consistent with the general trend reported for the lattice Thirring model, e.g., $\delta = 2.75(9)$ for $N_\mathrm{stagg} = 1$ [69]. [We note however that $N_\mathrm{stagg} = 1$ corresponds to two four-component continuum flavors, whereas our $\mathrm{U}(1) \otimes \mathrm{U}(1)$ model in Chap. 3 is defined with solely one four-component fermion.] In Refs. [70, 97] the question has been raised whether for $N_\mathrm{f} = 2$ the distinction between chiral GN and Thirring model might be unimportant

[c] Of course, hyperscaling may not hold at a fixed point with two relevant directions.

and both models might actually coincide. In such a scenario the fixed point pertaining to the χSB phase transition would incidentally lie in a U(4)-symmetric IR attractive subspace of the theory space. While certainly possible, we know of no argument supporting such a conjecture; it is also not favored by our results for chiral GN and Thirring model.

In order to clarify these uncertainties, it would be very interesting to simulate the Thirring model in a formulation in which either the restoration of the U($2N_\mathrm{f}$) symmetry can be explicitly verified in the continuum limit or in which it is manifest. In the two-component fermion formulation developed in this chapter the latter option might be pursued using standard methods (e.g., Wilson fermions [219]), since in this formulation there is no notion of chirality and the U($2N_\mathrm{f}$) is just a flavor symmetry. Alternatively, in the four-component language, one could employ more advanced chiral-fermion techniques, such as domain-wall [220–222] or overlap [223] fermions, both of which are explicitly chiral symmetric and deserve to be studied on their own rights due to their relevance to lattice QCD_4.

We would finally like to comment on the unorthodox behavior of the chiral condensate far from the critical point, as reported in the lattice study [72]. There, it has been found that $\langle\bar{\psi}\psi\rangle$ decreases again for large (current-current) coupling g_V. The corresponding peak position at $g_V = g_{V,\mathrm{max}}$ is independent of both lattice volume and bare fermion mass, indicating that its origin is at the UV scale. The effect has then been attributed to the fact that the vector propagator in the lattice regularization violates the transversity condition, the latter being crucial to the renormalizability of the $1/N_\mathrm{f}$ expansion. The impact of the extra divergence can however be absorbed by a coupling renormalization $g_V' = g_V(1 - g_V/g_{V,\mathrm{lim}})^{-1}$, such that the strong coupling limit is recovered at $g_V = g_{V,\mathrm{lim}}$. $g_{\mathrm{V,\,lim}}$ is thereupon identified with the peak position $g_{V,\mathrm{max}}$. By contrast, the present work suggests that the 3d Thirring model can in fact be renormalized nonperturbatively *without* insisting on a transverse vector propagator, if one allows for a microscopic definition in the two-dimensional coupling plane spanned, for instance, by the couplings g_V and g_ϕ. [In fact, within our truncation we find that the flow of transverse and longitudinal parts of the vector propagator coincide.] If this remains robust beyond our approximation, it could provide a natural explanation for the nonmonotonic behavior of the condensate as a function of g_V: Since the numerical value of any IR observable (in units of a fixed UV cutoff Λ) is first and foremost given by "duration" of RG time $t = \ln(k/\Lambda)$ before the flow freezes out or enters the IR fixed point regime, it could well be that for a theory defined on the pure Thirring axis with bare $g_\phi = 0$ an IR quantity decreases again for large g_V far from criticality. Loosely speaking, just because we start the flow with a large current-current interaction does not mean we are closer to the χSB regime. In order to check the possible substance of these considerations we computed the order parameter for different bare couplings g_V on the Thirring axis and initially decoupled scalar sector, showing indeed a maximum far from criticality $g_V \gg g_\mathrm{cr}$ and a subsequent decrease; see inset of Fig. 5.10.

5.9 Conclusions

In this chapter, we enhanced the results of the purely fermionic RG by including composite bosonic degress of freedom in the context of the Hubbard-Stratonovich transformation. In particular, we included a NJL-type scalar matrix field ϕ^{ab} and a Thirring-type massive vector field V_μ. Therewith, we analyzed both UV structure and IR behavior of the theory in the usual formulation with fixed fields as well as for dynamically bosonized fields, that is to say, by applying a scale-dependent Hubbard-Stratonovich transformation. Both formulations show the existence of a Thirring fixed point with one RG relevant direction. For small N_f it is located close to the scalar-channel subspace, while it approaches the vector-channel subspace (the pure Thirring axis) for increasing N_f. All this is well compatible with our previous findings in the purely fermionic description. For quantitative reliability however, we have shown that it proves necessary to employ the adapted RG flow in the dynamically bosonized setting, which overcomes the Fierz ambiguity. We therewith confirmed previous results from DSE studies and Monte-Carlo simulations indicating that chiral symmetry breaking, corresponding to a condensation in the scalar channel, occurs for large enough coupling if the number of fermion flavors N_f is smaller than a critical value N_f^cr, while it is shown to be absent for $N_\mathrm{f} > N_\mathrm{f}^\mathrm{cr}$, independently of the coupling. The results, obtained for different regularization schemes, estimate $N_\mathrm{f}^\mathrm{cr} \simeq 5.1(7)$, while the dependence on the regulator has been taken as a rough indication for the error induced by our truncation. Since all previous studies we know of rely on a microscopic definition of the 3d Thirring model with pure current-current (Thirring-like) interaction, the mechanism behind the quantum phase transition at N_f^cr has so far been rather unclear. The present work has shown for the first time that the critical flavor number may occur due to a competition between different condensation channels: the NJL-type scalar channel on the one hand, dominating for small N_f and triggering χSB, and the Thirring-type vector channel on the other hand, dominating for large N_f and prohibiting χSB.

Admittedly, our approximation with pointlike vector channel does not allow a reliable prediction of the IR properties of the system for $N_\mathrm{f} \gtrsim N_\mathrm{f}^\mathrm{cr}$, since for small vector mass $m_V^2 \lesssim \mathcal{O}(1)$ momentum dependent terms $\propto Z_{V,k}, \bar{A}_{V,k}, \bar{\zeta}_k$ in the effective action (5.27) are expected to become important. In this sense, one may view the estimate obtained within our truncation as a lower bound for the true critical flavor number N_f^cr. Thus, we consider our findings for N_f^cr to be well compatible with the lattice results [72]. In any case however, it would be very interesting to see in how far the inclusion of momentum dependent terms in the vector sector would modify the IR flow of the large-N_f theory. This is in particular true for the term $\propto \bar{\zeta}_k V_\mu V_\mu \partial_\nu V_\nu$, which has no analogue in scalar field theories and thus could lead to a qualitatively different IR behavior as compared to the latter. Furthermore, at this point we also cannot exclude with certainty that this term does not change the UV structure of our theory in the large-N_f limit. This deserves further investigation.

The RG approach is *per constructionem* particularly useful for predicting the critical phenomena associated with a given universality class. We have computed the critical behavior for fixed

$N_\mathrm{f} < N_\mathrm{f}^\mathrm{cr}$ as a function of the bare coupling in terms of the exponents ν, η_ϕ, β, and γ both for a microscopic definition of the model at the Thirring fixed point as well as on the pure Thirring axis. For $N_\mathrm{f} = 2$, we have checked the hyperscaling assumption and have shown that it is well fulfilled for both definitions of the model. We also explicitly verified that both models for any N_f are in fact in the same universality class; albeit, this statement ultimately only holds for our specific regularization scheme. Strictly speaking, the model starting on the pure Thirring axis is not itself a UV complete quantum field theory. We can, however, think of it as belonging to an RG trajectory (line of constant physics) that emanates from fixed point $\mathcal{B}$ and thus has a definite UV completion. For the theory defined at the Thirring fixed point, we have also computed the corrections-to-scaling exponent ω.

Close to the quantum critical point $N_\mathrm{f} \nearrow N_\mathrm{f}^\mathrm{cr}$, we have discussed the scaling behavior as a function of N_f (for fixed couplings above their critical values). We have found no indication of essential scaling. As a drawback, the deep IR behavior of our flow equations is strongly affected by the Goldstone-mode fluctuations. We expect that this IR dominance is in fact an artifact of our approximation, since our ansatz does not allow for different flows of the various scalar-mode couplings in the χSB regime. This issue was circumvented by stopping the flow as soon as the IR fixed-point regime is reached. Therewith, we have computed the dynamically generated fermion mass $\bar{m}^2_{\mathrm{R},\mathrm{f}}$ and the τ-mode mass $\bar{m}^2_{\mathrm{R},\tau}$ in units of the radial mass $\bar{m}^2_{\mathrm{R},\rho}$. Though in principle (for fixed radial mass) universal, the explicit values of our IR quantities should not be taken too literally, since their systematic uncertainty introduced by our truncation with uniform scalar-coupling flow in the χSB regime remains undetermined at present. In fact, this important question arises in any three-dimensional system with spontaneously broken continuous symmetry; it deserves an own study in a possibly simpler system. By contrast however, the critical behavior for $N_\mathrm{f} < N_\mathrm{f}^\mathrm{cr}$ as a function of the bare coupling is solely determined by the UV structure of the theory and thus remains unaffected by this issue. More than our IR predictions, we therefore consider our results for the correlation-length exponent ν to be well reliable on the percent level, whereas the predictions for anomalous dimension η_ϕ and corrections-to-scaling exponent ω might be somewhat less accurate.

6 Summary

In this work, we have investigated three-dimensional relativistic fermion systems from the perspective of the renormalization group (RG). We have classified these systems with respect to their symmetry and have focussed in particular on the chiral Gross-Neveu (GN) model and the Thirring model with $\mathrm{U_L}(N_\mathrm{L}) \otimes \mathrm{U_R}(N_\mathrm{R})$ and $\mathrm{U}(2N_\mathrm{f})$ symmetry, respectively. While perturbatively nonrenormalizable, we have shown that these models can indeed be defined nonperturbatively, exhibiting the same amount of universality as any perturbatively renormalizable field theory.

We have generalized the 3d chiral GN model by allowing for a different number of left- and right-handed fermion flavors, reminiscent of the Higgs-Yukawa sector of the particle-physics' standard model (where $N_\mathrm{L} = 2$ and $N_\mathrm{R} = 1$). By means of the functional RG in terms of the Wetterich equation, we have been able to identify a non-Gaußian fixed point for any $N_\mathrm{L} \in [1, \infty]$ with $N_\mathrm{R} = 1$, corresponding to a second-order chiral phase transition. We have provided quantitative predictions for the critical behavior in terms of the universal critical exponents ν, η_ϕ, η_ψ, and ω. Our results support the conjecture that in the $N_\mathrm{L} \to \infty$ limit our $\mathrm{U_L}(N_\mathrm{L}) \otimes \mathrm{U_R}(1)$ is in the universality class of the purely bosonic $\mathrm{O}(2N_\mathrm{L})$ model, in which case the critical exponents are known to very high accuracy. For $N_\mathrm{L} = 1$, our model coincides with the usual one-flavor chiral GN model. In this sense, for intermediate N_L our models "interpolate" between the purely bosonic $\mathrm{O}(2N_\mathrm{L})$ model and the purely fermionic GN model with continuous chiral symmetry. Beyond these two limits, our models define new universality classes, the critical behavior of which has previously been unknown. In general, fluctuating chiral fermions in strongly-correlated systems embody a challenging problem, which so far has been lacking a simpler benchmark example where nonperturbative methods can be tested and optimized. The universality classes defined by our models could fill this gap. For the functional RG, very refined techniques are available for the purely bosonic models [89, 90, 153, 171]; our models, which always allow a cross check on the $\mathrm{O}(2N_\mathrm{L})$ results, could possibly be used to apply these expertise to fermion systems.

Within a simple truncation of the effective action in terms of solely fermionic degrees of freedom, we have obtained a unified picture of the class of maximally symmetric 3d fermion systems, exhibiting $\mathrm{U}(2N_\mathrm{f})$ chiral and a set of discrete symmetries. The Thirring and the NJL model in three dimensions are of this type and we have shown that both are in fact in the same universality class, governed by the same interacting fixed point. We have also identified another interacting fixed point, governing the discrete symmetry breaking of the 3d GN model in the irreducible

representation. While exhibiting the same explicit symmetry, Thirring and GN model at criticality therefore define distinct universality classes. Our findings support the previous results that the chiral symmetry in both the Thirring and the NJL model may be spontaneously broken at small number of fermion flavors and is preserved above a critical flavor number $N_{\mathrm{f}}^{\mathrm{cr}}$ for arbitrary coupling. However, while so far the mechanism for the quantum phase transition at $N_{\mathrm{f}}^{\mathrm{cr}}$ has been rather unknown, we have for the first time provided a possible microscopic explanation: for small N_{f}, the system is dominated by the NJL-type scalar interaction, triggering chiral symmetry breaking; for large N_{f}, the Thirring-type vector interaction governs the flow, prohibiting chiral symmetry breaking.

In order to further elaborate on this scenario, we have advanced our truncation by allowing for composite bosonic degrees of freedom by means of the bosonization technique. For a quantitatively reliable investigation of the competition between the different condensation channels, we have shown that it is necessary to employ a formulation which does not suffer from the Fierz ambiguity. We have done this by performing the Hubbard-Stratonovich transformation at each RG step in terms of dynamical bosonization. As a function of N_{f} for fixed over-critical coupling, we have found a phase transition at a critical flavor number $N_{\mathrm{f}}^{\mathrm{cr}} \simeq 5.1(7)$, which is governed by the *IR* dynamics of the system. By contrast, the phase transition as a function of the bare coupling for fixed $N_{\mathrm{f}} < N_{\mathrm{f}}^{\mathrm{cr}}$ is determined by the RG flow in the *UV* regime. The respective critical phenomena of the two transitions are therefore completely unrelated. For the latter, our RG approach allows to yield very precise predictions; we have computed in detail the values of the universal critical exponents ν, η_ϕ, and ω as a function of N_{f}. We have explicitly shown that the critical behavior of the model defined with pure Thirring-like coupling is in fact governed by our Thirring fixed point. For $N_{\mathrm{f}} = 2$, we have (independently of our results on ν and η_ϕ) also computed the exponents β and γ, showing consistency with the hyperscaling relations below the percent level. In comparison to our UV results, our predictions for the chiral phase transition for fixed coupling with N_{f} as control parameter may be slightly more affected by the systematic errors; nevertheless, our findings clearly advocate a scenario with the transition at $N_{\mathrm{f}}^{\mathrm{cr}}$ being of *second* order.

Whereas most [63, 65–72] (but not all [64]) of the previous studies agree at least on the very existence of a critical flavor number at order $N_{\mathrm{f}}^{\mathrm{cr}} \sim \mathcal{O}(2 \ldots 7)$, the nature of the phase transition has so far been a substantially delicate issue. Based on our detailed predictions, in particular in terms of the universal exponents ν and η_ϕ for the transition at fixed $N_{\mathrm{f}} < N_{\mathrm{f}}^{\mathrm{cr}}$, we believe that it may now be possible to resolve the discrepancies in the literature. For that purpose, we propose an independent investigation of the critical behavior of the 3d Thirring model, for instance, by means of a Monte Carlo simulation with a lattice action exhibiting manifest $\mathrm{U}(2N_{\mathrm{f}})$ symmetry.

To conclude, we suggest that we cannot presume to say that we understand chiral symmetry breaking in the complicated 4d non-Abelian gauge theories with fermions, if we do not even understand flavor symmetry breaking in the putatively simple 3d fermion systems [202].

Bibliography

[1] W. Thirring, *Cosmic impressions: Traces of God in the Laws of Nature* (Templeton Press, 2007).

[2] E. C. G. Stueckelberg and A. Petermann, *Normalization of constants in the quanta theory*, Helv. Phys. Acta **26**, 499 (1953).

[3] M. Gell-Mann and F. E. Low, *Quantum electrodynamics at small distances*, Phys. Rev. **95**, 1300 (1954).

[4] N. N. Bogolyubov and D. V. Shirkov, *Charge renormalization group in quantum field theory*, Nuovo Cim. **3**, 845 (1956).

[5] K. G. Wilson, *Renormalization group and critical phenomena. 1. Renormalization group and the Kadanoff scaling picture*, Phys. Rev. **B4**, 3174 (1971).

[6] K. G. Wilson, *Renormalization group and critical phenomena. 2. Phase space cell analysis of critical behavior*, Phys. Rev. **B4**, 3184 (1971).

[7] K. G. Wilson, *The Renormalization Group and Strong Interactions*, Phys. Rev. **D3**, 1818 (1971).

[8] K. G. Wilson, *Feynman graph expansion for critical exponents*, Phys. Rev. Lett. **28**, 548 (1972).

[9] J. Binney, N. Dowrick, A. Fisher, and M. Newman, *The theory of critical phenomena: an introduction to the renormalization group* (Oxford University Press, New York, 1992).

[10] J. Zinn-Justin, *Quantum field theory and critical phenomena* (Oxford University Press, New York, 1996).

[11] I. Herbut, *A modern approach to critical phenomena* (Cambridge University Press, New York, 2007).

[12] H. D. Politzer, *Reliable perturbative results for strong interactions?*, Phys. Rev. Lett. **30**, 1346 (1973).

[13] D. J. Gross and F. Wilczek, *Ultraviolet behavior of non-abelian gauge theories*, Phys. Rev. Lett. **30**, 1343 (1973).

[14] J. Bardeen, L. N. Cooper, and J. R. Schrieffer, *Theory of superconductivity*, Phys. Rev. **108**, 1175 (1957).

[15] Y. Nambu, *Quasi-particles and gauge invariance in the theory of superconductivity*, Phys. Rev. **117**, 648 (1960).

[16] Y. Nambu, *A 'superconductor' model of elementary particles and its consequences*, Int. J. Mod. Phys. **A23**, 4063 (2008).

[17] P. Kopietz, L. Bartosch, and F. Schütz, *Introduction to the functional renormalization group* (Springer Verlag, Berlin, 2010).

[18] W. E. Thirring, *A soluble relativistic field theory*, Annals Phys. **3**, 91 (1958).

[19] M. Franz and Z. Tesanovic, *Algebraic Fermi Liquid from Phase Fluctuations: 'Topological' Fermions, Vortex 'Berryons', and QED3 Theory of Cuprate Superconductors*, Phys. Rev. Lett. **87**, 257003 (2001).

[20] M. Franz, Z. Tesanovic, and O. Vafek, *QED3 theory of pairing pseudogap in cuprates I: From d- wave superconductor to antiferromagnet via algebraic Fermi liquid*, Phys. Rev. **B66**, 054535 (2002).

[21] I. F. Herbut, *Antiferromagnetism from phase disordering of a d-wave superconductor*, Phys. Rev. Lett. **88**, 047006 (2002).

[22] I. F. Herbut, *QED3 theory of underdoped high temperature superconductors*, Phys. Rev. **B66**, 094504 (2002).

[23] I. F. Herbut, *Effective theory of high-temperature superconductors*, Phys. Rev. Lett. **94**, 237001 (2005).

[24] N. E. Mavromatos and J. Papavassiliou, *Novel Phases and Old Puzzles in QED3 and related models*, Recent Res. Devel. Phys. **5**, 369 (2004).

[25] G. W. Semenoff, *Condensed matter simulation of a three-dimensional anomaly*, Phys. Rev. Lett. **53**, 2449 (1984).

[26] I. F. Herbut, *Interactions and phase transitions on graphene's honeycomb lattice*, Phys. Rev. Lett. **97**, 146401 (2006).

[27] I. F. Herbut, V. Juricic, and B. Roy, *Theory of interacting electrons on the honeycomb lattice*, Phys. Rev. **B79**, 085116 (2009).

[28] J. Drut and T. Lähde, *Is graphene in vacuum an insulator?*, Phys. Rev. Lett. **102**, 26802 (2009).

[29] S. Hands and C. Strouthos, *Quantum Critical Behaviour in a Graphene-like Model*, Phys. Rev. **B78**, 165423 (2008).

[30] W. Armour, S. Hands, and C. Strouthos, *Monte Carlo Simulation of the Semimetal-Insulator Phase Transition in Monolayer Graphene*, Phys. Rev. **B81**, 125105 (2010).

[31] V. P. Gusynin, S. G. Sharapov, and J. P. Carbotte, *AC conductivity of graphene: from tight-binding model to 2+1-dimensional quantum electrodynamics*, Int. J. Mod. Phys. **B21**, 4611 (2007).

[32] K. Novoselov, A. Geim, S. Morozov, D. Jiang, Y. Zhang, S. Dubonos, I. Grigorieva, and A. Firsov, *Electric field effect in atomically thin carbon films*, Science **306**, 666 (2004).

[33] K. Novoselov, A. Geim, S. Morozov, D. Jiang, M. Grigorieva, S. Dubonos, and A. Firsov, *Two-dimensional gas of massless dirac fermions in graphene*, Nature **438**, 197 (2005).

[34] O. Klein, *Die Reflexion von Elektronen an einem Potentialsprung nach der relativistischen Dynamik von Dirac*, Z. Phys. **53**, 157 (1929).

[35] M. Katsnelson, K. Novoselov, and A. Geim, *Chiral tunnelling and the Klein paradox in graphene*, Nature Phys. **2**, 620 (2006).

[36] E. Schroedinger, *Über die kräftefreie Bewegung in der relativistischen Quantenmechanik*, Sitzber. Preuss. Akad. Wiss. Phys.-Math. Kl. **24**, 418 (1930).

[37] M. Katsnelson, *Zitterbewegung, chirality, and minimal conductivity in graphene*, Eur. Phys. J. **C51**, 157 (2006).

[38] J. Tworzydlo, B. Trauzettel, M. Titov, A. Rycerz, and C. Beenakker, *Quantum-limited shot noise in graphene*, Phys. Rev. Lett. **96**, 246802 (2006).

[39] A. Geim and K. Novoselov, *The rise of graphene*, Nature Mat. **6**, 183 (2007).

[40] A. Geim, *Graphene: status and prospects*, Science **324**, 1530 (2009).

[41] A. H. C. Neto, F. Guinea, N. M. R. Peres, K. S. Novoselov, and A. K. Geim, *The electronic properties of graphene*, Rev. Mod. Phys. **81**, 109 (2009).

[42] A. Cortijo, F. Guinea, and M. A. H. Vozmediano, *Geometrical and topological aspects of graphene and related materials*, arXiv:1112.2054 [cond-mat.mes-hall].

[43] R. D. Pisarski, *Chiral Symmetry Breaking in Three-Dimensional Electrodynamics*, Phys. Rev. **D29**, 2423 (1984).

[44] J. M. Cornwall, *Confinement and Chiral Symmetry Breakdown: Estimates of f_π and of Effective Quark Masses*, Phys. Rev. **D22**, 1452 (1980).

[45] S. Rao and R. Yahalom, *Dynamical Breakdown of Symmetries in QED in Three Dimensions*, Phys. Rev. **D34**, 1194 (1986).

[46] T. W. Appelquist, M. J. Bowick, D. Karabali, and L. C. R. Wijewardhana, *Spontaneous Chiral Symmetry Breaking in Three-Dimensional QED*, Phys. Rev. **D33**, 3704 (1986).

[47] T. Appelquist, M. J. Bowick, D. Karabali, and L. C. R. Wijewardhana, *Spontaneous breaking of parity in (2+1)-dimensional QED*, Phys. Rev. **D33**, 3774 (1986).

[48] T. Appelquist, D. Nash, and L. C. R. Wijewardhana, *Critical Behavior in (2+1)-Dimensional QED*, Phys. Rev. Lett. **60**, 2575 (1988).

[49] D. Nash, *Higher Order Corrections in (2+1)-Dimensional QED*, Phys. Rev. Lett. **62**, 3024 (1989).

[50] P. Maris, *The influence of the full vertex and vacuum polarization on the fermion propagator in QED3*, Phys. Rev. **D54**, 4049 (1996).

[51] K. Kubota and H. Terao, *Dynamical symmetry breaking in QED(3) from the Wilson RG point of view*, Prog. Theor. Phys. **105**, 809 (2001).

[52] K. Kaveh and I. F. Herbut, *Chiral symmetry breaking in QED(3) in presence of irrelevant interactions: A renormalization group study*, Phys. Rev. **B71**, 184519 (2005).

[53] S. J. Hands, J. B. Kogut, and C. G. Strouthos, *Non-compact QED(3) with $N_f \geq 2$*, Nucl. Phys. **B645**, 321 (2002).

[54] S. J. Hands, J. B. Kogut, L. Scorzato, and C. G. Strouthos, *Non-compact QED(3) with $N_f = 1$ and $N_f = 4$*, Phys. Rev. **B70**, 104501 (2004).

[55] V. P. Gusynin and M. Reenders, *Infrared cutoff dependence of the critical flavor number in QED(3)*, Phys. Rev. **D68**, 025017 (2003).

[56] C. S. Fischer, R. Alkofer, T. Dahm, and P. Maris, *Dynamical chiral symmetry breaking in unquenched QED(3)*, Phys. Rev. **D70**, 073007 (2004).

[57] A. Bashir, A. Raya, S. Sanchez-Madrigal, and C. D. Roberts, *Gauge invariance of a critical number of flavours in QED3*, Few Body Syst. **46**, 229 (2009).

[58] W. Li and G.-Z. Liu, *Dynamical chiral symmetry breaking in QED_3 at finite density and impurity potential*, Phys. Rev. **D81**, 045006 (2010).

[59] V. P. Gusynin, V. A. Miransky, and A. V. Shpagin, *Effective action and conformal phase transition in QED(3)*, Phys. Rev. **D58**, 085023 (1998).

[60] G. Parisi, *The Theory of Nonrenormalizable Interactions. 1. The Large N Expansion*, Nucl. Phys. **B100**, 368 (1975).

[61] S. Hikami and T. Muta, *Fixed Points and Anomalous Dimensions in O(n) Thirring Model at Two + Epsilon Dimensions*, Prog. Theor. Phys. **57**, 785 (1977).

[62] S. Hands, *$O(1/N_f)$ corrections to the Thirring model in $2 < d < 4$*, Phys. Rev. **D51**, 5816 (1995).

[63] M. Gomes, R. S. Mendes, R. F. Ribeiro, and A. J. da Silva, *Gauge structure, anomalies and mass generation in a three- dimensional Thirring model*, Phys. Rev. **D43**, 3516 (1991).

[64] D. K. Hong and S. H. Park, *Large N analysis of (2+1)-dimensional Thirring model*, Phys. Rev. **D49**, 5507 (1994).

[65] T. Itoh, Y. Kim, M. Sugiura, and K. Yamawaki, *Thirring model as a gauge theory*, Prog. Theor. Phys. **93**, 417 (1995).

[66] M. Sugiura, *Fermion mass generation in the D-dimensional Thirring model as a gauge theory*, Prog. Theor. Phys. **97**, 311 (1997).

[67] K. Kondo, *Thirring model as a gauge theory*, Nucl. Phys. **B450**, 251 (1995).

[68] S. Kim and Y. Kim, *Lattice gauge theory of three-dimensional Thirring model*, arXiv:hep-lat/9605021.

[69] L. Del Debbio, S. J. Hands, and J. C. Mehegan (UKQCD), *Three-dimensional Thirring model for small N_f*, Nucl. Phys. **B502**, 269 (1997).

[70] L. Del Debbio and S. J. Hands, *The three dimensional Thirring model for $N_f = 4$ and $N_f = 6$*, Nucl. Phys. **B552**, 339 (1999).

[71] S. Hands and B. Lucini, *The phase diagram of the three dimensional Thirring model*, Phys. Lett. **B461**, 263 (1999).

[72] S. Christofi, S. Hands, and C. Strouthos, *Critical flavor number in the three dimensional Thirring model*, Phys. Rev. **D75**, 101701 (2007).

[73] S. Chandrasekharan and A. Li, *Fermion bags, duality and the three dimensional massless lattice Thirring model*, arXiv:1111.7204 [hep-lat].

[74] V. A. Miransky and K. Yamawaki, *Conformal phase transition in gauge theories*, Phys. Rev. **D55**, 5051 (1997), [Erratum-ibid.D56:3768,1997].

[75] T. Appelquist, J. Terning, and L. C. R. Wijewardhana, *The Zero Temperature Chiral Phase Transition in SU(N) Gauge Theories*, Phys. Rev. Lett. **77**, 1214 (1996).

[76] M. Harada, M. Kurachi, and K. Yamawaki, *Meson masses in large N_f QCD from Bethe-Salpeter equation*, Phys. Rev. **D68**, 076001 (2003).

[77] Y. Iwasaki, K. Kanaya, S. Kaya, S. Sakai, and T. Yoshie, *Phase structure of lattice QCD for general number of flavors*, Phys. Rev. **D69**, 014507 (2004).

[78] H. Gies and J. Jaeckel, *Chiral phase structure of QCD with many flavors*, Eur. Phys. J. **C46**, 433 (2006).

[79] T. A. Ryttov and F. Sannino, *Supersymmetry Inspired QCD Beta Function*, Phys. Rev. **D78**, 065001 (2008).

[80] H. S. Fukano and F. Sannino, *Conformal Window of Gauge Theories with Four-Fermion Interactions and Ideal Walking*, Phys. Rev. **D82**, 035021 (2010).

[81] L. Vecchi, *The Conformal Window of deformed CFT's in the planar limit*, Phys. Rev. **D82**, 045013 (2010).

[82] L. Del Debbio, B. Lucini, A. Patella, C. Pica, and A. Rago, *The infrared dynamics of Minimal Walking Technicolor*, Phys. Rev. **D82**, 014510 (2010).

[83] J. Braun and H. Gies, *Running coupling at finite temperature and chiral symmetry restoration in QCD*, Phys. Lett. **B645**, 53 (2007).

[84] J. Braun and H. Gies, *Chiral phase boundary of QCD at finite temperature*, JHEP **06**, 024 (2006).

[85] J. Braun and H. Gies, *Scaling laws near the conformal window of many-flavor QCD*, JHEP **05**, 060 (2010).

[86] J. Braun, C. S. Fischer, and H. Gies, *Beyond Miransky Scaling*, Phys. Rev. **D84**, 034045 (2011).

[87] J. Braun, *Fermion Interactions and Universal Behavior in Strongly Interacting Theories*, J. Phys. **G39**, 033001 (2012).

[88] M. Hasenbusch, *A finite size scaling study of lattice models in the three-dimensional ising universality class*, Phys. Rev. **B82**, 174433 (2010).

[89] D. F. Litim and D. Zappala, *Ising exponents from the functional renormalisation group*, Phys. Rev. **D83**, 085009 (2011).

[90] F. Benitez *et al.*, *Non-perturbative renormalization group preserving full momentum dependence: implementation and quantitative evaluation*, arXiv:1110.2665 [cond-mat.stat-mech].

[91] J. Sengers and J. Shanks, *Experimental critical-exponent values for fluids*, Journal of Statistical Physics **137**, 857 (2009).

[92] D. J. Gross and A. Neveu, *Dynamical Symmetry Breaking in Asymptotically Free Field Theories*, Phys. Rev. **D10**, 3235 (1974).

[93] Y. Nambu and G. Jona-Lasinio, *Dynamical model of elementary particles based on an analogy with superconductivity. I*, Phys. Rev. **122**, 345 (1961).

[94] Y. Nambu and G. Jona-Lasinio, *Dynamical model of elementary particles based on an analogy with superconductivity. II*, Phys. Rev. **124**, 246 (1961).

[95] V. P. Gusynin, V. A. Miransky, and I. A. Shovkovy, *Catalysis of dynamical flavor symmetry breaking by a magnetic field in (2+1)-dimensions*, Phys. Rev. Lett. **73**, 3499 (1994), [Erratum-ibid.76:1005,1996].

[96] J. A. Gracey, *The Beta function of the chiral Gross-Neveu model at $O(1/N^2)$*, Phys. Rev. **D50**, 2840 (1994), [Erratum-ibid.D59:109904,1999].

[97] I. M. Barbour, N. Psycharis, E. Focht, W. Franzki, and J. Jersak (UKQCD), *Strongly coupled lattice gauge theory with dynamical fermion mass generation in three dimensions*, Phys. Rev. **D58**, 074507 (1998).

[98] S. J. Hands, J. B. Kogut, and C. G. Strouthos, *The (2+1)-dimensional Gross-Neveu model with a U(1) chiral symmetry at non-zero temperature*, Phys. Lett. **B515**, 407 (2001).

[99] S. Christofi and C. Strouthos, *Three dimensional four-fermion models - A Monte Carlo study*, JHEP **05**, 088 (2007).

[100] J. A. Gracey, *Computation of $\beta'(g_c)$ at $O(1/N^2)$ in the O(N) Gross-Neveu model in arbitrary dimensions*, Int. J. Mod. Phys. **A9**, 567 (1994).

[101] L. Karkkainen, R. Lacaze, P. Lacock, and B. Petersson, *Critical behavior of the 3d Gross-Neveu and Higgs-Yukawa models*, Nucl. Phys. **B415**, 781 (1994), [Erratum-ibid.B438:650,1995].

[102] J. A. Gracey, *The Nambu-Jona-Lasinio model at $O(1/N^2)$*, Phys. Lett. **B308**, 65 (1993).

[103] J. A. Gracey, *Computation of critical exponent eta at $O(1/N^3)$ in the four Fermi model in arbitrary dimensions*, Int. J. Mod. Phys. **A9**, 727 (1994).

[104] S. Hands, A. Kocic, and J. B. Kogut, *Four Fermi theories in fewer than four-dimensions*, Ann. Phys. **224**, 29 (1993).

[105] L. Rosa, P. Vitale, and C. Wetterich, *Critical exponents of the Gross-Neveu model from the effective average action*, Phys. Rev. Lett. **86**, 958 (2001).

[106] F. Hofling, C. Nowak, and C. Wetterich, *Phase transition and critical behaviour of the $d = 3$ Gross-Neveu model*, Phys. Rev. **B66**, 205111 (2002).

[107] J. Braun, H. Gies, and D. D. Scherer, *Asymptotic safety: a simple example*, Phys. Rev. **D83**, 085012 (2011).

[108] T. Banks, L. Susskind, and J. B. Kogut, *Strong Coupling Calculations of Lattice Gauge Theories: (1+1)-Dimensional Exercises*, Phys. Rev. **D13**, 1043 (1976).

[109] L. Susskind, *Lattice Fermions*, Phys. Rev. **D16**, 3031 (1977).

[110] C. Burden and A. N. Burkitt, *Lattice fermions in odd dimensions*, Europhys. Lett. **3**, 545 (1987).

[111] C. Wetterich, *Exact evolution equation for the effective potential*, Phys. Lett. **B301**, 90 (1993).

[112] J. Berges, N. Tetradis, and C. Wetterich, *Non-perturbative renormalization flow in quantum field theory and statistical physics*, Phys. Rept. **363**, 223 (2002).

[113] C. Bagnuls and C. Bervillier, *Exact renormalization group equations: An introductory review*, Phys. Rept. **348**, 91 (2001).

[114] K. Aoki, *Introduction to the nonperturbative renormalization group and its recent applications*, Int. J. Mod. Phys. **B14**, 1249 (2000).

[115] J. Polonyi, *Lectures on the functional renormalization group method*, Central Eur. J. Phys. **1**, 1 (2003).

[116] J. M. Pawlowski, *Aspects of the functional renormalisation group*, Annals Phys. **322**, 2831 (2007).

[117] H. Gies, *Introduction to the functional RG and applications to gauge theories*, arXiv:hep-ph/0611146.

[118] B. Delamotte, *An introduction to the nonperturbative renormalization group*, arXiv:cond-mat/0702365.

[119] H. Sonoda, *The Exact Renormalization Group – renormalization theory revisited –*, arXiv:0710.1662 [hep-th].

[120] W. Metzner, M. Salmhofer, C. Honerkamp, V. Meden, and K. Schonhammer, *Functional renormalization group approach to correlated fermion systems*, arXiv:1105.5289 [cond-mat.str-el].

[121] P. J. Redmond and J. L. Uretsky, *Conjecture concerning the properties of nonrenormalizable field theories*, Phys. Rev. Lett. **1**, 147 (1958).

[122] K. Symanzik, *Renormalization Problem in Nonrenormalizable Massless ϕ^4 Theory*, Commun. Math. Phys. **45**, 79 (1975).

[123] K. Gawedzki and A. Kupiainen, *Renormalizing the Nonrenormalizable*, Phys. Rev. Lett. **55**, 363 (1985).

[124] G. Felder and G. Gallavotti, *Perturbation Theory and Nonrenormalizable Scalar Fields*, Commun. Math. Phys. **102**, 549 (1986).

[125] B. Rosenstein, B. J. Warr, and S. H. Park, *The Four Fermi Theory Is Renormalizable in (2+1)- Dimensions*, Phys. Rev. Lett. **62**, 1433 (1989).

[126] B. Rosenstein, B. Warr, and S. H. Park, *Dynamical symmetry breaking in four Fermi interaction models*, Phys. Rept. **205**, 59 (1991).

[127] S. Weinberg, in S. Hawking and W. Israel, eds., *General Relativity* (Cambridge University Press, Cambridge, 1979), pp. 790–831.

[128] M. Niedermaier and M. Reuter, *The Asymptotic Safety Scenario in Quantum Gravity*, Living Rev. Rel. **9**, 5 (2006).

[129] R. Percacci, *Asymptotic Safety*, arXiv:0709.3851 [hep-th].

[130] O. J. Rosten, *Fundamentals of the Exact Renormalization Group*, arXiv:1003.1366 [hep-th].

[131] H. Gies, L. Janssen, S. Rechenberger, and M. M. Scherer, *Phase transition and critical behavior of d=3 chiral fermion models with left-right asymmetry*, Phys. Rev. **D81**, 025009 (2010).

[132] S. Rechenberger, *Asymptotic Safety of Yukawa Systems*, Diploma thesis, University of Jena (2010).

[133] M. M. Scherer, *Effective and fundamental quantum fields at criticality*, Ph.D. thesis, University of Jena (2010).

[134] H. Gies and L. Janssen, *UV fixed-point structure of the three-dimensional Thirring model*, Phys. Rev. **D82**, 085018 (2010).

[135] L. O'Raifeartaigh, A. Wipf, and H. Yoneyama, *The constraint effective potential*, Nucl. Phys. **B271**, 653 (1986).

[136] F. Schuetz, L. Bartosch, and P. Kopietz, *Collective fields in the functional renormalization group for fermions, ward identities, and the exact solution of the tomonaga-luttinger model*, Phys. Rev. **B72**, 035107 (2005).

[137] J. Keitel and L. Bartosch, *The zero-dimensional O(N) vector model as a benchmark for perturbation theory, the large-N expansion and the functional renormalization group*, J. Phys. **A45**, 105401 (2012).

[138] R. D. Ball, P. E. Haagensen, I. J. Latorre, and E. Moreno, *Scheme independence and the exact renormalization group*, Phys. Lett. **B347**, 80 (1995).

[139] S.-B. Liao, J. Polonyi, and M. Strickland, *Optimization of renormalization group flow*, Nucl. Phys. **B567**, 493 (2000).

[140] D. F. Litim, *Optimisation of the exact renormalisation group*, Phys. Lett. **B486**, 92 (2000).

[141] D. F. Litim, *Optimised renormalisation group flows*, Phys. Rev. **D64**, 105007 (2001).

[142] L. Canet, B. Delamotte, D. Mouhanna, and J. Vidal, *Optimization of the derivative expansion in the nonperturbative renormalization group*, Phys. Rev. **D67**, 065004 (2003).

[143] L. Canet, B. Delamotte, D. Mouhanna, and J. Vidal, *Nonperturbative renormalization group approach to the Ising model: a derivative expansion at order ∂^4*, Phys. Rev. **B68**, 064421 (2003).

[144] M. Reuter and F. Saueressig, *Renormalization group flow of quantum gravity in the Einstein-Hilbert truncation*, Phys. Rev. **D65**, 065016 (2002).

[145] F. Freire and D. F. Litim, *Charge cross-over at the U(1)-Higgs phase transition*, Phys. Rev. **D64**, 045014 (2001).

[146] K. G. Wilson and M. E. Fisher, *Critical exponents in 3.99 dimensions*, Phys. Rev. Lett. **28**, 240 (1972).

[147] M. Fisher and R. Burford, *Theory of critical-point scattering and correlations. I. The Ising model*, Phys. Rev. **156**, 583 (1967).

[148] D. Ritchie and M. Fisher, *Theory of critical-point scattering and correlations. II. Heisenberg models*, Phys. Rev. **B5**, 2668 (1972).

[149] H. Tarko and M. Fisher, *Theory of critical point scattering and correlations. III. The Ising model below T_c and in a field*, Phys. Rev. **B11**, 1217 (1975).

[150] N. Tetradis and C. Wetterich, *Critical exponents from effective average action*, Nucl. Phys. **B422**, 541 (1994).

[151] H. Gies and M. M. Scherer, *Asymptotic safety of simple Yukawa systems*, Eur. Phys. J. **C66**, 387 (2010).

[152] H. Gies, S. Rechenberger, and M. M. Scherer, *Towards an Asymptotic-Safety Scenario for Chiral Yukawa Systems*, Eur. Phys. J. **C66**, 403 (2010).

[153] F. Benitez *et al.*, *Solutions of renormalization group flow equations with full momentum dependence*, Phys. Rev. **E80**, 030103 (2009).

[154] K. Osterwalder and R. Schrader, *Axioms for Euclidean Green's functions*, Commun. Math. Phys. **31**, 83 (1973).

[155] C. Wetterich, *Spinors in euclidean field theory, complex structures and discrete symmetries*, Nucl. Phys. **B852**, 174 (2011).

[156] C. Wetterich, *Quadratic renormalization of the average potential and the naturalness of quadratic mass relations for the top quark*, Z. Phys. **C48**, 693 (1990).

[157] R. Jackiw and S. Templeton, *How Superrenormalizable Interactions Cure their Infrared Divergences*, Phys. Rev. **D23**, 2291 (1981).

[158] I. Affleck, J. A. Harvey, and E. Witten, *Instantons and (Super)Symmetry Breaking in (2+1)-Dimensions*, Nucl. Phys. **B206**, 413 (1982).

[159] B.-J. Schaefer and H.-J. Pirner, *The equation of state of quarks and mesons in a renormalization group flow picture*, Nucl. Phys. **A660**, 439 (1999).

[160] B.-J. Schaefer and J. Wambach, *The phase diagram of the quark meson model*, Nucl. Phys. **A757**, 479 (2005).

[161] H. Gies and C. Wetterich, *Renormalization flow of bound states*, Phys. Rev. **D65**, 065001 (2002).

[162] H. Gies and C. Wetterich, *Universality of spontaneous chiral symmetry breaking in gauge theories*, Phys. Rev. **D69**, 025001 (2004).

[163] J. Braun, *The QCD Phase Boundary from Quark-Gluon Dynamics*, Eur. Phys. J. **C64**, 459 (2009).

[164] J. Braun, *Thermodynamics of QCD low-energy models and the derivative expansion of the effective action*, Phys. Rev. **D81**, 016008 (2010).

[165] D. U. Jungnickel and C. Wetterich, *Effective action for the chiral quark-meson model*, Phys. Rev. **D53**, 5142 (1996).

[166] M. C. Birse, B. Krippa, J. A. McGovern, and N. R. Walet, *Pairing in many-fermion systems: An exact renormalisation group treatment*, Phys. Lett. **B605**, 287 (2005).

[167] S. Diehl, H. Gies, J. M. Pawlowski, and C. Wetterich, *Renormalisation Flow and Universality for Ultracold Fermionic Atoms*, Phys. Rev. **A76**, 053627 (2007).

[168] S. Diehl, H. Gies, J. M. Pawlowski, and C. Wetterich, *Flow Equations for the BCS-BEC Crossover*, Phys. Rev. **A76**, 021602 (2007).

[169] S. Floerchinger, M. Scherer, S. Diehl, and C. Wetterich, *Particle-hole fluctuations in the BCS-BEC Crossover*, Phys. Rev. **B78**, 174528 (2008).

[170] S. Floerchinger, M. M. Scherer, and C. Wetterich, *Modified Fermi-sphere, pairing gap and critical temperature for the BCS-BEC crossover*, Phys. Rev. **A81**, 063619 (2010).

[171] J. P. Blaizot, R. Mendez Galain, and N. Wschebor, *A new method to solve the non perturbative renormalization group equations*, Phys. Lett. **B632**, 571 (2006).

[172] J.-P. Blaizot, *Renormalization group flow equations with full momentum dependence*, Phil. Trans. Roy. Soc. Lond. **A369**, 2735 (2011).

[173] Y. Nambu, in *Kazimierz 1988, Proceedings, New Theories in Physics* (World Scientific, 1989), pp. 1–10.

[174] V. A. Miransky, M. Tanabashi, and K. Yamawaki, *Dynamical Electroweak Symmetry Breaking with Large Anomalous Dimension and t Quark Condensate*, Phys. Lett. **B221**, 177 (1989).

[175] V. A. Miransky, M. Tanabashi, and K. Yamawaki, *Is the t Quark Responsible for the Mass of W and Z Bosons?*, Mod. Phys. Lett. **A4**, 1043 (1989).

[176] W. A. Bardeen, C. T. Hill, and M. Lindner, *Minimal Dynamical Symmetry Breaking of the Standard Model*, Phys. Rev. **D41**, 1647 (1990).

[177] J. Zinn-Justin, *Four fermion interaction near four-dimensions*, Nucl. Phys. **B367**, 105 (1991).

[178] A. Hasenfratz, P. Hasenfratz, K. Jansen, J. Kuti, and Y. Shen, *The Equivalence of the top quark condensate and the elementary Higgs field*, Nucl. Phys. **B365**, 79 (1991).

[179] K.-I. Aoki, K.-I. Morikawa, J.-I. Sumi, H. Terao, and M. Tomoyose, *Non-perturbative renormalization group analysis of the chiral critical behaviors in QED*, Prog. Theor. Phys. **97**, 479 (1997).

[180] A. N. Vasiliev, S. E. Derkachov, N. A. Kivel, and A. S. Stepanenko, *The 1/n expansion in the Gross-Neveu model: Conformal bootstrap calculation of the index eta in order* $1/n^3$, Theor. Math. Phys. **94**, 127 (1993), [Teor.Mat.Fiz.94:179-192,1993].

[181] C. J. Halboth and W. Metzner, *d-Wave Superconductivity and Pomeranchuk Instability in the Two-Dimensional Hubbard Model*, Phys. Rev. Lett. **85**, 5162 (2000).

[182] C. J. Halboth and W. Metzner, *Renormalization-group analysis of the two-dimensional Hubbard model*, Phys. Rev. **B61**, 7364 (2000).

[183] M. Salmhofer and C. Honerkamp, *Fermionic renormalization group flows: Technique and theory*, Prog. Theor. Phys. **105**, 1 (2001).

[184] C. Honerkamp and W. Hofstetter, *Ultracold fermions and the SU(N) Hubbard model*, Phys. Rev. Lett. **92**, 170403 (2004).

[185] H. C. Krahl, J. A. Müller, and C. Wetterich, *Generation of d-wave coupling in the two-dimensional hubbard model from functional renormalization*, Phys. Rev. **B79**, 094526 (2009).

[186] M. Reuter, *Nonperturbative Evolution Equation for Quantum Gravity*, Phys. Rev. **D57**, 971 (1998).

[187] O. Lauscher and M. Reuter, *Ultraviolet fixed point and generalized flow equation of quantum gravity*, Phys. Rev. **D65**, 025013 (2002).

[188] W. Souma, *Non-trivial ultraviolet fixed point in quantum gravity*, Prog. Theor. Phys. **102**, 181 (1999).

[189] P. Forgacs and M. Niedermaier, *A fixed point for truncated quantum Einstein gravity*, arXiv:hep-th/0207028.

[190] R. Percacci and D. Perini, *Asymptotic safety of gravity coupled to matter*, Phys. Rev. **D68**, 044018 (2003).

[191] A. Codello, R. Percacci, and C. Rahmede, *Ultraviolet properties of f(R)-gravity*, Int. J. Mod. Phys. **A23**, 143 (2008).

[192] D. Benedetti, P. F. Machado, and F. Saueressig, *Asymptotic safety in higher-derivative gravity*, Mod. Phys. Lett. **A24**, 2233 (2009).

[193] D. Benedetti, P. F. Machado, and F. Saueressig, *Taming perturbative divergences in asymptotically safe gravity*, Nucl. Phys. **B824**, 168 (2010).

[194] A. Eichhorn, H. Gies, and M. M. Scherer, *Asymptotically free scalar curvature-ghost coupling in Quantum Einstein Gravity*, Phys. Rev. **D80**, 104003 (2009).

[195] H. Gies, *Renormalizability of gauge theories in extra dimensions*, Phys. Rev. **D68**, 085015 (2003).

[196] H. Gies, J. Jaeckel, and C. Wetterich, *Towards a renormalizable standard model without fundamental Higgs scalar*, Phys. Rev. **D69**, 105008 (2004).

[197] S. Floerchinger and C. Wetterich, *Exact flow equation for composite operators*, Phys. Lett. **B680**, 371 (2009).

[198] M. Salmhofer, C. Honerkamp, W. Metzner, and O. Lauscher, *Renormalization group flows into phases with broken symmetry*, Prog. Theor. Phys. **112**, 943 (2004).

[199] P. Strack, S. Takei, and W. Metzner, *Anomalous scaling of fermions and order parameter fluctuations at quantum criticality*, Phys. Rev. **B81**, 125103 (2010).

[200] T. Baier, E. Bick, and C. Wetterich, *Spontaneous symmetry breaking in the colored Hubbard model*, Phys. Rev. **B62**, 15471 (2000).

[201] J. Jaeckel and C. Wetterich, *Flow equations without mean field ambiguity*, Phys. Rev. **D68**, 025020 (2003).

[202] R. D. Pisarski, *Fermion mass in three-dimensions and the renormalization group*, Phys. Rev. **D44**, 1866 (1991).

[203] M. Q. Huber and J. Braun, *Algorithmic derivation of functional renormalization group equations and Dyson-Schwinger equations*, arXiv:1102.5307 [hep-th].

[204] Y. Hosotani, *Spontaneously broken Lorentz invariance in three- dimensional gauge theories*, Phys. Lett. **B319**, 332 (1993).

[205] Y. Hosotani, *Spontaneous breakdown of the Lorentz invariance*, Phys. Rev. **D51**, 2022 (1995).

[206] D. Wesolowski and Y. Hosotani, *Spontaneous magnetization in Lorentz invariant theories*, Phys. Lett. **B354**, 396 (1995).

[207] K. Higashijima and N. Yokoi, *Spontaneous Lorentz symmetry breaking by anti-symmetric tensor field*, Phys. Rev. **D64**, 025004 (2001).

[208] V. R. Khalilov, *A (2+1)-dimensional gauge model with electrically charged fermions*, Theor. Math. Phys. **140**, 1229 (2004), [Teor.Mat.Fiz.140N3:396-409,2004].

[209] S. Hands, *Fixed point four-Fermi theories*, arXiv:hep-lat/9706018.

[210] F. Lamprecht, *Confinement in Polyakov-Eichung und Flussgleichungen dynamischer Freiheitsgrade*, Diploma thesis, University of Heidelberg (2007).

[211] Z. Yang, *1/N expansion and vector-fermion couplings in odd dimensions*, Texas preprint UTTG-40-90 (1990) (unpublished).

[212] P. I. Fomin, V. P. Gusynin, V. A. Miransky, and Y. A. Sitenko, *Dynamical Symmetry Breaking and Particle Mass Generation in Gauge Field Theories*, Riv. Nuovo Cim. **6N5**, 1 (1983).

[213] V. A. Miransky, *Dynamics of Spontaneous Chiral Symmetry Breaking and Continuum Limit in Quantum Electrodynamics*, Nuovo Cim. **A90**, 149 (1985).

[214] V. L. Berezinsky, *Destruction of long range order in one-dimensional and two-dimensional systems possessing a continuous symmetry group. I. Classical systems*, Sov. Phys. JETP **32**, 493 (1971).

[215] V. L. Berezinsky, *Destruction of long-range order in one-dimensional and two-dimensional systems possessing a continuous symmetry group. II. Quantum systems*, Sov. Phys. JETP **34**, 610 (1972).

[216] J. M. Kosterlitz and D. J. Thouless, *Ordering, metastability and phase transitions in two-dimensional systems*, J. Phys. **C6**, 1181 (1973).

[217] J. M. Kosterlitz, *The critical properties of the two-dimensional xy model*, J. Phys. **C7**, 1046 (1974).

[218] D. B. Kaplan, J.-W. Lee, D. T. Son, and M. A. Stephanov, *Conformality Lost*, Phys. Rev. **D80**, 125005 (2009).

[219] K. G. Wilson, in A. Zichichi, ed., *New Phenomena in Subnuclear Physics* (Plenum Press, New York, 1977).

[220] D. B. Kaplan, *A Method for simulating chiral fermions on the lattice*, Phys. Lett. **B288**, 342 (1992).

[221] Y. Shamir, *Chiral fermions from lattice boundaries*, Nucl. Phys. **B406**, 90 (1993).

[222] V. Furman and Y. Shamir, *Axial symmetries in lattice QCD with Kaplan fermions*, Nucl. Phys. **B439**, 54 (1995).

[223] H. Neuberger, *Exactly massless quarks on the lattice*, Phys. Lett. **B417**, 141 (1998).

Appendix A

Fierz identities

Let $(\gamma_A, \gamma_B) \coloneqq \mathrm{Tr}(\gamma_A \gamma_B)$ define an inner product on the space of 4×4 Dirac matrices. The 16 matrices $\{\gamma_A\}$ in Eq. (4.22) are orthogonal with respect to this product,

$$\mathrm{Tr}(\gamma_A \gamma_B) = 4\delta_{AB}, \tag{A.1}$$

and thus define a complete basis of the 4×4 Dirac matrices (which generically have 16 independent matrix elements),

$$\sum_{A=1}^{16} \frac{1}{4} (\gamma_A)_{m\ell} (\gamma_A)_{ik} = \delta_{mk}\delta_{i\ell}. \tag{A.2}$$

The Fierz identities are straightforwardly obtained by multiplying the completeness relation (A.2) by each of the four-fermi terms $\bar{\psi}^a_m (\gamma_A \psi^b)_k \bar{\psi}^c_i (\gamma_A \psi^d)_\ell$ and, where appropriate, decomposing multiple products of Dirac matrices into basis elements γ_A. We find

$$\left(\bar{\psi}^a \gamma_A \psi^b\right) \left(\bar{\psi}^c \gamma_A \psi^d\right) = \sum_{B=1}^{16} C_{AB} \left(\bar{\psi}^a \gamma_B \psi^d\right) \left(\bar{\psi}^c \gamma_B \psi^b\right) \tag{A.3}$$

with

$$(C_{AB}) = \frac{1}{4} \begin{pmatrix} -1 & -1 & -1 & -1 & -1 & -1 & -1 & -1 \\ -3 & 1 & 3 & 1 & -1 & -1 & -3 & 3 \\ -1 & 1 & -1 & -1 & 1 & -1 & 1 & 1 \\ -3 & 1 & -3 & 1 & 1 & 1 & -3 & -3 \\ -3 & -1 & 3 & 1 & 1 & -1 & 3 & -3 \\ -3 & -1 & -3 & 1 & -1 & 1 & 3 & 3 \\ -1 & -1 & 1 & -1 & 1 & 1 & -1 & 1 \\ -1 & 1 & 1 & -1 & -1 & 1 & 1 & -1 \end{pmatrix} \tag{A.4}$$

and $(\gamma_A) = (\mathbb{1}_4, \gamma_\mu, \gamma_4, \gamma_{\mu\nu}, \mathrm{i}\gamma_\mu\gamma_4, \mathrm{i}\gamma_\mu\gamma_5, \gamma_{45}, \gamma_5)$. With these preliminaries one can simply read off the Fierz relations (4.27) between the invariant four-fermi interactions in Eqs. (4.24), (4.25) and (4.26).

Everything is much simpler in the irreducible two-component representation as outlined in Sec. 4.1. Here, the completeness relation is given by

$$\sum_{A=0}^{3} \frac{1}{2} (\sigma_A)_{m\ell} (\sigma_A)_{ik} = \delta_{mk} \delta_{i\ell}, \tag{A.5}$$

where we have used the fact that the standard Pauli matrices $\{\sigma_\mu\}_{\mu=1,2,3}$ together with the unit matrix $\sigma_0 \equiv \mathbb{1}_2$ define a complete basis of the 2×2 Dirac matrices. Therewith, the Fierz identities read

$$\left(\bar{\chi}^a \sigma_A \chi^b\right) \left(\bar{\chi}^c \sigma_A \chi^d\right) = \sum_{B=0}^{3} C_{AB} \left(\bar{\chi}^a \sigma_B \chi^d\right) \left(\bar{\chi}^c \sigma_B \chi^b\right) \tag{A.6}$$

with $\sigma_A = (\mathbb{1}, \sigma_\mu)$ and

$$(C_{AB}) = \frac{1}{2} \begin{pmatrix} -1 & -1 \\ -3 & 1 \end{pmatrix}, \tag{A.7}$$

in consistency with Eqs. (A.4) and (4.27).

Appendix B

Computation of loop integrals

The regulator functions R_k are often written in terms of dimensionless shape functions r_k via

$$R_{\phi,k}(q) = Z_{\phi,k} q^2 r_{\phi,k}(q^2), \qquad R_{\psi,k}(q) = -Z_{\psi,k} \not{q} r_{\psi,k}(q^2), \tag{B.1}$$

with collective bosonic and fermionic fields $\phi = (\phi^{ab}, V_\mu, \dots)$ and $\psi = (\psi^a, \dots)$, respectively. The linear cutoff, which satisfies an optimization criterion [141], reads

$$r^{\text{opt}}_{\phi,k}(q^2) = \left(\frac{k^2}{q^2} - 1\right)\Theta(k^2 - q^2), \qquad r^{\text{opt}}_{\psi,k}(q^2) = \left(\sqrt{\frac{k^2}{q^2}} - 1\right)\Theta(k^2 - q^2). \tag{B.2}$$

The sharp cutoff is defined as the $a \to \infty$ limit of the class of regulators given by

$$r^{\text{sc}}_{\phi,k}(q^2) = a\left(\frac{k^2}{q^2} - 1\right)\Theta(k^2 - q^2), \quad r^{\text{sc}}_{\psi,k}(q^2) = \left(\sqrt{a\left(\frac{k^2}{q^2} - \frac{a-1}{a}\right)} - 1\right)\Theta(k^2 - q^2), \tag{B.3}$$

where we demand for definiteness that the sharp-cutoff limit $a \to \infty$ is to be taken *after* the integration over the internal momentum q, i.e., after the substitution into the threshold functions [144].

The one-loop structure of the Wetterich equation guarantees that the flow equations can always be written in terms of single integrals—the threshold functions, which encode the details of the regularization scheme. Their definitions are

$$\ell_0^{(\text{B/F})d}(\omega; \eta_{\phi/\psi}) = \frac{1}{2} k^{-d}\, \tilde{\partial}_t \int_0^\infty \mathrm{d}x\, x^{\frac{d}{2}-1} \log\left[P_{\phi/\psi}(x) + \omega k^2\right], \tag{B.4}$$

$$\begin{aligned}\ell_n^{(\text{B/F})d}(\omega; \eta_{\phi/\psi}) &= \frac{(-1)^n}{(n-1)!}\partial_\omega^n \ell_0^{(\text{B/F})d}(\omega; \eta_{\phi/\psi}) \\ &= -\frac{1}{2} k^{2n-d}\, \tilde{\partial}_t \int_0^\infty \mathrm{d}x\, x^{\frac{d}{2}-1} \left[P_{\phi/\psi}(x) + \omega k^2\right]^{-n},\end{aligned} \tag{B.5}$$

$$\ell^{(\text{BB})d}_{n_1,n_2}(\omega_1, \omega_2; \eta_\phi, \eta_V) = -\frac{1}{2} k^{2(n_1+n_2)-d}\, \tilde{\partial}_t \int_0^\infty \mathrm{d}x\, x^{\frac{d}{2}-1} \left[P_\phi(x) + \omega_1 k^2\right]^{-n_1} \left[P_V(x) + \omega_2 k^2\right]^{-n_2}, \tag{B.6}$$

$$\ell^{(\text{FB})d}_{n_1,n_2}(\omega_1, \omega_2; \eta_\psi, \eta_\phi) = -\frac{1}{2} k^{2(n_1+n_2)-d}\, \tilde{\partial}_t \int_0^\infty \mathrm{d}x\, x^{\frac{d}{2}-1} \left[P_\psi(x) + \omega_1 k^2\right]^{-n_1} \left[P_\phi(x) + \omega_2 k^2\right]^{-n_2}, \tag{B.7}$$

$$\ell^{(\mathrm{FBB})d}_{n_1,n_2,n_3}(\omega_1,\omega_2,\omega_3;\eta_\psi,\eta_\phi) = -\frac{1}{2}k^{2(n_1+n_2+n_3)-d}\,\tilde{\partial}_t \int_0^\infty \mathrm{d}x\, x^{\frac{d}{2}-1}\left[P_\psi(x)+\omega_1 k^2\right]^{-n_1} \times \left[P_\phi(x)+\omega_2 k^2\right]^{-n_2}\left[P_\phi(x)+\omega_3 k^2\right]^{-n_3}, \quad \text{(B.8)}$$

$$m^{(\mathrm{B})d}_{2,2}(\omega_1,\omega_2;\eta_\phi) = -\frac{1}{2}k^{6-d}\,\tilde{\partial}_t \int_0^\infty \mathrm{d}x\, x^{\frac{d}{2}}\left[\partial_x \frac{1}{P_\phi(x)+\omega_1 k^2}\right]\left[\partial_x \frac{1}{P_\phi(x)+\omega_2 k^2}\right], \quad \text{(B.9)}$$

$$m^{(\mathrm{F})d}_{2}(\omega;\eta_\psi) = -\frac{1}{2}k^{6-d}\,\tilde{\partial}_t \int_0^\infty \mathrm{d}x\, x^{\frac{d}{2}}\left[\partial_x \frac{1}{P_\psi(x)+\omega k^2}\right]^2, \quad \text{(B.10)}$$

$$m^{(\mathrm{F})d}_{4}(\omega;\eta_\psi) = -\frac{1}{2}k^{4-d}\,\tilde{\partial}_t \int_0^\infty \mathrm{d}x\, x^{\frac{d}{2}+1}\left[\partial_x \frac{1+r_\psi(x)}{P_\psi(x)+\omega k^2}\right]^2, \quad \text{(B.11)}$$

$$m^{(\mathrm{FB})d}_{1,2}(\omega_1,\omega_2;\eta_\psi,\eta_{\phi/V}) = \frac{1}{2}k^{4-d}\,\tilde{\partial}_t \int_0^\infty \mathrm{d}x\, x^{\frac{d}{2}}\frac{1+r_\psi(x)}{P_\psi(x)+\omega_1 k^2}\partial_x \frac{1}{P_{\phi/V}(x)+\omega_2 k^2}, \quad \text{(B.12)}$$

with $n_i \in \mathbb{N}$ and where we have suppressed the scale index k for the sake of simplicity. Moreover, we have abbreviated the (inverse) regularized propagator parts by

$$P_\phi(x) \coloneqq x\left[1+r_\phi(x)\right], \qquad P_\psi(x) \coloneqq x\left[1+r_\psi(x)\right]^2. \quad \text{(B.13)}$$

For the integrations, we have substituted $q^2 \mapsto x$, that is to say

$$\int \frac{\mathrm{d}^d q}{(2\pi)^d} = 4v_d \int \mathrm{d}q\, q^{d-1} = 2v_d \int \mathrm{d}x\, x^{\frac{d}{2}-1} \qquad \text{with} \qquad v_d \coloneqq \frac{1}{4}\frac{\mathrm{Vol}(S^{d-1})}{(2\pi)^d} = [2^{d+1}\pi^{d/2}\Gamma(d/2)]^{-1}. \quad \text{(B.14)}$$

$\tilde{\partial}_t$ is defined to act only on the regulator's t-dependence,

$$\tilde{\partial}_t \coloneqq \sum_{\Phi=\phi,V,\psi}\int \mathrm{d}x' \frac{\partial_t\left[Z_\Phi r_\Phi(x')\right]}{Z_\Phi}\frac{\delta}{\delta r_\Phi(x')} \quad \text{(B.15)}$$

$$= \int \mathrm{d}x' x' \left\{\frac{\partial_t\left[Z_\phi r_\phi(x')\right]}{Z_\phi}\frac{\delta}{\delta P_\phi(x')} + \frac{\partial_t\left[Z_V r_\phi(x')\right]}{Z_V}\frac{\delta}{\delta P_V(x')} + 2\left[1+r_\psi(x')\right]\frac{\partial_t\left[Z_\psi r_\psi(x')\right]}{Z_\psi}\frac{\delta}{\delta P_\psi(x')}\right\}. \quad \text{(B.16)}$$

Both the linear and sharp regulators have the very convenient feature that all loop integrals can be performed explicitly. For the linear cutoff the results are

$$\ell^{(\mathrm{B})d}_0(\omega;\eta_\phi) = \frac{2}{d}\left(1-\frac{\eta_\phi}{d+2}\right)\frac{1}{1+\omega}, \quad \text{(B.17)}$$

$$\ell^{(\mathrm{B})d}_n(\omega;\eta_\phi) = \frac{2}{d}\left(1-\frac{\eta_\phi}{d+2}\right)\frac{n}{(1+\omega)^{n+1}}, \quad \text{(B.18)}$$

$$\ell^{(\mathrm{F})d}_0(\omega;\eta_\psi) = \frac{2}{d}\left(1-\frac{\eta_\psi}{d+1}\right)\frac{1}{1+\omega}, \quad \text{(B.19)}$$

$$\ell^{(\mathrm{F})d}_n(\omega;\eta_\psi) = \frac{2}{d}\left(1-\frac{\eta_\psi}{d+1}\right)\frac{n}{(1+\omega)^{n+1}}, \quad \text{(B.20)}$$

$$\ell^{(\mathrm{BB})d}_{n_1,n_2}(\omega_1,\omega_2;\eta_\phi,\eta_V) = \frac{2}{d}\left[\left(1-\frac{\eta_\phi}{d+2}\right)\frac{n_1}{1+\omega_1}+\left(1-\frac{\eta_V}{d+2}\right)\frac{n_2}{1+\omega_2}\right]\frac{1}{(1+\omega_1)^{n_1}(1+\omega_2)^{n_2}}, \quad \text{(B.21)}$$

$$\ell^{(\mathrm{FB})d}_{n_1,n_2}(\omega_1,\omega_2;\eta_\psi,\eta_\phi) = \frac{2}{d}\left[\left(1-\frac{\eta_\psi}{d+1}\right)\frac{n_1}{1+\omega_1}+\left(1-\frac{\eta_\phi}{d+2}\right)\frac{n_2}{1+\omega_2}\right]\frac{1}{(1+\omega_1)^{n_1}(1+\omega_2)^{n_2}}, \tag{B.22}$$

$$\ell^{(\mathrm{FBB})d}_{n_1,n_2,n_3}(\omega_1,\omega_2,\omega_3;\eta_\psi,\eta_\phi) = \frac{2}{d}\left[\left(1-\frac{\eta_\psi}{d+1}\right)\frac{n_1}{1+\omega_1}+\left(1-\frac{\eta_\phi}{d+2}\right)\left(\frac{n_2}{1+\omega_2}+\frac{n_3}{1+\omega_3}\right)\right] \times \frac{1}{(1+\omega_1)^{n_1}(1+\omega_2)^{n_2}(1+\omega_3)^{n_3}}, \tag{B.23}$$

$$m^{(\mathrm{B})d}_{2,2}(\omega_1,\omega_2;\eta_\phi) = \frac{1}{(1+\omega_1)^2(1+\omega_2)^2}, \tag{B.24}$$

$$m^{(\mathrm{F})d}_{2}(\omega;\eta_\psi) = \frac{1}{(1+\omega)^4}, \tag{B.25}$$

$$m^{(\mathrm{F})d}_{4}(\omega;\eta_\psi) = \frac{1}{(1+\omega)^4}+\frac{1-\eta_\psi}{d-2}\frac{1}{(1+\omega)^3}-\left(\frac{1-\eta_\psi}{2d-4}+\frac{1}{4}\right)\frac{1}{(1+\omega)^2}, \tag{B.26}$$

$$m^{(\mathrm{FB})d}_{1,2}(\omega_1,\omega_2;\eta_\psi,\eta_{\phi/V}) = \left(1-\frac{\eta_{\phi/V}}{d+1}\right)\frac{1}{(1+\omega_1)(1+\omega_2)^2}. \tag{B.27}$$

For the sharp cutoff we find

$$\ell^{(\mathrm{B/F})d}_{0}(\omega;\eta_{\phi/\psi}) = -\log(1+\omega)+\ell^{(\mathrm{B/F})d}_{0}(0;\eta_{\phi/\psi}), \tag{B.28}$$

$$\ell^{(\mathrm{B/F})d}_{n}(\omega;\eta_{\phi/\psi}) = \frac{1}{(1+\omega)^n}, \tag{B.29}$$

$$\ell^{(\mathrm{BB})d}_{n_1,n_2}(\omega_1,\omega_2;\eta_\phi,\eta_V) = \frac{1}{(1+\omega_1)^{n_1}(1+\omega_2)^{n_2}}, \tag{B.30}$$

$$\ell^{(\mathrm{FB})d}_{n_1,n_2}(\omega_1,\omega_2;\eta_\psi,\eta_{\phi/V}) = \frac{1}{(1+\omega_1)^{n_1}(1+\omega_2)^{n_2}}, \tag{B.31}$$

$$\ell^{(\mathrm{FBB})d}_{n_1,n_2,n_3}(\omega_1,\omega_2,\omega_3;\eta_\psi,\eta_\phi) = \frac{1}{(1+\omega_1)^{n_1}(1+\omega_2)^{n_2}(1+\omega_3)^{n_3}}, \tag{B.32}$$

$$m^{(\mathrm{B})d}_{2,2}(\omega_1,\omega_2;\eta_\phi) = \frac{1}{(1+\omega_1)^2(1+\omega_2)^2}, \tag{B.33}$$

$$m^{(\mathrm{F})d}_{2}(\omega;\eta_\psi) = \frac{1}{(1+\omega)^4}, \tag{B.34}$$

$$m^{(\mathrm{F})d}_{4}(\omega;\eta_\psi) = \frac{1}{(1+\omega)^4}, \tag{B.35}$$

$$m^{(\mathrm{FB})d}_{1,2}(\omega_1,\omega_2;\eta_\psi,\eta_\phi) = \frac{1}{(1+\omega_1)(1+\omega_2)^2}. \tag{B.36}$$

Acknowledgments

I do not want to miss the opportunity to thank those who have supported me during the development of this work. In particular, I am deeply indepted to my supervisor Holger Gies; thank you for setting such a great example as scientist and beyond.

Let me thank Lorenz von Smekal, Igor Herbut, and Christian Fischer for their willingness to take the time to examine this thesis. I am grateful to Björn Wellegehausen, Daniel Scherer, and Michael Scherer for proofreading parts of the manuscript and for their useful comments. Many helpful discussions with Jens Braun, Simon Hands, Igor Herbut, Markus Huber, Stefan Rechenberger, Daniel Scherer, Michael Scherer, Lorenz von Smekal, Björn Wellegehausen, and Andreas Wipf are gratefully acknowledged.

This work has been supported by the DFG under GRK 1523 and FOR 723.

I would like to thank my parents, Bettina and Wolfgang Janssen, for their participation and support for this work.

Naively, one would expect the things that matter to be explained by the father to the daughter. In our family, it is sometimes the other way round. Thank you, little Rebekka, for sharing with me your insights on phase transitions and critical phenomena.

I am more than thankful to my precious wife Maria. You have an at least equal part in the completion of this thesis.

Zusammenfassung

In der vorliegenden Arbeit werden kritische Phänomene in (2+1)-dimensionalen relativistischen Fermiontheorien untersucht. Diese Systeme modellieren einerseits das Niederenergieverhalten von neuartigen zweidimensionalen Festkörpern; darüber hinaus zeigen sie andererseits eine derart reichhaltige Phasenstruktur, welche an sich bereits lohnenswert zu erforschen ist. Oft können Effekte, die in komplizierteren Feldtheorien auftreten, bis zu einem gewissen Grad auf solche niederdimensionalen Modelle abgebildet werden. Mithilfe von quantitativen Vergleichen in den Modellen können quantenfeldtheoretische Methoden getestet und verfeinert werden. In früheren Studien hat sich allerdings herausgestellt, dass diese Systeme sehr viel schwieriger zu handhaben sind als ursprünglich gedacht: In QED_3 und dem Thirring-Modell wird erwartet, dass chirale Symmetriebrechung oberhalb einer kritischen Fermionzahl N_f^cr verboten ist; die erhaltenen Werte für N_f^cr und noch mehr die Vorhersagen für das Wesen des Phasenübergangs unterscheiden sich aber ganz erheblich.

In dieser Arbeit wird das Thirring-Modell sowie eine Variante des chiralen Gross-Neveu-Modells mithilfe der funktionalen Renormierungsgruppe (RG) untersucht. Dabei handelt es sich um einen analytischen Zugang zu stark wechselwirkenden Systemen, mit dessen Hilfe in der Vergangenheit äußerst präzise Vorhersagen für kritische Exponenten in vergleichbaren Systemen getroffen werden konnten. Für das chirale Gross-Neveu-Modell werden die kritischen Exponenten ν, η_ϕ und ω berechnet, wobei eine unterschiedliche Anzahl von links- und rechtshändigen Fermionen erlaubt wird – in diesem Sinne können diese Systeme als Spielzeugmodelle für den Higgs-Yukawa-Sektor im Standardmodell der Elementarteilchenphysik angesehen werden. Die RG Analyse im Thirring-Modell basiert auf einer vollständigen Basis von fermionischen 4-Punkt-Funktionen. Es wird gezeigt, dass das UV vollständige (asymptotisch sichere) Thirring-Modell in einer zweidimensionalen Kopplungsebene liegt, welche nur im Limes großer Fermionzahl mit der konventionellen Thirring-Kopplung zusammenfällt. Dies erlaubt erstmalig ein mikroskopisches Verständnis des Quantenphasenübergangs bei N_f^cr: Demnach wird chirale Symmetriebrechung für große N_f aufgrund von konkurrierenden Ordnungsparametern verhindert. Basierend auf der fermionischen Analyse werden schließlich mithilfe von dynamischer Bosonisierung detaillierte quantitative Vorhersagen für das kritische Verhalten in Form der universellen Exponenten ν, η_ϕ, β, γ und ω gemacht.

Ehrenwörtliche Erklärung

Ich erkläre hiermit ehrenwörtlich, dass ich die vorliegende Arbeit selbständig, ohne unzulässige Hilfe Dritter und ohne Benutzung anderer als der angegebenen Hilfsmittel und Literatur angefertigt habe. Die aus anderen Quellen direkt oder indirekt übernommenen Daten und Konzepte sind unter Angabe der Quelle gekennzeichnet. Ergebnisse, die in Zusammenarbeit mit Mitarbeitern des Theoretisch-Physikalischen Institutes in Jena entstanden sind, sind in der Arbeit entsprechend benannt.

Weitere Personen waren an der inhaltlich-materiellen Erstellung der vorliegenden Arbeit nicht beteiligt. Insbesondere habe ich hierfür nicht die entgeltliche Hilfe von Vermittlungs- bzw. Beratungsdiensten (Promotionsberater oder andere Personen) in Anspruch genommen. Niemand hat von mir unmittelbar oder mittelbar geldwerte Leistungen für Arbeiten erhalten, die im Zusammenhang mit dem Inhalt der vorgelegten Dissertation stehen.

Die Arbeit wurde bisher weder im In- noch im Ausland in gleicher oder ähnlicher Form einer anderen Prüfungsbehörde vorgelegt.

Die geltende Promotionsordnung der Physikalisch-Astronomischen Fakultät ist mir bekannt.

Ich versichere ehrenwörtlich, dass ich nach bestem Wissen die reine Wahrheit gesagt und nichts verschwiegen habe.

Jena, 20.03.2012